



UNIVERSITÀ DEGLI STUDI DI MILANO

Department of Food, Environmental and Nutritional Sciences

Ph.D. School in Food Systems

XXXII Cycle

**Thermodynamic stability of
ISG-like model lipid membranes:
inspecting the contributions of lipid-lipid
interaction and action of free fatty acids
in the frame of type 2 diabetes mellitus disease**

CHIM/02

Ph.D. Candidate:

Francesca SAITTA (R11565)

Tutor: Prof. Dimitrios FESSAS

Dean: Prof. Ella PAGLIARINI

Academic Year 2018/2019

Contents

Abstract	1
1 Introduction	5
1.1. Type 2 diabetes mellitus and molecular hypotheses	5
1.2. Free fatty acids	10
1.3. Phospholipid bilayers and vesicles	12
1.4. Cell membrane thermodynamics and differential scanning calorimetry	15
1.5. References	21
2 Aims and objectives	29
2.1. Research purposes	29
2.2. References	33
3 Cell membrane thermodynamics: dissecting the contributions	35
3.1. Introduction	35
3.2. Materials and methods	37

3.2.1. Materials	37
3.2.2. Liposomes preparation	38
3.2.2.1. Preparation of giant unilamellar vesicles (GUVs)	38
3.2.2.2. Preparation of large unilamellar vesicles (LUVs)	38
3.2.2.3. Preparation of small unilamellar vesicles (SUVs)	38
3.2.2.4. Preparation of multilamellar lipid bilayers (MLBs)	39
3.2.2.5. Preparation of multilamellar lipid vesicles (MLVs)	39
3.2.3. Spectroscopic characterization	39
3.2.4. Thermal analysis measurements	40
3.3. Results and discussion	42
3.3.1. Lamellarity and size effects	42
3.3.2. Mixing effects	45
3.3.3. Effects of unsaturated phospholipid acyl chains	55
3.3.4. Hierarchy of thermodynamic contributions	56
3.3.5. Spectroscopic characterization	57
3.4. References	59
4 ISG-representative model membranes	63
4.1. Introduction	63
4.2. Materials and methods	65
4.2.1. Materials	65
4.2.2. Selection of vesicles constituents	65
4.2.3. Liposomes preparation	65
4.2.4. Thermal analysis measurements	66

4.3. Results and discussion	68
4.3.1. From five to fourteen-components vesicles	68
4.3.2. ISG-like membrane: influence of cholesterol	73
4.4. References	75
5 Free fatty acids effects on lipid membranes	80
5.1. Introduction	80
5.2. Materials and methods	82
5.2.1. Materials	82
5.2.2. Liposomes preparation	82
5.2.3. Spectroscopic characterization	83
5.2.4. Thermal analysis measurements	83
5.3. Results and discussion	83
5.3.1. Spectroscopic characterization	83
5.3.2. FFAs on simple model membranes	84
5.3.3. FFAs on ISG-like membranes	90
5.4. References	95
6 Peptide-membrane interaction	100
6.1. Introduction	100
6.2. Materials and methods	102
6.2.1. Materials	102
6.2.2. Liposomes preparation	102
6.2.3. Nisin purification and stock solutions preparation	103
6.2.4. Thermal analysis measurements	103

6.2.5. Spectroscopic characterization	104
6.2.5.1. Fluorescence spectroscopy	104
6.2.5.2. Dynamic light scattering	105
6.3. Results and discussion	105
6.3.1. Model membrane design	105
6.3.2. Differential scanning calorimetry and fluorescence spectroscopy	109
6.3.3. Dynamic light scattering	119
6.4. References	124
7 General conclusions	128
8 Implications and future directions	131
Appendices	133
A. Side projects	134
i. Thermodynamic Stability of Myoglobin-Poly(Ethylene Glycol) Bioconjugates: a Calorimetric Study	134
ii. pH-responsive chimeric liposomes: from nanotechnology to in vivo application	136
iii. The DSC monitoring of oil melting to follow the oil curing	139
iv. Thermodynamic studies of AgamOBP4 and AgamOBP5 from Anopheles gambiae with different semiochemicals	141
v. Mechanism of action of Sakacin-A, a bacteriocin with potential	145
B. List of publications	148
i. Papers with impact factor	148

ii. Parts in books	149
iii. Communications to scientific meetings	150
C. Honours and awards	154
D. Other activities	156
Acknowledgments	159

Abstract

A stepwise study of vesicles with different morphology and lipid composition was performed through high-sensitivity differential scanning calorimetry at physiological pH with the purpose of comprehending the role played by some of the main factors that contribute to the thermodynamic stability of cell membranes, achieving the preparation of artificial lipid vesicles that highly resembled the phospholipid bilayer of Insulin Secretory Granules (ISGs), vesicles located in the pancreatic Langerhans β -cells and which are responsible for insulin and amylin storage and secretion in response to nutrient intake. All the considered vesicle preparations were aimed at representing only the lipid component of ISGs membrane, *i.e.* the phospholipid bilayer, but we will refer to all as “model membranes” in this thesis for simplicity' sake.

Curvature effects were considered by analysing the micro-DSC profiles of small, large and giant unilamellar vesicles prepared as pure and mixed systems of DMPC, DPPC, DSPC. The cross-study of binary systems composed by DMPC, DPPC, DSPC and DPPC, DPPS, DPPE allowed the dissection of the role played by several phospholipid headgroups and tails on the thermotropic behaviour of cell membranes, whilst the addition of DOPC, an unsaturated phospholipid, to a completely saturated ternary membrane characterized by only a specific phospholipid headgroup (choline) revealed the strong influence of unsaturated tails on membrane lipid organization.

Therefore, a hierarchy of contribution to the overall thermodynamic stability of membranes was depicted as

membrane curvature < phospholipid headgroup < phospholipid tail <
phospholipid unsaturation.

The following inclusion of sphingomyelins and lysophosphatidylcholines to a DPPC:DPPE:DPPS ternary membrane, whose composition already reflected the proportions in ISGs, together with a more complete fatty acids distribution characterizing the phospholipid bilayer of the ISGs allowed us to achieve the preparation of a high-complexity fourteen-components model membrane that reflected the 80% of phospholipids present in such a real system. The inclusion of cholesterol was finally considered for the achievement of the final ISG-like membrane.

Furthermore, the effect of Free Fatty Acids (FFAs), whose levels are recurrently altered in diabetic and/or obese subjects, on the thermodynamic stability of selected membranes was investigated. The results highlighted strong stabilizing effects on the membranes as well as pronounced phase segregations in the case of saturated acids (palmitic and stearic acids), moderate stabilizing effects for a *trans*-unsaturated FFA (elaidic acid), whereas the opposite effect was observed in the case of a *cis*-unsaturated one (oleic acid).

Finally, in order to investigate the interaction between model membranes and a pore-forming peptide (nisin), calorimetric and spectroscopic measurements were carried out. With this purpose, a simplified model membrane that resembled the thermodynamics of the ISG-like membrane was modelled by combining specific percentages of DMPC, DPPS and DOPC. Nisin-membrane interaction was studied on the simplified membrane through micro-DSC, fluorescence anisotropy and DLS at physiological pH, also highlighting the role of six different FFAs on peptide-membrane interaction, namely two saturated FFAs (palmitic and stearic acids), two monounsaturated FFAs (the *cis*-unsaturated oleic acid and the *trans*-unsaturated elaidic acid)

and two polyunsaturated FFAs (the ω -6 linoleic acid and the ω -3 docosahexaenoic acid or DHA).

Italian version

Allo scopo di comprendere il ruolo giocato da alcuni dei principali fattori che contribuiscono alla stabilità termodinamica delle membrane cellulari, è stato effettuato uno studio progressivo di vescicole con diversa morfologia e composizione lipidica a pH fisiologico mediante calorimetria a scansione differenziale ad alta sensibilità (High-Sensitivity DSC), raggiungendo la preparazione di vescicole lipidiche artificiali che rappresentano abbondantemente il doppio strato fosfolipidico dei granuli secretori di insulina (ISGs), vescicole presenti nelle cellule β di Langerhans del pancreas e addette alla conservazione e cosecrezione di insulina e amilina in seguito al consumo di alimenti. Tutte le vescicole sono state preparate allo scopo di rappresentare solamente la componente lipidica delle membrane delle ISGs, ovvero il bilayer fosfolipidico, ma per motivi di semplicità saranno tutte indicate come "membrane modello" in questa tesi.

Gli effetti della curvatura di membrana sono stati considerati analizzando i profili micro-DSC di vescicole unilamellari piccole, grandi e giganti preparate come sistemi puri e misti di DMPC, DPPC e DSPC. Lo studio incrociato di sistemi binari composti da DMPC, DPPC, DSPC e DPPC, DPPS, DPPE ha consentito la discriminazione dei ruoli giocati dalle diverse teste e code fosfolipidiche riguardo al comportamento termotropico delle membrane cellulari, mentre l'aggiunta di DOPC, un fosfolipide insaturo, ad una membrane ternaria completamente satura e caratterizzata da solo una specifica testa fosfolipidica (colina) ha rivelato la forte influenza che le code insature hanno sull'organizzazione dei lipidi in membrana. Quindi, è stato

possibile delineare una gerarchia di contributi alla stabilità complessiva delle membrane:

curvatura di membrana < testa fosfolipidica < coda fosfolipidica <
insaturazione fosfolipidica.

La successiva inclusione di sfingomieline e lisofosfatidilcoline alla membrana ternaria DPPC:DPPE:DPPS, la cui composizione rifletteva già le proporzioni delle ISGs, insieme ad una distribuzione più completa di acidi grassi presenti nel bilayer fosfolipidico delle ISGs ha permesso di giungere alla preparazione di una membrana modello complessa costituita da quattordici componenti che riflette l'80% dei fosfolipidi presenti nel sistema reale. Infine, è stata considerata anche l'inclusione del colesterolo portando all'ottenimento della membrana simil-ISG finale.

L'effetto di acidi grassi liberi (FFAs), i cui livelli sono spesso elevati in soggetti diabetici e/o obesi, sulla stabilità termodinamica di membrane selezionate è stato inoltre investigato. I risultati hanno evidenziato forti effetti stabilizzanti sulle membrane e pronunciate segregazioni di fase nel caso di acidi saturi (acidi palmitico e stearico), moderati effetti stabilizzanti per un acido insaturo *trans* (acido elaidico), mentre effetti opposti sono stati riscontrati per un acido insaturo *cis* (acido oleico).

Infine, sono state effettuate misure calorimetriche e spettroscopiche allo scopo di investigare l'interazione tra membrane modello e un peptide in grado di formare pori (nisina). A tale scopo, è stata progettata una membrana modello semplificata rappresentante la termodinamica della membrana simil-ISG combinando specifiche percentuali di DMPC, DPPS e DOPC. L'interazione nisina-membrana è stata studiata sulla membrana semplificata mediante micro-DSC, anisotropia di fluorescenza e DLS a pH fisiologico, evidenziando inoltre il ruolo di sei diversi FFAs sull'interazione peptide-membrana, ossia due FFAs saturi (acidi palmitico e stearico), due monoinsaturi (acido oleico come acido insaturo *cis* e acido elaidico come acido insaturo *trans*) e due acidi grassi polinsaturi (l'acido linoleico come ω -6 e l'acido docosaesaenoico o DHA come ω -3).

Introduction

1.1. Type 2 diabetes mellitus and molecular hypotheses

Type 2 Diabetes Mellitus is a chronic disease that is increasingly spreading in developed countries, as among the Italian population (ISTAT, 2018a), and in developing ones. Moreover, subjects affected by diabetes mellitus (both type 1 and type 2) are now near to 400 million and, according to global estimates (Guariguata et al., 2014), they will reach 600 million by 2035 (Fig.1.1).

Factors that influence the rapid spreading of such disease are not only genetic nature, but may also derive from environmental conditions: socio-economic modifications, ageing of the population, variations in society nutrition habits and life-style have contributed in incrementing the percentage of overweight and/or obese individuals, which in turn have led to a higher diffusion of diabetes and related complications among adults. Indeed, the increase in weight strictly correlated to the insurgence of insulin-resistance (ISTAT, 2018b; Kahn and Flier, 2000), which is considered as the starting point for the development of the disease. Furthermore, an inversely correlation between the average Body Mass Index (BMI) and the age at diagnosis of diabetes has been shown: the higher the BMI, the sooner diabetes is manifested (Logue et al., 2011). In spite of the numerous campaigns and recommendations intended to diffuse a healthier lifestyle (for instance based on a Mediterranean diet), ISTAT data show that over-65 subjects represent

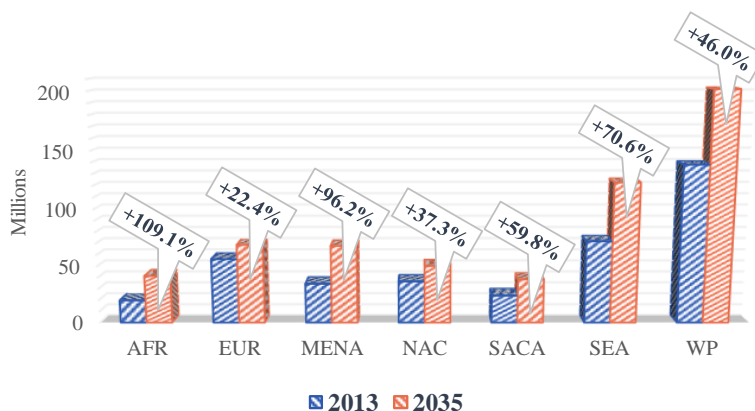


Figure 1.1: *Diabetes prevalence and number of people affected by diabetes (20-79 years) by International Diabetes Federation (IDF) Region for 2013 and 2035. IDF regions considered are Africa (AFR), Europe (EUR), Middle East and North Africa (MENA), North America and Caribbean (NAC), South and Central America (SACA), South-East Asia (SEA) and Western Pacific (WP). (Guariguata et al., 2014)*

the higher percentage of population to be affected by obesity and/or overweight (ISTAT, 2018b). Nevertheless, the reason and the manner in which obesity and, generally, factors related to nutrition are related to the onset of Type 2 Diabetes Mellitus have not been completely comprehended yet.

Diabetes mellitus is a disease that is characterized by a high glucose concentration in blood and can be differentiated from diabetes insipidus, which instead does not manifest altered glucose concentration in the bloodstream. Different types of diabetes mellitus can be identified depending on the factors that cause the high blood glucose levels. The term “diabetes” commonly refers to the one more properly referred to as type 2 diabetes mellitus (T2DM), which is more widespread than type 1 diabetes (or juvenile diabetes) and gestational diabetes, for instance. It is a metabolic disorder that occurs after a reduction in insulin activity, the hormone which is responsible for the regulation of blood glucose level: this hormone promotes glucose access into the cytosol of cells

of insulin-dependent organs by binding to a receptor outside the cell membrane. In particular, diabetes can be due to a reduced availability of this hormone, to an impediment to its normal action, or a combination of these two factors.

Normally, glucose and all nutrients are absorbed through the gut wall upon nutrition and enter the bloodstream. The increase in blood glucose level stimulates the insulin secretion by the pancreatic Langerhans β -cells which in turn promotes glucose absorption (Fig.1.2).

If insulin-resistance appears, cells do not properly respond to insulin and glucose input is thus reduced. In an attempt to lower the high glycaemic concentration, pancreatic β -cells start to secrete larger amounts of insulin. This is the reason why individuals affected by insulin resistance are also characterized by high insulin levels. However, though at the beginning the higher insulin concentration seems to compensate for the lack in cellular

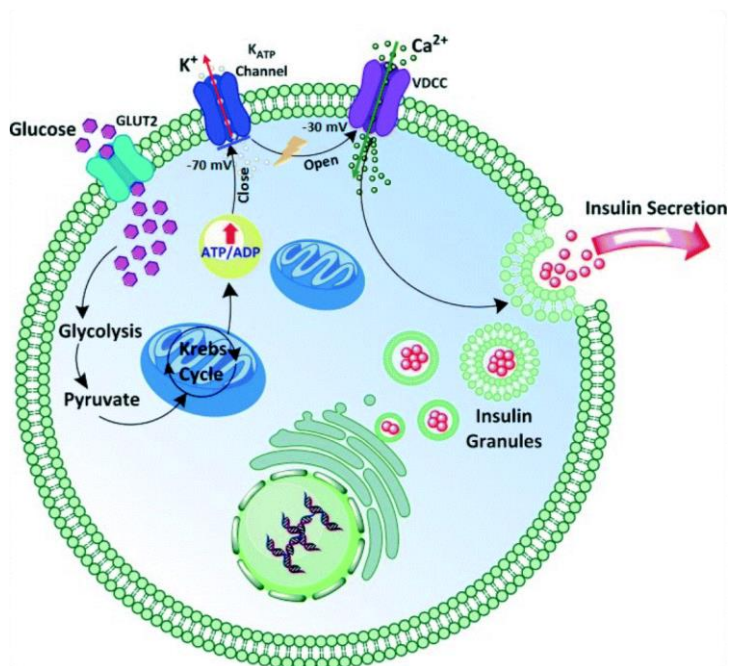


Figure 1.2: *Glucose-stimulated insulin secretion pathway in pancreatic β -cells.* (Castiello et al., 2016)

response, β -cells efforts are insufficient too in the long run. Therefore, the initial "simple" insulin-resistance can turn into T2DM without treatments.

Despite the research of the last twenty years, the causes and the molecular mechanisms that trigger the disease onset are not completely understood yet. It is clear today that two main phenomena are involved, each based on different mechanisms: the decrease of insulin effectiveness (insulin resistance) and the pancreatic β -cells failure. The second one includes a reduction both in the β -cells mass and function and, besides several biochemical mechanisms leading to apoptosis, the literature reports the possible involvement of an amyloidogenic protein (Westermarck et al., 2011) (Fig.1.3). The Islet Amyloid Polypeptide (IAPP), also known as Amylin, is a hormone which is cosecreted and costored with insulin in vesicles named Insulin Secretory Granules (ISGs), complex intracellular organelles of the pancreatic Langerhans β -cell dedicated to insulin storage and secretion in response to nutrient intake (Young, 2005). These subcellular vesicles have been characterized as phospholipid bilayer spheres of about 300nm of diameter (Hutton, 1989; Olofsson et al., 2002) containing a crystalline core of insulin and zinc surrounded by a halo region of amylin together with other additional molecules (Hutton et al., 1982; Westermarck et al., 1996). However, such a granule is far more than just a repository of the hormones in the cell since it is the site of insulin proteolytic activation and it is involved in intercellular communication. Moreover, its membrane contains a variety of proteins which are key components for secretion control, different catalytic activities and messenger functions (Hutton, 1989).

Studies performed in vitro, tissue culture and post-mortem analysis showed that, for unknown reasons, human IAPP (hIAPP) starts to form aggregates that are involved in Langerhans β -cells death (Aitken et al., 2010) and also affect the severity of the disease. Moreover, it seems that hIAPP oligomeric species might be involved in membrane fragmentation processes, whereas mature fibers seem to be inert since they do not manifest any cytotoxic action.

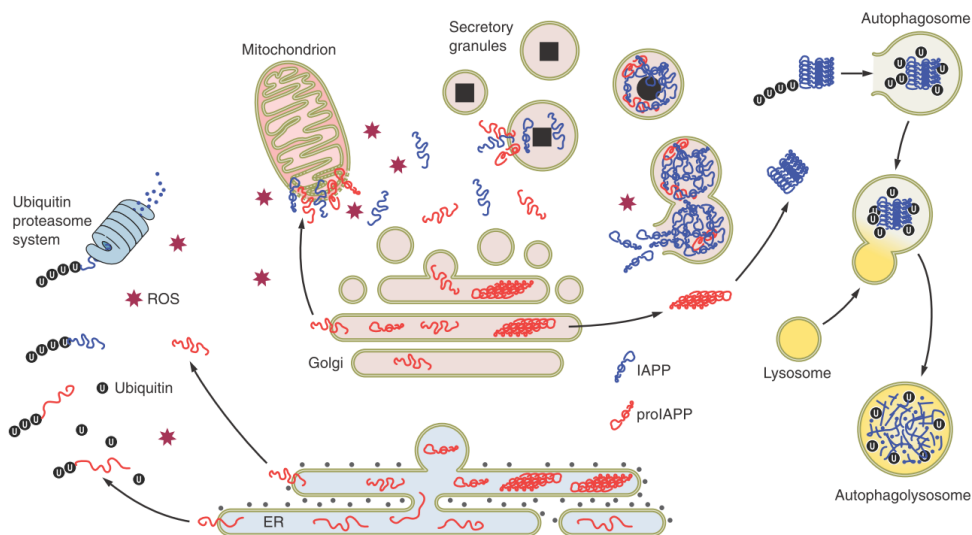


Figure 1.3: Hypothetical ways by which IAPP aggregates may develop and be toxic. (Westermarck et al., 2011)

As for the action of hIAPP oligomers, the water/plasma membrane interface seems to play a key role in the aggregation process of amyloid fibres (Zhang et al., 2012) and then in the onset and progression of T2DM. It has been hypothesized that oligomers could damage the cell membrane through four processes: by changing the fluidity of the phospholipid bilayer, by forming pores stabilized by proteins, by forming a layer on the membrane, or by removing the lipid components from the membrane through a detergent-like mechanism (Anguiano et al., 2002; Hebda and Miranker, 2009; Sciacca et al., 2012a, 2012b). The main goal of several studies has been to understand the mechanism by which hIAPP acts against the phospholipid bilayer and a recent research has allowed to hypothesize a mechanism with two independent steps of each other that could describe such a mechanism. The first step would be characterized by the formation of pores as a result of the penetration of oligomeric or monomeric species into the hydrophobic core of the bilayer. These protein structures would interfere with the lipids packing and may cause a local deformation of the membrane at high concentrations. This deformation

would not be energetically favoured and proteins clustering would occur in order to reduce such deformation (Pannuzzo et al., 2013). Instead, the second step would be characterized by membrane destruction as a result of the aggregation of amyloid fibres on the surface of the bilayer, which would cause the dissolution of the bilayer itself through a detergent-like mechanism (Sciacca et al., 2012a, 2012b).

Among several factors, the “resistance” against such a fragmentation process strongly depends on the thermodynamic stability of the membranes, which in turn is strictly correlated to the phospholipid composition and the morphology of the bilayer and to the environmental composition.

1.2. Free fatty acids

Most dietary fats are provided in the form of triglycerides, which must be hydrolyzed to fatty acids and monoacylglycerols in order to be absorbed. The free fatty acids and monoglycerides are absorbed by the enterocytes, cells responsible for nutrients absorption, of the intestinal wall. In general, fatty acids which have a chain length of less than 14 carbons have direct access to the portal vein to be transported to the liver. Fatty acids with 14 or more carbons units are re-esterified within the enterocytes and enter the circulation via the lymphatic route as chylomicrons or via the portal route as well (McDonald et al., 1980).

Because of their hydrophobicity, most of free fatty acids (FFAs) are conveyed by albumin in plasma. Albumin-bound FFAs are unable to enter cells or bind to proteins, whereas the effectively physiologically active FFAs correspond to the tiny unbound fraction which is typically $<10^{-4}$ of the total FFAs concentration in human serum (Huber and Kleinfeld, 2017). Unbound-FFAs levels increase exponentially when the total FFAs-to-albumin ratio increases, making the unbound-FFAs levels very sensitive to physiologic changes (Richieri and Kleinfeld, 1995).

Low levels of FFAs are normally present in cell membranes (around 0.3-10% of total lipids) (O'Connor et al., 1999) as they may take part to exchange processes with lipid membranes (Jespersen et al., 2012), as well as done by other amphiphilic molecules (Needham and Zhelev, 1995). FFAs have been shown to be involved in several membrane-mediated cellular processes as membrane-bound enzyme activity (Schmalzing and Kutschera, 1982), lipid-assisted protein transport across the bilayer (La Rosa et al., 2016), fusion of lipid vesicles and cells (Creutz, 1981) and/or alteration of the microdomains of cell phospholipid bilayers as well as their physical properties (Ibarguren et al., 2014; Klausner et al., 1980). Moreover, they also act as signalling molecules for several cell mechanisms (Brash, 2001; Desbois and Smith, 2010; Kenny et al., 2009; Khan et al., 1995; Ruzin and Novick, 2000), for instance insulin secretion (Itoh et al., 2003).

However, altered FFAs are generally associated to pathological conditions. For instance, plasma FFA concentration is generally high in obese subjects. Indeed, the amount of FFA tends to be increasingly high with the increase in weight since more FFA are released from an enlarged adipose tissue and the clearance of these fatty acids is reduced (Björntorp et al., 1969).

Elevated plasma FFAs levels also characterize diabetic people. Indeed, the concentration of FFAs detected during meals and fasting displays more elevated values for individuals affected by severe type 2 diabetes than those registered for mildly diabetic subjects and healthy ones (Reaven et al., 1988). Furthermore, FFAs have been shown to have particular effects on pancreatic β -cells turnover and function depending on their chemical structure maybe modifying the fluidity of pancreatic β -cells phospholipid bilayer or through specific metabolic pathways. Indeed, Maedler et al. (2001) showed how the saturated palmitic acid is able to reduce the proliferative capacity of β -cells and to induce β -cell death mainly by apoptosis, whilst the monounsaturated palmitoleic acid exhibits the opposite effects by promoting β -cell proliferation and counteracting the toxic effects of saturated FFAs. In addition, the synergic action of saturated FFAs as palmitate with increasing levels of glucose typical

of diabetes mellitus have been shown to be deleterious for the architecture of cell compartments (Molina et al., 2009).

On the other hand, besides the direct action of FFAs on cell membranes, an active role of FFAs in protein transport through the phospholipid bilayers has been recently highlighted by molecular dynamics (La Rosa et al., 2016). Several surfactants have been tested, exhibiting a lipid chain length depending protein absorption, with maximum rates corresponding to medium-sized surfactants (*e.g.*, long chain FFAs), whereas this lipid-assisted protein transport is less promoted by large (*e.g.*, double-tail phospholipids) and small amphiphilic molecules.

1.3. Phospholipid bilayers and vesicles

The investigation of the forces that drive the self-assembly of phospholipid bilayers and that induce a particular thermodynamic behaviour is crucial for the determination of their roles in biological environments. For this reason, the thermodynamics of phospholipid bilayers and vesicles has been largely studied in the last years.

Liposomes are small artificial vesicles of spherical shape that may be made of phospholipids. Such molecules are amphiphilic molecules composed by a hydrophilic polar headgroup, as choline, serine, ethanolamine, etc., and two hydrophobic tails which consist in acyl chains that may be characterized by different length and unsaturation level (Fig.1.4). Phospholipids have been displayed to spontaneously form closed structures when they are hydrated in aqueous solutions by arranging themselves in order to direct all the hydrophilic headgroups toward the aqueous medium, whereas the hydrophobic tails of the facing lipid leaflets are protected from water by the polar heads (Fig.1.4). The resulting vesicles may consist of one or more phospholipid bilayers whose flexibility, permeability and surface charge may be tuned through the selection of specific phospholipids and compositional proportions. For instance, saturated phospholipids provide compact, rigid and impermeable bilayers,

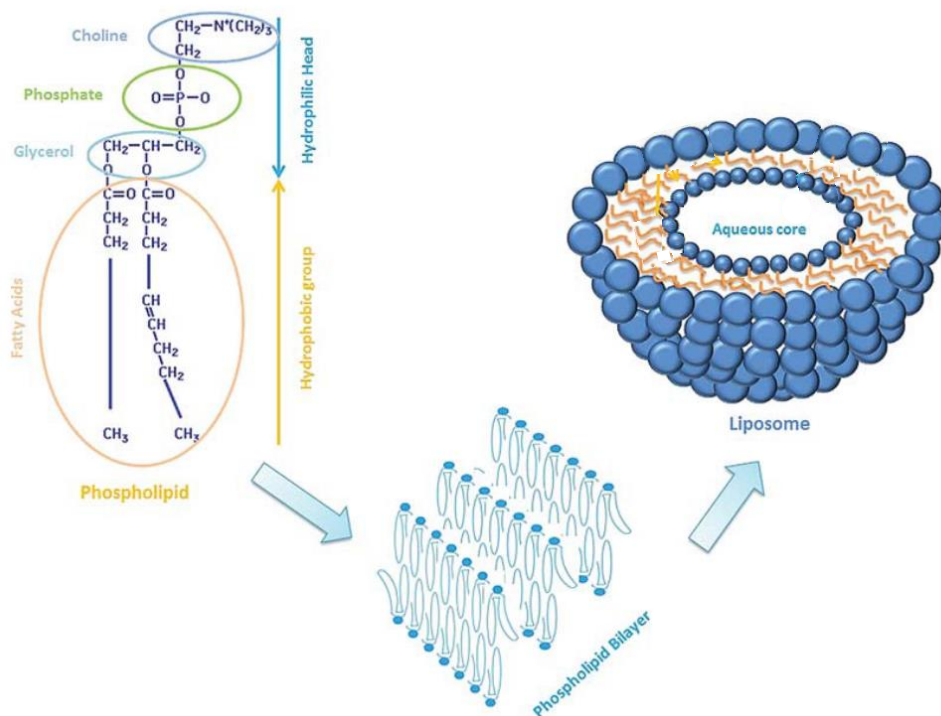


Figure 1.4: Chemical structure of a phospholipid and schematic drawing of liposomes. (Laouini et al., 2012).

whereas unsaturated phospholipids form more permeable, fluid and less stable structure (Allen, 1997; Gabizon et al., 1998; Sahoo and Labhasetwar, 2003).

Due to their biocompatibility, size and hydrophobic/hydrophilic character, liposomes have found several applications in biochemical, medical and pharmaceutical fields as novel nanotechnologies like biosensors and drug carriers in which apolar drugs are trapped within the hydrophobic region, whilst polar drugs are enclosed into the aqueous cavity (Bozzuto and Molinari, 2015; Gardikis et al., 2010, 2011; Pippa et al., 2015; Testa et al., 2001). Of course, besides the aforementioned applications, lipid vesicles are also exemplary model systems able to provide simulations of both cytoplasmic membrane and cell compartments.

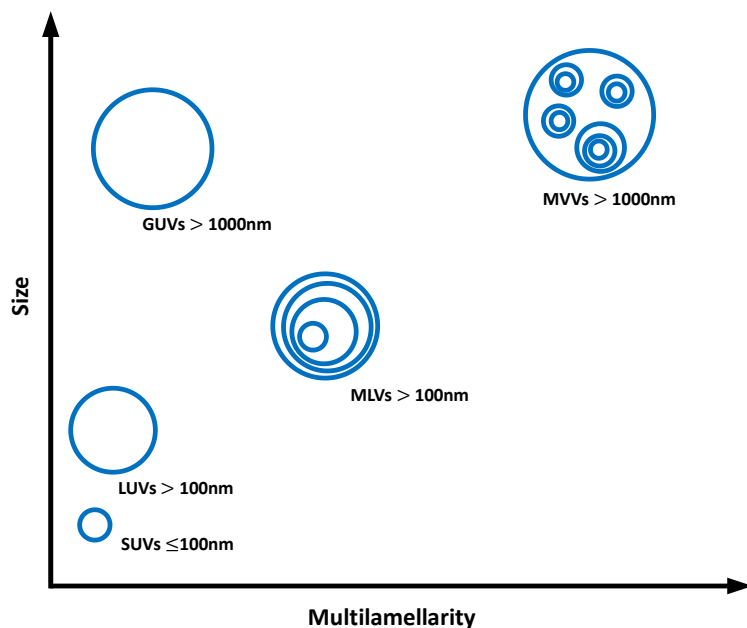


Figure 1.5: Liposomes classification based on size and lamellarity.

Generally, liposomes are classified basing on their particle size and number of bilayers (Fig.1.5):

- i. Small unilamellar vesicles (SUVs, $\leq 100\text{nm}$);
- ii. Large unilamellar vesicles (LUVs, $> 100\text{nm}$);
- iii. Giant unilamellar vesicles (GUVs, $> 1000\text{nm}$);
- iv. Multilamellar vesicles (MLVs);
- v. Multivesicular vesicles (MVVs).

Different liposome preparation methods maybe applied depending on the desired physical properties (e.g. size and lamellarity) (Laouini et al., 2012; Moscho et al., 1996).

Modification in lipid composition and morphological characteristics are able to produce adjustments of liposome structure, which in turn might lead to variations of their physicochemical properties. Based on X-ray scattering data (Brzustowicz and Brunger, 2005), in the last decades molecular dynamic investigations (Marrink and Mark, 2003; Risselada and Marrink, 2009) have

provided structural information on high curved liposomes prepared by using mixtures of phospholipids which differ in headgroups and tails (saturated and unsaturated) in order to test the relation between their molecular shape and the response to curvature stress (Mouritsen, 2011). For instance, high curved phospholipid bilayers undergo demixing phenomena due to differences in packing which lead to a heavy asymmetry between inner and outer leaflets: the inner leaflet becomes enriched in phospholipids with smaller headgroups compared to tails (cone shaped phospholipids) allowing the last ones to assume a more disordered conformation; on the other hand, the outer one becomes mainly composed of cylindrically and inverted-cone shaped phospholipids (such as lysophospholipids), leading to a backfolding of polyunsaturated tails towards the outside. As a consequence of these stressed geometry and asymmetry, high curved liposomes have a different phase behaviour showing a radius-dependent main phase transition below a certain threshold (Biltonen and Lichtenberg, 1993; Koynova and Caffrey, 1998). Furthermore, Bacia et al. (2005) showed how the molecular and structural properties of sterols make them capable of producing lipid segregation and rafts in giant unilamellar vesicles (GUVs) prepared with a mixture of dioleoyl-phosphatidylcholine (DOPC), sphingomyelin and sterol as well as negative and positive curvature at the rafts' boundaries.

Investigations on model membranes may be mainly carried out through calorimetric, spectroscopic and imaging techniques and allow to obtain significant information for the comprehension of the behaviour and functionality of real cell membranes.

1.4. Cell membrane thermodynamics and differential scanning calorimetry

Calorimetry is a key tool when we are dealing with membrane thermodynamics. Approaches based on several calorimetric techniques are feasible, such as differential scanning calorimetry (DSC) (Drazenovic et al.,

2015; Gardikis et al., 2010, 2011; Shaikh et al., 2009) and isothermal titration calorimetry (ITC) (Høytrup et al., 2001; Yokoyama et al., 2013), even though DSC is maybe the most used technique for such a purpose (Demetzos, 2008).

A DSC experiment consists in the measurement of the difference in heat flow between the sample and the reference systems while the two cells are constrained to a predetermined temperature program at constant pressure. Specifically for a power-compensating DSC (Fig.1.6), two identical crucibles (one for the sample and one for the reference), whose material has not to interact with the examined sample, are located into two separate small furnaces each of which is provided with a heating unit and a temperature

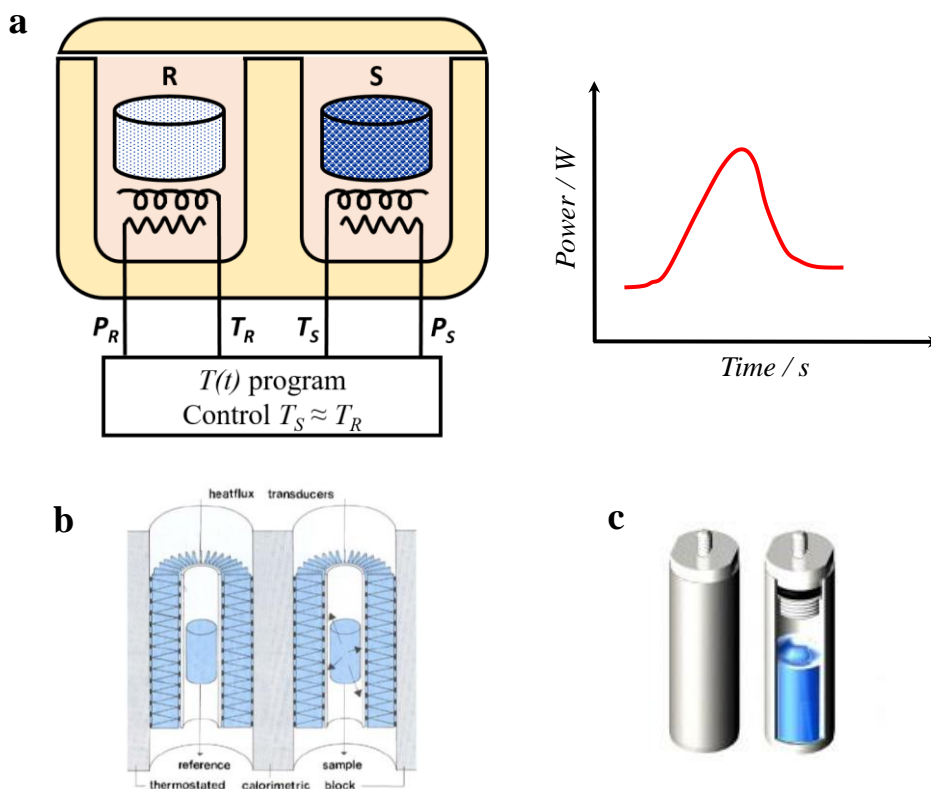


Figure 1.6: a) General scheme of a power-compensating DSC apparatus (left) and a common DSC thermogram (right); b) Graphical representation of a power-compensating high-sensitivity DSC as Setaram micro-DSCIII employed for the research discussed in this thesis; c) hermetically closed cylindrical crucibles used with Setaram micro-DSCIII.

sensor. During the measurement, the difference between the temperature of sample's and the reference's furnaces is kept at a minimum thanks to the presence of a control heater that adapts the heating powers. If there are not asymmetries between reference and sample, any difference in temperature between the compartments is proportional to the difference in power provided to both. If a difference in the resulting temperatures occurs, for instance because of differences in the heat capacity between sample and reference sample or to exothermic/endothermic transformations in the sample, an additionally heating power is provided in order to maintain such a temperature difference as small as possible and a proportional power signal is traced in the thermogram. All the measurements are performed by using an inert atmosphere with a continuous and uniform flow of dry N₂ within the furnace in order to avoid air humidity.

Differential scanning calorimetry finds applications in several topics as thermal characterization of protein denaturation processes (conformational transitions) (Pelosi et al., 2019), lipid model membrane thermotropic behaviour (phase transition) (Kontogiannopoulos et al., 2018) and polymers glass transition. Moreover, the determination of the effect of pH, solvent, ionic strength and sample composition is allowed, together with the investigation of the influence of ligands, chaotropes or other perturbing molecules.

The instrumental output generally reports the variation of heat flow as power signal ($P = dQ/dt$) against temperature and time. Nevertheless, the power trace is usually converted to heat capacity at constant pressure, C_p , that is defined as

$$C_p \equiv \left(\frac{\partial H}{\partial T} \right)_{p,n} \quad (1.1)$$

and H is enthalpy, T is the temperature, p is the pressure and n is the moles number. Indeed, according to both the definition of enthalpy and the first thermodynamic principle, the heat Q involved in the process corresponds to the enthalpy variation when $p=\text{const}$ and $n=\text{const}$:

$$P(t) = \frac{dQ}{dt} = \frac{dH}{dt} \quad (1.2)$$

Therefore, the signal may be converted to molar heat capacity through the application of a correction factor that strictly depends on the temperature scanning rate and sample mass or moles number:

$$C_p(T) = P \frac{1}{\beta} \frac{1}{n} = \frac{dH}{dt} \frac{dt}{dT} \frac{1}{n} \quad (1.3)$$

being β the scanning rate, n the moles number and T the temperature. The obtained trace reveals the *apparent* molar heat capacity trace, $C_p^{app}(T)$, since such a signal depends on instrumental aspects, experimental conditions, etc. In the resulting thermogram, the apparent molar heat capacity trace is generally scaled with respect to the pre-transition trace to obtain the excess molar heat capacity, $C_p^{exc}(T)$. Since the thermogram reports $C_p^{exc}(T)$ versus T , the peak area represents the transition ΔH^p as obtained after the integration of Eq.1.1:

$$Q = \Delta H = \int_{T_1}^{T_2} C_p \cdot dT \quad (1.4)$$

As regards the application of DSC technique for the study of the thermodynamic stability of cell membranes, phospholipid bilayers formed in aqueous media show a peculiar polymorphism that strictly depends on the temperature as well as on the molecular geometry of the constituents, hence the application of heating/cooling ramps lead to transitions between the various polymorphic phases (Fig.1.7). For instance, 1,2-dipalmitoyl-sn-glycero-3-phosphocholine (DPPC) is a cylindrically-shaped phospholipid with choline as headgroup and two palmitoyl chains as tails. At room temperature, DPPC bilayers display a lipid organization named *planar gel phase* (L_{β}^{\prime}) in which phospholipid molecules are compacted tidily and compactly packed maximizing the Van der Waals chain-to-chain interactions. As the temperature increases, acyl chains become more mobile and a transition commonly indicated as pretransition from *planar gel phase* (L_{β}^{\prime}) to *rippled gel phase* (P_{β}^{\prime})

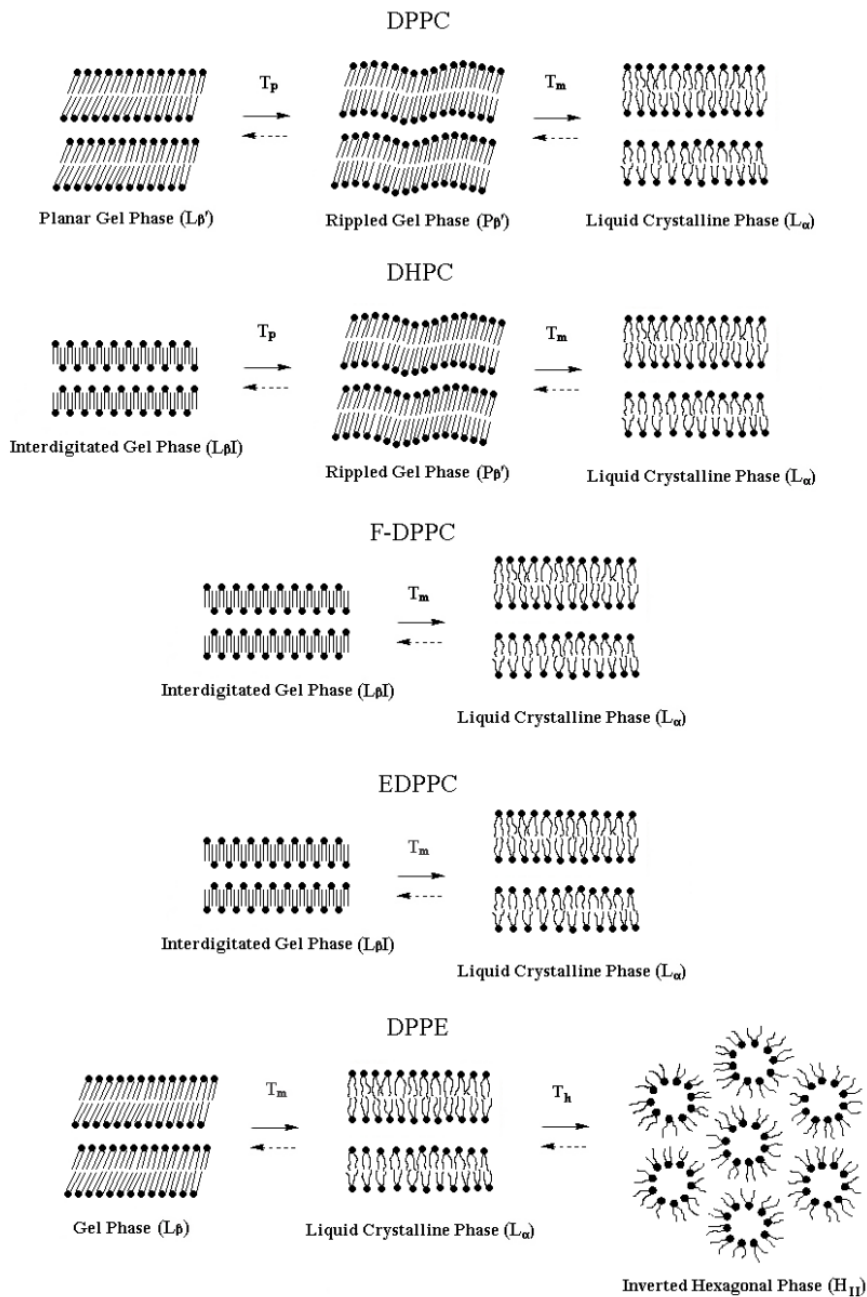


Figure 1.7: Phase transitions of representative lipids. (Smith and Dea, 2013)

DPPC = 1,2-dipalmitoyl-*sn*-glycero-3-phosphocholine

DHPC = 1,2-di-*O*-hexadecyl-*sn*-glycero-3-phosphocholine

F-DPPC = 1-palmitoyl-2-(16-fluoropalmitoyl)-*sn*-glycero-3-phosphocholine

EDPPC = 1,2-dipalmitoyl-*sn*-glycero-3-ethylphosphocholine

DPPE = 1,2-dipalmitoyl-*sn*-glycero-3-phosphoethanolamine

Table 1.1: Main factors that may influence cell membrane thermodynamics and functionality.

Factor	Example
Morphology	Multilamellarity Curvature
Composition	Phospholipid tails length and presence of unsaturations Phospholipid headgroups (size and charge) Presence of non-phospholipid constituents (e.g. cholesterol, etc.)
Inner and/or outer environment	pH Cations' charge Presence of "perturbing" agents (e.g. FFAs, membrane's proteins, peptide oligomers or fibrils, etc.)

occurs. When DPPC reaches about 41°C, the *rippled gel phase* (P_{β}') undergoes the so-called main transition toward the *liquid crystalline phase* (L_{α}) in which the mobility of the phospholipid tails is the highest (Smith and Dea, 2013). Almost all phospholipids display the main transition and the only exceptions are ascribable to a lipid molecular structure that does not allow the peculiar organization of the involved polymorphic phases (e.g. lysophospholipids), whilst not all phospholipids show the pretransition (e.g. DPPE). By contrast, some phospholipid may give rise to transition involving other phases because of their molecular structure, such as micelles and the *interdigitated gel phase* of lysophosphocholines (Lu et al., 2001) and the *inverted hexagonal phase* typical of phosphoethanolamines (Smith and Dea, 2013).

The described phase transitions are well detected through the DSC, which is therefore able to describe the thermotropic behaviour of lipid bilayers and vesicles (Gardikis et al., 2010; Kontogiannopoulos et al., 2018). Moreover,

they show asymmetric signals that may be influenced by several factors, some of which are reported in Table 1.1.

1.5. References

Aitken, J.F., Loomes, K.M., Scott, D.W., Reddy, S., Phillips, A.R.J., Prijic, G., Fernando, C., Zhang, S., Broadhurst, R., L'Huillier, P., Cooper, G.J.S., 2010. Tetracycline treatment retards the onset and slows the progression of diabetes in human amylin/islet amyloid polypeptide transgenic mice. *Diabetes* 59, 161–71.

Allen, T.M., 1997. Liposomes. Opportunities in drug delivery. *Drugs* 54, 8–14.

Anguiano, M., Nowak, R.J., Lansbury, P.T., 2002. Protofibrillar Islet Amyloid Polypeptide Permeabilizes Synthetic Vesicles by a Pore-like Mechanism that May Be Relevant to Type II Diabetes †. *Biochemistry* 41, 11338–11343.

Bacia, K., Schwille, P., Kurzchalia, T., 2005. From The Cover: Sterol structure determines the separation of phases and the curvature of the liquid-ordered phase in model membranes. *Proc. Natl. Acad. Sci.* 102, 3272–3277.

Biltonen, R.L., Lichtenberg, D., 1993. The use of differential scanning calorimetry as a tool to characterize liposome preparations. *Chem. Phys. Lipids* 64, 129–142.

Björntorp, P., Bergman, H., Varnauskas, E., 1969. Plasma free fatty acid turnover rate in obesity. *Acta Med. Scand.* 185, 351–356.

Bozzuto, G., Molinari, A., 2015. Liposomes as nanomedical devices. *Int. J. Nanomedicine* 10, 975.

Brash, A.R., 2001. Arachidonic acid as a bioactive molecule. *J. Clin. Invest.* 107, 1339–1345.

- Brzustowicz, M.R., Brunger, A.T., 2005. X-ray scattering from unilamellar lipid vesicles. *J. Appl. Crystallogr.* 38, 126–131.
- Castiello, F.R., Heileman, K., Tabrizian, M., 2016. Microfluidic perfusion systems for secretion fingerprint analysis of pancreatic islets: Applications, challenges and opportunities. *Lab Chip* 16, 409–431.
- Creutz, C.E., 1981. cis-Unsaturated fatty acids induce the fusion of chromaffin granules aggregated by synexin. *J. Cell Biol.* 91, 247–256.
- Demetzos, C., 2008. Differential Scanning Calorimetry (DSC): A Tool to Study the Thermal Behavior of Lipid Bilayers and Liposomal Stability. *J. Liposome Res.* 18, 159–173.
- Desbois, A.P., Smith, V.J., 2010. Antibacterial free fatty acids: activities, mechanisms of action and biotechnological potential. *Appl. Microbiol. Biotechnol.* 85, 1629–1642.
- Drazenovic, J., Wang, H., Roth, K., Zhang, J., Ahmed, S., Chen, Y., Bothun, G., Wunder, S.L., 2015. Effect of lamellarity and size on calorimetric phase transitions in single component phosphatidylcholine vesicles. *Biochim. Biophys. Acta - Biomembr.* 1848, 532–543.
- Gabizon, A., Goren, D., Cohen, R., Barenholz, Y., 1998. Development of liposomal anthracyclines: from basics to clinical applications. *J. Control. Release* 53, 275–9.
- Gardikis, K., Fessas, D., Signorelli, M., Dimas, K., Tsimplouli, C., Ionov, M., Demetzos, C., 2011. A New Chimeric Drug Delivery Nano System (chi-aDDnS) Composed of PAMAM G 3.5 Dendrimer and Liposomes as Doxorubicin's Carrier. *In Vitro Pharmacological Studies. J. Nanosci. Nanotechnol.* 11, 3764–3772.
- Gardikis, K., Hatziantoniou, S., Signorelli, M., Pusceddu, M., Micha-Screttas, M., Schiraldi, A., Demetzos, C., Fessas, D., 2010. Thermodynamic and

- structural characterization of Liposomal-Locked in-Dendrimers as drug carriers. *Colloids Surfaces B Biointerfaces* 81, 11–19.
- Guariguata, L., Whiting, D.R., Hambleton, I., Beagley, J., Linnenkamp, U., Shaw, J.E., 2014. Global estimates of diabetes prevalence for 2013 and projections for 2035. *Diabetes Res. Clin. Pract.* 103, 137–149.
- Hebda, J.A., Miranker, A.D., 2009. The Interplay of Catalysis and Toxicity by Amyloid Intermediates on Lipid Bilayers: Insights from Type II Diabetes. *Annu. Rev. Biophys.* 38, 125–152.
- Høytrup, P., Davidsen, J., Jørgensen, K., 2001. Lipid Membrane Partitioning of Lysolipids and Fatty Acids: Effects of Membrane Phase Structure and Detergent Chain Length. *J. Phys. Chem. B* 105, 2649–2657.
- Huber, A.H., Kleinfeld, A.M., 2017. Unbound free fatty acid profiles in human plasma and the unexpected absence of unbound palmitoleate. *J. Lipid Res.* 58, 578–585.
- Hutton, J.C., 1989. The insulin secretory granule. *Diabetologia* 32, 271–281.
- Hutton, J.C., Penn, E.J., Peshavaria, M., 1982. Isolation and characterisation of insulin secretory granules from a rat islet cell tumour. *Diabetologia* 23, 365–373.
- Ibarguren, M., López, D.J., Escibá, P. V., 2014. The effect of natural and synthetic fatty acids on membrane structure, microdomain organization, cellular functions and human health. *Biochim. Biophys. Acta - Biomembr.* 1838, 1518–1528.
- ISTAT, 2018a. *Annuario statistico italiano 2018*.
- ISTAT, 2018b. *Indagine multiscopo sulle famiglie: Aspetti della vita quotidiana*.

- Itoh, Y., Kawamata, Y., Harada, M., Kobayashi, M., Fujii, R., Fukusumi, S., Ogi, K., Hosoya, M., Tanaka, Y., Uejima, H., Tanaka, H., Maruyama, M., Satoh, R., Okubo, S., Kizawa, H., Komatsu, H., Matsumura, F., Noguchi, Y., Shinohara, T., Hinuma, S., Fujisawa, Y., Fujino, M., 2003. Free fatty acids regulate insulin secretion from pancreatic β cells through GPR40. *Nature* 422, 173–176.
- Jespersen, H., Andersen, J.H., Ditzel, H.J., Mouritsen, O.G., 2012. Lipids, curvature stress, and the action of lipid prodrugs: Free fatty acids and lysolipid enhancement of drug transport across liposomal membranes. *Biochimie* 94, 2–10.
- Kahn, B.B., Flier, J.S., 2000. Obesity and insulin resistance. *J. Clin. Invest.* 106, 473–81.
- Kenny, J.G., Ward, D., Josefsson, E., Jonsson, I.-M., Hinds, J., Rees, H.H., Lindsay, J.A., Tarkowski, A., Horsburgh, M.J., 2009. The *Staphylococcus aureus* Response to Unsaturated Long Chain Free Fatty Acids: Survival Mechanisms and Virulence Implications. *PLoS One* 4, e4344.
- Khan, W.A., Blobel, G.C., Hannun, Y.A., 1995. Arachidonic acid and free fatty acids as second messengers and the role of protein kinase C. *Cell. Signal.* 7, 171–184.
- Klausner, R.D., Kleinfeld, A.M., Hoover, R.L., Karnovsky, M.J., 1980. Lipid domains in membranes. Evidence derived from structural perturbations induced by free fatty acids and lifetime heterogeneity analysis. *J. Biol. Chem.* 255, 1286–1295.
- Kontogiannopoulos, K.N., Dasargyri, A., Ottaviani, M.F., Cangiotti, M., Fessas, D., Papageorgiou, V.P., Assimopoulou, A.N., 2018. Advanced Drug Delivery Nanosystems for Shikonin: A Calorimetric and Electron Paramagnetic Resonance Study. *Langmuir*.

- Koynova, R., Caffrey, M., 1998. Phases and phase transitions of the phosphatidylcholines. *Biochim. Biophys. Acta - Rev. Biomembr.* 1376, 91–145.
- La Rosa, C., Scalisi, S., Lolicato, F., Pannuzzo, M., Raudino, A., 2016. Lipid-assisted protein transport: A diffusion-reaction model supported by kinetic experiments and molecular dynamics simulations. *J. Chem. Phys.* 144, 184901.
- Laouini, A., Jaafar-Maalej, C., Limayem-Blouza, I., Sfar, S., Charcosset, C., Fessi, H., 2012. Preparation, Characterization and Applications of Liposomes: State of the Art. *J. Colloid Sci. Biotechnol.* 1, 147–168.
- Logue, J., Walker, J.J., Colhoun, H.M., Leese, G.P., Lindsay, R.S., McKnight, J.A., Morris, A.D., Pearson, D.W., Petrie, J.R., Philip, S., Wild, S.H., Sattar, N., Group, on behalf of T.S.D.R.N.E., 2011. Do men develop type 2 diabetes at lower body mass indices than women? *Diabetologia* 54, 3003–3006.
- Lu, J.-Z., Hao, Y.-H., Chen, J.-W., 2001. Effect of Cholesterol on the Formation of an Interdigitated Gel Phase in Lysophosphatidylcholine and Phosphatidylcholine Binary Mixtures. *J. Biochem.* 129, 891–898.
- Maedler, K., Spinass, G.A., Dyntar, D., Moritz, W., Kaiser, N., Donath, M.Y., 2001. Distinct Effects of Saturated and Monounsaturated Fatty Acids on β -Cell Turnover and Function. *Diabetes* 50, 69–76.
- Marrink, S.J., Mark, A.E., 2003. Molecular Dynamics Simulation of the Formation, Structure, and Dynamics of Small Phospholipid Vesicles. *J. Am. Chem. Soc.* 125, 15233–15242.
- McDonald, G.B., Saunders, D.R., Weidman, M., Fisher, L., 1980. Portal venous transport of long-chain fatty acids absorbed from rat intestine. *Am. J. Physiol. Liver Physiol.* 239, G141–G150.

- Molina, A.J.A., Wikstrom, J.D., Stiles, L., Las, G., Mohamed, H., Elorza, A., Walzer, G., Twig, G., Katz, S., Corkey, B.E., Shirihai, O.S., 2009. Mitochondrial Networking Protects β -Cells from Nutrient-Induced Apoptosis. *Diabetes* 58, 2303–2315.
- Moscho, A., Orwar, O., Chiu, D.T., Modi, B.P., Zare, R.N., 1996. Rapid preparation of giant unilamellar vesicles. *Proc. Natl. Acad. Sci.* 93, 11443–11447.
- Mouritsen, O.G., 2011. Lipids, curvature, and nano-medicine. *Eur. J. Lipid Sci. Technol.* 113, 1174–1187.
- Needham, D., Zhelev, D. V., 1995. Lysolipid exchange with lipid vesicle membranes. *Ann. Biomed. Eng.* 23, 287–298.
- O'Connor, L.J., Nicholas, T., Levin, R.M., 1999. Subcellular Distribution of Free Fatty Acids, Phospholipids, and Endogenous Lipase Activity of Rabbit Urinary Bladder Smooth Muscle and Mucosa. In: *Advances in Bladder Research*. Springer, Boston, MA, pp. 265–273.
- Olofsson, C.S., Göpel, S.O., Barg, S., Galvanovskis, J., Ma, X., Salehi, A., Rorsman, P., Eliasson, L., 2002. Fast insulin secretion reflects exocytosis of docked granules in mouse pancreatic β -cells. *Pflügers Arch - Eur J Physiol* 444, 43–51.
- Pannuzzo, M., Milardi, D., Raudino, A., Karttunen, M., La Rosa, C., 2013. Analytical model and multiscale simulations of A β peptide aggregation in lipid membranes: towards a unifying description of conformational transitions, oligomerization and membrane damage. *Phys. Chem. Chem. Phys.* 15, 8940.
- Pelosi, C., Saitta, F., Wurm, F.R., Fessas, D., Tinè, M.R., Duce, C., 2019. Thermodynamic stability of myoglobin-poly(ethylene glycol) bioconjugates: A calorimetric study. *Thermochim. Acta* 671, 26–31.

- Pippa, N., Meristoudi, A., Pispas, S., Demetzos, C., 2015. Temperature-dependent drug release from DPPC:C12H25-PNIPAM-COOH liposomes: Control of the drug loading/release by modulation of the nanocarriers' components. *Int. J. Pharm.* 485, 374–382.
- Reaven, G.M., Hollenbeck, C., Jeng, C.Y., Wu, M.S., Chen, Y.D.I., 1988. Measurement of plasma glucose, free fatty acid, lactate, and insulin for 24 h in patients with NIDDM. *Diabetes* 37, 1020–1024.
- Richieri, G. V., Kleinfeld, A.M., 1995. Unbound free fatty acid levels in human serum. *J. Lipid Res.* 36, 229–240.
- Risselada, H.J., Marrink, S.J., 2009. Curvature effects on lipid packing and dynamics in liposomes revealed by coarse grained molecular dynamics simulations. *Phys. Chem. Chem. Phys.* 11, 2056.
- Ruzin, A., Novick, R.P., 2000. Equivalence of Lauric Acid and Glycerol Monolaurate as Inhibitors of Signal Transduction in *Staphylococcus aureus*. *J. Bacteriol.* 182, 2668–2671.
- Sahoo, S.K., Labhasetwar, V., 2003. Nanotech approaches to drug delivery and imaging. *Drug Discov. Today* 8, 1112–1120.
- Schmalzing, G., Kutschera, P., 1982. Modulation of ATPase activities of human erythrocyte membranes by free fatty acids or phospholipase A2. *J. Membr. Biol.* 69, 65–76.
- Sciacca, M.F.M., Brender, J.R., Lee, D.-K., Ramamoorthy, A., 2012a. Phosphatidylethanolamine Enhances Amyloid Fiber-Dependent Membrane Fragmentation. *Biochemistry* 51, 7676–7684.
- Sciacca, M.F.M., Kotler, S.A., Brender, J.R., Chen, J., Lee, D., Ramamoorthy, A., 2012b. Two-Step Mechanism of Membrane Disruption by A β through Membrane Fragmentation and Pore Formation. *Biophys. J.* 103, 702–710.

- Shaikh, S.R., LoCascio, D.S., Soni, S.P., Wassall, S.R., Stillwell, W., 2009. Oleic- and docosahexaenoic acid-containing phosphatidylethanolamines differentially phase separate from sphingomyelin. *Biochim. Biophys. Acta - Biomembr.* 1788, 2421–2426.
- Smith, E.A., Dea, P.K., 2013. Differential Scanning Calorimetry Studies of Phospholipid Membranes: The Interdigitated Gel Phase. In: *Applications of Calorimetry in a Wide Context - Differential Scanning Calorimetry, Isothermal Titration Calorimetry and Microcalorimetry.* pp. 407–444.
- Testa, B., van de Waterbeemd, H., Folkers, G., Guy, R., 2001. *Pharmacokinetic Optimization in Drug Research.* Verlag Helvetica Chimica Acta, Zürich.
- Westermark, P., Andersson, A., Westermark, G.T., 2011. Islet Amyloid Polypeptide, Islet Amyloid, and Diabetes Mellitus. *Physiol. Rev.* 91, 795–826.
- Westermark, P., Li, Z.-C., Westermark, G.T., Leckström, A., Steiner, D.F., 1996. Effects of beta cell granule components on human islet amyloid polypeptide fibril formation. *FEBS Lett.* 379, 203–206.
- Yokoyama, H., Ikeda, K., Wakabayashi, M., Ishihama, Y., Nakano, M., 2013. Effects of Lipid Membrane Curvature on Lipid Packing State Evaluated by Isothermal Titration Calorimetry. *Langmuir* 29, 857–860.
- Young, A., 2005. Tissue Expression and Secretion of Amylin. In: *Advances in Pharmacology.* pp. 19–45.
- Zhang, Y., Luo, Y., Deng, Y., Mu, Y., Wei, G., 2012. Lipid Interaction and Membrane Perturbation of Human Islet Amyloid Polypeptide Monomer and Dimer by Molecular Dynamics Simulations. *PLoS One* 7, e38191.

Aims and objectives

The reason and the manner in which obesity and, in general, factors related to nutrition are linked to type 2 diabetes mellitus (T2DM) have not been fully understood yet. However, literature reports that T2DM and obesity have several of common points (Bhupathiraju and Hu, 2016; Mantzoros, 2006; Profenno et al., 2010; Rosenberg et al., 2005; Van Steenberghe and Lanckmans, 1995) among which there are high levels of free fatty acids (FFAs) in plasma. Such high levels are recognised as pathological conditions since high concentrations of FFAs are reported to be involved in several deleterious processes for an organism, as mentioned in section 1.2.

For the research discussed in this thesis, the direct action of FFAs with cell membranes was drawn as case study, hence focusing on the thermodynamic study of cell membranes. Since a synergic action of FFAs and amylin has been hypothesized to be involved in T2DM onset and progression, the phospholipid bilayer of the vesicles appointed for amylin and insulin storage and secretion (Insulin Secretory Granules, ISGs) was selected as reference membrane.

2.1. Research purposes

The main purpose of the thesis was to investigate stepwise some of the main factors that influence the thermodynamics of the phospholipid bilayers of cell

membranes, finding out the hierarchy of thermodynamic contributions behind the membrane stability, and to dissect the effect of the presence of some FFAs that may be found in typical food of the Mediterranean diet as well as in industrially processed food in order to better comprehend and correlate the molecular mechanisms hidden behind the pathogenesis of T2DM.

Furthermore, the investigation on the interaction between model membranes and nisin, a simpler pore-forming peptide than the amyloidogenic hIAPP (or amylin), allowed the evaluation of the influence of various FFAs on peptide-membrane interaction, also paving the way for the study of hIAPP action in the frame of T2DM. The selection of nisin as simpler case study was driven by its growing use as food preservative as well as antibiotic in health care.

The work was divided into three chronologically overlapping parts.

Part I

The first part was aimed to the stepwise physicochemical study of relatively simple model membranes in order to investigate the influence of both morphology and composition on the thermodynamic stability of cell membranes. The work was carried out at physiological pH by using High Sensitivity DSC and dynamic light scattering techniques.

As for vesicle morphology, DMPC, DPPC and DSPC, three phospholipids with the same headgroup (choline) and saturated tails with different length, were used for the preparation of single-component MLBs and LUVs and their calorimetric profiles were compared for the description of the effect of multilamellarity. Furthermore, in order to find out how the curvature may affect the vesicle calorimetric profiles, DMPC, DPPC and DSPC were also used for the comparison of GUVs and SUVs prepared as single-component liposomes or as 1:1 molar ratio binary systems.

As for the vesicle composition, the above-mentioned systems were also considered for detecting the influence of saturated acyl chains with different length, whereas the effect of different phospholipid headgroups, both in terms

of size and charge, was revealed through the investigations of binary systems prepared as 1:1 molar ratio of DPPC, DPPE and DPPS, *i.e.* all phospholipids with palmitoyl chains and different headgroups (choline, ethanolamine and serine, respectively). With the same purpose, liposomes with two ternary compositions that reflected the constituents' proportions in real ISGs were also considered by maintaining either the phospholipid tails or the headgroup the same. The effect of the presence of phospholipid tails unsaturation was finally assessed by the addition of DOPC, an unsaturated lipid, to the ternary membrane constituted by DMPC, DPPC and DSPC since the effect of unsaturations concerns tail properties.

The discrimination of all these factors allowed the depiction of a hierarchy of contribution to cell membrane thermodynamic stability.

Part II

The second part was focused on the achievement of a highly representative membrane by counting up to fifteen lipid constituents. The stepwise investigation was continued by also including 16:0 LysoPC (lysophosphocholine) and egg sphingomyelin to the headgroups ternary membrane in order to reflect the major macro-categories constituting the ISGs. Therefore, a wider fatty acids distribution considering different tails length and unsaturation was integrated to the resulting five-components vesicles, followed by the further addition of cholesterol. The final ISG-like membrane represented the 80% of phospholipids in real ISGs in terms of both tails and headgroups.

Part III

The third part was focused on the study of the effects of FFAs on cell membranes. After some preliminary evaluation of such influences on ternary, quaternary and ISG-like vesicles, the results achieved in the previous parts were taken into consideration for the modelling of an *ad hoc* simpler ISG-like vesicle in order to further investigate the influence of six different FFAs on such vesicles (Table 2.1), namely two saturated FFAs (palmitic acid and

Table 2.1: List of the free fatty acids considered in this thesis and respective sources examples.

Name	C atoms and unsaturations	Short illustration	Source examples (Chow, 2007)
<i>Palmitic acid</i>	C16:0	16:0	Animal and vegetable fats
<i>Stearic acid</i>	C18:0	18:0	Animal and vegetable fats
<i>Oleic acid</i>	C18:1	18:1, <i>cis</i> - Δ^9	Olive oil and other natural fats
<i>Elaidic acid</i>	C18:1	18:1, <i>trans</i> - Δ^9	Ruminants fats and hydrogenated fats
<i>Linoleic acid</i>	C18:2	18:2, <i>cis,cis</i> - Δ^9,Δ^{12}	Linseed and sunflower oils
<i>Docosahexaenoic Acid (DHA)</i>	C22:6	22:6, <i>cis,cis,cis,cis,cis,cis</i> - $\Delta^4,\Delta^7,\Delta^{10},\Delta^{13},\Delta^{16},\Delta^{19}$	Fish oil

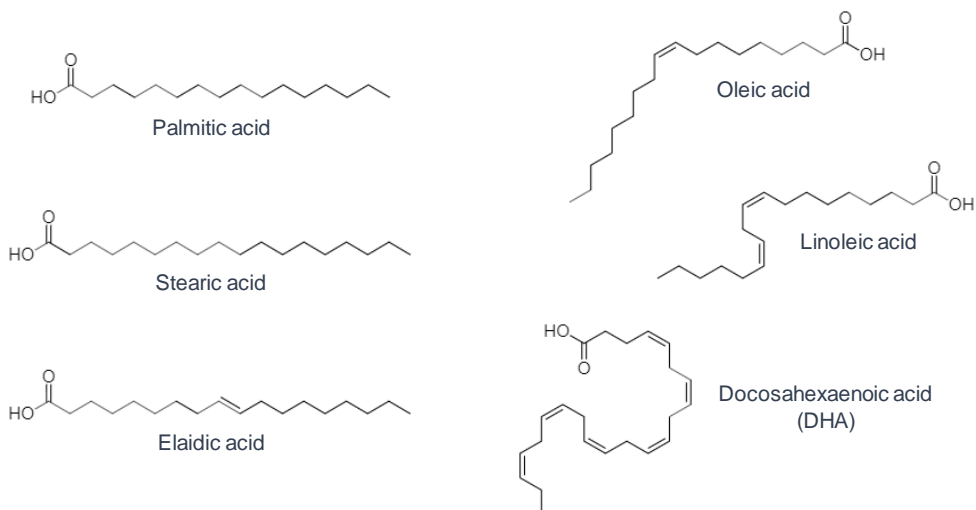


Figure 2.1: Chemical structure of the free fatty acids considered in this thesis.

stearic acid), two monounsaturated FFAs (the *cis*-unsaturated oleic acid and the *trans*-unsaturated elaidic acid) and two polyunsaturated FFAs (the ω -6 linoleic acid and the ω -3 docosahexaenoic acid or DHA).

Furthermore, the interaction of FFAs-containing vesicles with nisin, a pore-forming peptide, was also considered in order to highlight the weight of vesicle lipid composition and presence of FFAs on protein-cell membrane interaction.

With the purpose of deepen the knowledge on thermal analysis and calorimetry, as well as on thermodynamics, side projects were also undertaken. Such parallel activities involved the thermodynamics study of biological macromolecules, as proteins in solution (conformational stability, specific and/or aspecific macromolecule - ligand binding phenomena), physicochemical investigation on liposomes thermotropic behaviour for pharmaceutical application, as well as the calorimetric characterization of cultural heritage biomaterials (phase transitions as crystallization/melting, glass transitions, etc.). Details about the undertaken side projects are described in appendices.

2.2. References

Bhupathiraju, S.N., Hu, F.B., 2016. Epidemiology of Obesity and Diabetes and Their Cardiovascular Complications. *Circ. Res.* 118, 1723–1735.

Chow, C.K., 2007. Fatty acids in foods and their health implications, Third ed. CRC Press.

Mantzoros, C.S., 2006. Obesity and diabetes. Humana Press.

Profenno, L.A., Porsteinsson, A.P., Faraone, S. V., 2010. Meta-Analysis of Alzheimer's Disease Risk with Obesity, Diabetes, and Related Disorders. *Biol. Psychiatry* 67, 505–512.

Rosenberg, T.J., Garbers, S., Lipkind, H., Chiasson, M.A., 2005. Maternal Obesity and Diabetes as Risk Factors for Adverse Pregnancy Outcomes:

Differences Among 4 Racial/Ethnic Groups. *Am. J. Public Health* 95, 1545–1551.

Van Steenbergen, W., Lanckmans, S., 1995. Liver disturbances in obesity and diabetes mellitus. *Int. J. Obes. Relat. Metab. Disord.* 19 Suppl 3, S27-36.

Cell membrane thermodynamics: dissecting the contributions

This chapter reports a stepwise micro-DSC study of small, large and giant unilamellar vesicles prepared as pure and mixed systems of DMPC, DPPC, DSPC and DOPC. It allowed the discrimination of the thermodynamic contributions of some main factors dictating the thermodynamic stability of membranes, as vesicle size, phospholipid tails' length and unsaturation and composition. Small unilamellar vesicles obtained by mixing DPPC, DPPS and DPPE were also considered to investigate how phospholipid headgroups affect the membrane thermodynamics. The final multicomponent model membranes achieved reflected the real phospholipid proportions characterizing the Insulin Secretory Granules, vesicles located in the pancreatic Langerhans β -cells and which are responsible for insulin and amylin storage and secretion in response to nutrient intake.

The results allowed to discriminate the thermodynamic contributions to the overall cell membranes thermodynamics evidencing mainly entropic effects hierarchically summarized as membrane curvature < phospholipid headgroup < phospholipid tail length < phospholipid tail unsaturation.

3.1. Introduction

The structure of lipid vesicles makes them exemplary model systems able to provide simulations of either cytoplasmic membrane or cell compartments,

such as organelles and vesicles involved in endo- and exocytosis. It is hard to perfectly mime a real biological membrane. However, despite the numerous studies on model membranes carried out mainly through calorimetric, spectroscopic and imaging techniques, such model systems were characterized by a simple composition which does not keep into consideration the contribution deriving from the single lipid components and from their mixing in real systems (Prince et al., 2016; Sciacca et al., 2009). Besides that, some physical features were also not always considered in an appropriate manner, such as vesicle unilamellarity and curvature.

Cell membrane curvature is not only a mere consequence of the several mechanisms that take place during cell life, but local specific conformations are hallmarks of cell membranes (McMahon and Gallop, 2005). Indeed, the curvature of cell bilayers has an active role in cellular activity, above all cell division, vesicles trafficking and protein-membrane interactions (Mouritsen, 2011; Tonnesen et al., 2014), so much that the cell is able to modulate and remodel membranes by changing their lipid composition and causing lipid segregations (Bacia et al., 2005; McMahon and Gallop, 2005). Therefore, each modification in lipid composition and morphological characteristics might produce modifications of the molecular structure of such systems, which in turn might lead to variations of their physicochemical properties (Brzustowicz and Brunger, 2005; Marrink and Mark, 2003; Risselada and Marrink, 2009). For instance, high curved liposomes have a different phase behaviour showing a radius-dependent main phase transition below a certain threshold (Biltonen and Lichtenberg, 1993; Koynova and Caffrey, 1998).

In this frame, comprehending the contribution of the main parameters that rule the thermodynamic stability of a real cell membrane might be a key point for the correct interpretation of membrane-based mechanisms in cells since each factor might produce modifications in membrane thermodynamics, which in turn might lead to functionality modifications.

Through the following investigation, the morphological and compositional effects on the overall membrane stability were discriminated. On one hand, a

thermodynamic study of different Small, Large and Giant Unilamellar Vesicles (SUVs, LUVs and GUVs) prepared as pure and mixed system of DMPC, DPPC, DSPC and DOPC at physiological pH (pH 7.4) was performed by using High Sensitivity DSC. In order to better discriminate the thermodynamic contributions of vesicle size, phospholipid tails length, presence of unsaturations and components' molar ratio, in this case all the constituents were chosen with the same headgroup (choline). On the other hand, SUVs obtained by mixing DPPC, DPPS and DPPE were also considered in order to investigate how phospholipid headgroups affect the membrane thermodynamics. The mixing behaviour of systems with different phospholipid headgroup was carried out by using phospholipids with same tail length (16:0). The final ternary and quaternary model membranes achieved were prepared reflecting the real phospholipid proportions characterizing the Insulin Secretory Granules (MacDonald et al., 2015).

3.2. Materials and methods

3.2.1. Materials

1,2-distearoyl-sn-glycero-3-phosphocholine (DSPC), 1,2-dipalmitoyl-sn-glycero-3-phosphocholine (DPPC), 1,2-dimyristoyl-sn-glycero-3-phosphocholine (DMPC), 1,2-dioleoyl-sn-glycero-3-phosphocholine (DOPC), 1,2-dipalmitoyl-sn-glycero-3-phosphoethanolamine (DPPE) and 1,2-dipalmitoyl-sn-glycero-3-phospho-L-serine (DPPS, sodium salt) powders were purchased from Avanti Polar Lipids, whereas other chemicals were obtained from Sigma-Aldrich. The lipids were of the highest available purity ($\geq 99\%$ certified by the supplier) and were used without further purification. All solvents were of analytical grade.

3.2.2. *Liposomes preparation*

3.2.2.1. *Preparation of giant unilamellar vesicles (GUVs)*

GUVs were prepared following a procedure described elsewhere (Moscho et al., 1996). Briefly, the phospholipids were dissolved in chloroform obtaining a 2mM concentration. A volume equal to 1mL of this solution was transferred in a round-bottom flask where, subsequently, 7mL of 10mM phosphate buffer (pH 7.4) were added. The organic solvent was removed through rotary evaporation (Heidolph Laborota 4000 efficient, WB eco, Schwabach, Germany) under reduced pressure at 40°C and 40rpm, obtaining about 6.0mL dispersion of GUVs at high concentration (~0.3mM).

3.2.2.2. *Preparation of large unilamellar vesicles (LUVs)*

Large vesicles were obtained from GUVs dispersion. In order to obtain LUVs with a 400nm diameter, the appropriate volume of GUVs dispersion was extruded through polycarbonate filters (pore size of 400nm) mounted on a heated mini-extruder (Avanti Polar Lipids, Alabaster, AL, USA) fitted with two 1mL gastight syringes (Hamilton, Reno, NV, USA). An odd number of passages, usually 41, was performed to avoid any contamination by liposomes that might have not passed through the filters, as suggested elsewhere (MacDonald et al., 1991).

3.2.2.3. *Preparation of small unilamellar vesicles (SUVs)*

SUVs were prepared through thin-film hydration (Laouini et al., 2012). An amount of about 20mg phospholipids were dissolved in 2mL of chloroform in a round-bottomed flask (mixtures that contained the serine headgroup were dissolved in chloroform:methanol 3:1). Lipids were dried under a stream of dry nitrogen gas and evaporated to dryness through rotary evaporation (Heidolph Laborota 4000 efficient, WB eco, Schwabach, Germany) at 40°C. The films were kept under vacuum for at least 3 hours to remove solvent traces and

then aged overnight at 4°C. For the hydration, 10mM phosphate buffer (pH 7.4) at a temperature above the gel-to-liquid-crystal transition of the lipid system was added up to a 10mg lipid/mL medium concentration. After the complete dispersion of the lipid films, the obtained mixtures were slowly stirred in water bath, at the same temperature chosen for the buffer, for about an hour until the induction of a homogenous emulsion. Extrusion was performed through 100nm polycarbonate filters following the same precautions previously described.

3.2.2.4. Preparation of multilamellar lipid bilayers (MLBs)

MLBs samples were prepared by simply dispersing the adequate lipid powder amounts in 10mM phosphate buffer achieving a 0.2M lipid concentration.

3.2.2.5. Preparation of multilamellar lipid vesicles (MLVs)

Multilamellar vesicles were obtained from the same homogeneous lipid emulsion achieved for SUVs preparation. In order to obtain MLVs with a diameter of 400nm, the appropriate volume of lipid emulsion was extruded through 400nm polycarbonate filters following the same precautions previously described.

3.2.3. Spectroscopic characterization

The hydrodynamic diameter of some liposomal formulations was measured by Dynamic Light Scattering (DLS). Amounts of 100µL of SUVs preparations and 670µL of LUVs and GUVs preparations were diluted in buffer up to 3mL after the annealing of the dispersions. Measurements were performed at 25°C through a light-scattering instrument (Litesizer™ 500, Anton Paar, Graz, Austria) in side-scatter mode for SUVs and LUVs dispersion, whereas the back-scatter mode was used for GUVs dispersions. The results permitted to verify the specifications about the polycarbonate filters' pore sizes used for

the SUVs and LUVs extrusions (MacDonald et al., 1991) and to verify that the GUVs sizes was higher than 1 μm .

3.2.4. Thermal analysis measurements

Calorimetry was used to determine the stability of the membranes with specific reference to transitions of the lipid phases. Micro-DSC was selected as the most suitable technique for liposome investigation (Gardikis et al., 2010). The instrument used was a Setaram micro-DSCIII (Setaram Instrumentation, Caluire, France) operating with 1mL hermetically closed pans at 0.5°C/min scanning rate. After the conclusion of the liposomes' preparation protocols, each dispersion was allowed to anneal for at least 30 minutes at room temperature before launching the DSC measurement. SUVs samples were diluted up to 2.5mM phospholipids concentration, whereas GUVs and LUVs suspensions were used without further dilutions (~0.3mM). The final phospholipid concentration for all kind of vesicles was checked by using the Stewart assay (Stewart, 1980).

Instead, classic DSC technique was selected to obtain thermograms for Multilamellar Lipid Bilayers (MLBs) as references. A PerkinElmer DSC6 (PerkinElmer, Waltham, MA, USA) working with hermetically closed pans was used by choosing a 0.5°C/min scanning rate. MLBs samples were prepared by adding 10mM phosphate buffer (pH 7.4) to the adequate lipid amount achieving a 0.2M lipid concentration.

The raw data were worked out with the dedicated software "THESEUS" (Barone et al., 1992). Briefly, the apparent specific heat trace, $C_p^{app}(T)$, was scaled to obtain the excess specific heat, $C_p^{exc}(T)$, with respect to the low temperature lipids state. Due to such a treatment, the area beneath the recorded peaks directly corresponded to the relevant transition enthalpy ΔH° of the lipid phase. Two heating-cooling cycles were applied to each sample. All transitions were reversible and the second cycle heating curves were taken into account to evaluate the parameters of the thermotropic transitions

observed. Such cycle may be indicated as the thermodynamically meaningful one since any other following cycle would lead to almost the same calorimetric profile. Errors were evaluated on the basis of at least three replicas.

In case of single main peaks, the main transition temperature, T_m , is usually identified as the temperature of the calorimetric peak maximum, T_{max} , and the transition cooperativity is quantified by means of $\Delta T_{1/2}$ (full width at half maximum) that is of the order of 0.5°C for MLBs, while the unilamellar liposomes' values are generally 2-3 times higher according to the literature (Gardikis et al., 2010). However, in this work we often dealt with complex signals. In order to describe the overall stability of the systems, in addition to T_{max} we proposed the use of the transition average temperature, \bar{T} , defined here as

$$\bar{T} = \int_{T_0}^{T_f} T \cdot f(T) dT$$

where the frequency function $f(T)$ is just the normalized calorimetric peak distribution between T_0 and T_f , *i.e.* the initial and final limit of the observable peak:

$$f(T) = \frac{C_p^{exc}(T)}{\Delta H^\circ}.$$

Furthermore, to better estimate the cooperativity in multicomponent and/or multiphasic samples, we proposed an Average Cooperativity Index, *ACI*, defined here as

$$ACI = \sqrt{\int_{T_0}^{T_f} (T - \bar{T})^2 \cdot f(T) dT}.$$

This approach is just a classical statistical distribution approach applied to the calorimetric signal (for instance, *ACI* coincides with the standard deviation σ in the case of a gaussian distribution) and just for comparison we mention that in case of single peaks, as for the MLBs, a $\Delta T_{1/2}$ value of 0.5°C corresponds to $\sim 0.2^\circ\text{C}$ in *ACI* terms, whereas the $|\bar{T} - T_{max}|$ difference represents a peak asymmetry index (Saitta et al., 2019).

3.3. Results and discussion

3.3.1. Lamellarity and size effects

DSC thermograms for DMPC, DPPC and DSPC samples as MLBs and LUVs are shown in Fig.3.1.

All the transition reported showed total reversibility of the thermograms and the cooling traces evidenced hysteresis effects typical of “Ising” systems (Ising, 1924).

As regards the MLBs, the obtained thermograms exhibited the distinctive intense and sharp signal related to the main transition from the gel phase to the liquid crystalline phase, preceded by the typical smaller and broader pretransition (Gardikis et al., 2010) which corresponds to the generation of intermediate “ripples” along the bilayers in gel phase (planar-to-rippled gel phase transition) (Riske et al., 2009). All the three systems showed low

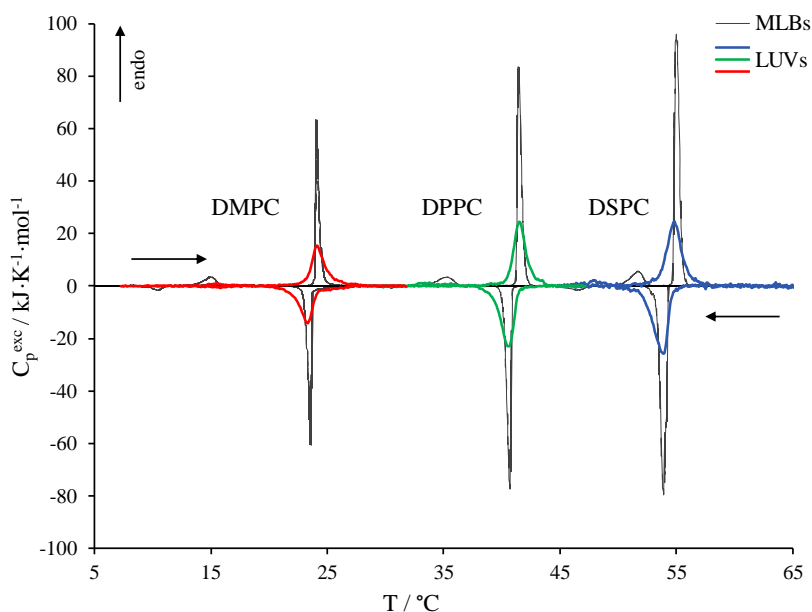


Figure 3.1: DSC thermograms for pure DMPC, DPPC and DSPC dispersions (from left to right) representing MLBs (black thin curves) versus LUVs (coloured bold curves).

Average Cooperativity Index (ACI – see materials and methods) values for the main peak (with an average value of $0.2 \pm 0.1^\circ\text{C}$) reflecting the high cooperativity of the involved phase transition due to the high longitudinal order. Moreover, the temperature ranges covered by these signals and the corresponding main transition enthalpies followed the trend outlined by the phospholipids' chain lengths increment (14, 16, 18 carbon atoms for DMPC, DPPC and DSPC respectively) (Koynova and Caffrey, 1998; Mabrey and Sturtevant, 1976).

As for LUVs, the DSC traces were mainly characterized by broader peaks than their MLBs counterparts even maintaining the same main transition temperature (Gardikis et al., 2010). Moreover, we observed that the differences between LUVs and MLBs for the same lipids were not due to enthalpic effects (any relevant enthalpy variation was recorded) but only to entropic factors, according to the fact that vesicles display lower longitudinal

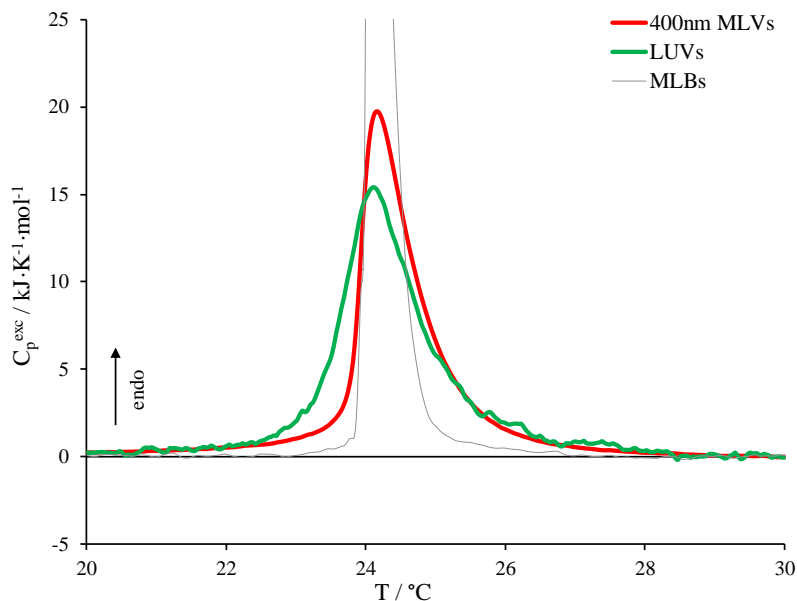


Figure 3.2: Micro-DSC thermograms for DMPC 400nm MLVs (red curve) and same size DMPC LUVs (green curve) dispersions. The grey thin curve, showing the DSC trace of DMPC MLBs for comparison, was smoothed in order to reduce the amplified noise because of curve magnification.

order because of curvature, leading to larger microstates distributions and lower cooperativity. This last point was well shown by the higher ACI values compared to the MLBs ones (the average ACI value among the three LUVs systems was equal to $1.0 \pm 0.1^\circ\text{C}$). Furthermore, LUVs showed less evident pretransition signals, which is in line with the fact that unilamellar vesicles are not constrained in a lipid lattice generated by multilayer stacks with high transversal order. Thus, the reorganization of “melted” lipid domains in the gel phase is not so strong to show a defined ripples formation since lipid out-of-plane fluctuation is sterically less confined (Heimburg, 2000).

Effects of lamellarity are still visible when MLVs and LUVs with the same nominal diameter of about 400nm are compared (Fig.3.2). Indeed, the profiles were clearly different and higher cooperativity was evidenced for the 400nm MLVs, as expected. As for the noisiest signal observed for LUVs dispersions, it was due to the lower lipid concentration dictated by the preparation method.

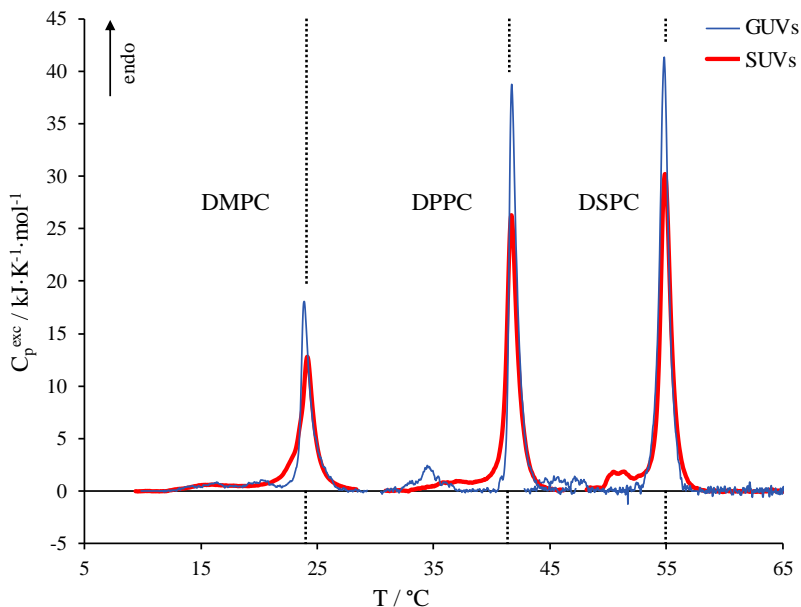


Figure 3.3: DSC thermograms for pure DMPC, DPPC and DSPC dispersions (from left to right) representing GUVs (blue thin curves) versus SUVs (red solid curves). The dotted vertical lines mark the T_{max} of the respective MLBs).

The micro-DSC thermograms obtained for DMPC, DPPC and DSPC samples as GUVs and SUVs are shown in Fig.3.3.

All GUVs and SUVs showed similar layouts compared to LUVs reported in Fig.3.1. However, peculiarities in the calorimetric profiles deriving from differences in vesicles size were evidenced. Indeed, it is well known that the cooperativity of the phase transition depends on the geometry of the membrane and decreases as the vesicle curvature increases (Gardikis et al., 2010; Ivanova and Heimburg, 2001). We observed that the higher the curvature (SUVs), the lower the cooperativity without any variation in terms of enthalpic contribution. In summary, the ACI values we obtained were of the same order for the DSPC, DPPC and DMPC systems, namely $0.6 \pm 0.1^\circ\text{C}$ for GUVs and $1.2 \pm 0.1^\circ\text{C}$ for SUVs, to be compared to the forenamed $1.0 \pm 0.1^\circ\text{C}$ for LUVs and $0.2 \pm 0.1^\circ\text{C}$ for MLBs.

As mentioned above, the main transition enthalpies remained correspondingly unaffected among all the four preparations (MLBs, GUVs, LUVs and SUVs) indicating that such curvature effects were of entropic nature in line with previous studies (Gardikis et al., 2010). In summary, for all the forms of the systems, as overall main transition values we obtained $\Delta H^\circ = 44 \pm 2\text{kJ}\cdot\text{mol}^{-1}$ and $T_{max} = 54.9 \pm 0.2^\circ\text{C}$ for DSPC, $\Delta H^\circ = 35 \pm 2\text{kJ}\cdot\text{mol}^{-1}$ and $T_{max} = 41.6 \pm 0.2^\circ\text{C}$ for DPPC, and $\Delta H^\circ = 24 \pm 2\text{kJ}\cdot\text{mol}^{-1}$ and $T_{max} = 24.0 \pm 0.2^\circ\text{C}$ for DMPC. The pretransition was better detected in the case of MLBs (enthalpy values of $7 \pm 1\text{kJ}\cdot\text{mol}^{-1}$, $5 \pm 1\text{kJ}\cdot\text{mol}^{-1}$ and $4 \pm 1\text{kJ}\cdot\text{mol}^{-1}$ for DSPC, DPPC and DMPC, respectively) whereas they became less evident going from GUVs, LUVs to SUVs (Heimburg, 1998, 2000).

3.3.2. *Mixing effects*

In order to evaluate the contribution of each phospholipid on the thermodynamic stability of a hypothetical model membrane, experiments on vesicles prepared by only mixing phospholipids with saturated acyl chains were carried out.

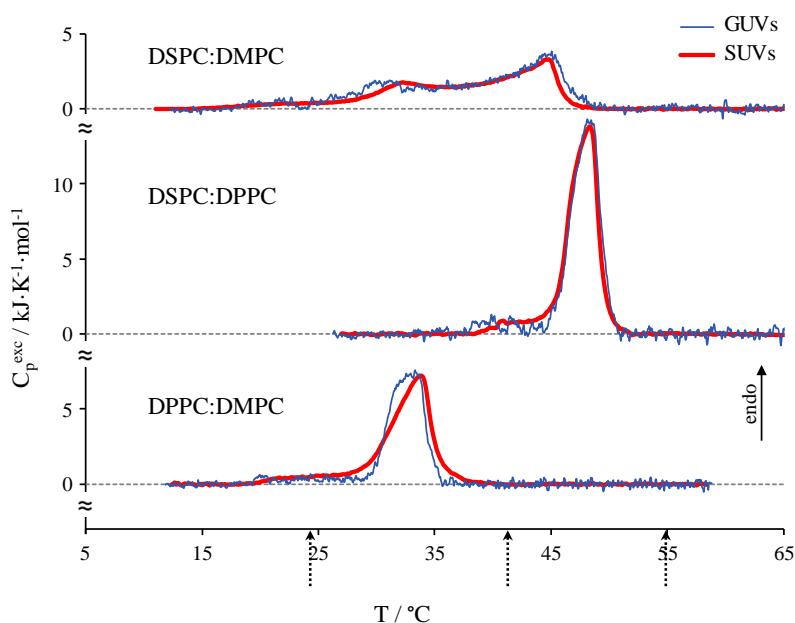


Figure 3.4: Micro-DSC thermograms for GUVs (blue thin curves) and SUVs (red solid curves) dispersions obtained by 1:1 DSPC:DPPC, DPPC:DMPC and DSPC:DMPC mixtures. The dotted vertical arrows mark the T_{max} of pure DMPC, DPPC, and DSPC MLBs (left to right).

As for the evaluation of the influence of the phospholipid tails length on the thermodynamics of membranes, binary systems prepared as 1:1 molar mixtures of DSPC:DPPC, DPPC:DMPC and DSPC:DMPC were investigated for the size border systems (GUVs and SUVs) and the resulting micro-DSC traces are respectively reported in Fig.3.4. The relevant thermodynamic data are reported in Table 3.1.

Starting with the effects ascribable to the curvature for vesicles with binary composition, it is possible to notice that the differences between GUVs and SUVs become almost negligible for the DSPC:DPPC mixture, whereas they are still visible in the cases of mixtures with the shortest phospholipid DMPC. This behaviour when DMPC is one of the component, above all in the case of DPPC:DMPC, may be related to the higher gap between the T_{max} values of the respective reference (single-component) systems if compared to the value

associated to the DSPC:DPPC mixture (for instance, ΔT_{max} is about 13.3°C for DSPC:DPPC, whereas it is about 17.6°C for DPPC:DMPC). However, it is less evident in the case of DSPC:DMPC because of the breadth of the profiles. In any case, the differences observed are less evident if compared to the single-component systems reported in Fig.3.3.

Therefore, though we do not exclude that local curvature modifications may be involved in some functionality in real membranes (Parthasarathy and Groves, 2007; Tonnesen et al., 2014), all the systems investigated from here on were only considered as SUVs dispersions since curvature effects become of minor importance increasing the vesicle complexity and further exploitations of these fine curvature aspects are beyond the scope of this thesis.

Proceeding with the analysis of the calorimetric profiles in Fig.3.4, for phospholipids mixtures with a chain lengths' deviation of two carbon units, *i.e.* DSPC:DPPC and DPPC:DMPC, we observed a main peak roughly placed in the middle of the temperature range defined by the T_{max} values of the single-component dispersions (considered as references), in line with the literature (Losada-Pérez et al., 2015). Such profiles indicate that phospholipids with slight differences in tails' length are in first approximation miscible, *i.e.* almost thermodynamically compatible. However, we may notice broader signals than the references' profiles, also presenting slight shoulders towards the phospholipids with the shortest tails.

Conversely, in the case of DSPC:DMPC mixture, *i.e.* phospholipids with a higher chain lengths' deviation (four carbon units), these effects were dramatically enhanced showing a complex asymmetric and mainly biphasic signal. Consequently, we may assess that the presence of phase separations, *i.e.* thermodynamic incompatibility, is strictly related to the lipid composition in terms of chain lengths' deviation (Bagatolli and Gratton, 2000). However, we remind that the conclusion at this point regards saturate phospholipids with the same headgroup.

Notwithstanding, the thermograms showed the formation of phases characterized by different lipid molar ratios for all the three mixtures. Indeed,

Table 3.1: Thermodynamic parameters evaluated from micro-DSC investigations for phospholipid tails and headgroups binary systems and compared with the arithmetical values calculated from single-component systems. The second cycle heating curves were used to obtain the main transition enthalpy (ΔH°), the peak maximum temperature (T_{max}), the transition average temperature (\bar{T}) and the Average Cooperativity Index (ACI).

	Expected		Experimental			
	ΔH° kJ·mol ⁻¹	$T_{expected}$ °C	ΔH° kJ·mol ⁻¹	T_{max} °C	\bar{T} °C	ACI °C
<i>Tails binary systems</i>						
DSPC:DPPC						
GUVs	40	48.3	46 ± 2	48.1 ± 0.3	47.3 ± 0.3	2.3 ± 0.2
SUVs			45 ± 2	48.4 ± 0.3	47.2 ± 0.3	2.0 ± 0.2
DPPC:DMPC						
GUVs	30	32.8	33 ± 2	33.3 ± 0.3	31.6 ± 0.3	3.0 ± 0.2
SUVs			35 ± 2	33.8 ± 0.3	31.9 ± 0.3	3.3 ± 0.2
DSPC:DMPC						
GUVs	34	39.5	38 ± 2	45.0 ± 0.3	37.4 ± 0.3	7.1 ± 0.2
SUVs			37 ± 2	44.8 ± 0.3	37.1 ± 0.3	6.9 ± 0.2
<i>Headgroups binary systems</i>						
DPPC:DPPS	38	48.3	37 ± 2	45.4 ± 0.2	46.5 ± 0.1	2.4 ± 0.1
DPPC:DPPE	36	53.1	36 ± 2	55.6 ± 0.3	53.1 ± 0.1	2.9 ± 0.1
DPPS:DPPE	38	59.8	37 ± 2	60.3 ± 0.2	59.5 ± 0.1	1.9 ± 0.2

it is easy to notice a small step at the beginning of the peaks in all the cases evidencing the presence of phases richer in the lower- T_m phospholipid (corresponding to DPPC-rich phase in DSPC:DPPC and to DMPC-rich phase in both DSPC:DMPC and DPPC:DMPC). However, regardless of the magnitude of the phase separations characterizing such systems, we observed that the lipids reorganization within the vesicles promoted the enrichment of the most stable domains against the phase transition and such a detail clearly emerges by the asymmetry of the peaks in Fig.3.4 in addition

to the phase separations. The overall enthalpies obtained for the three binary mixtures are collected in Table 3.1 and are compared with the respective arithmetical values calculated from single-component systems. We observed higher ΔH° than the calculated values for all the systems with deviations of about $4\text{-}5\text{kJ}\cdot\text{mol}^{-1}$ that are of the order of the pretransition values. Accordingly, we may argue that the enthalpic contributions are additive and that these differences may reflect the contribution of residual pretransitions of each constituent not clearly detectable because covered by the overall curves. In any case, no considerable enthalpic differences are evident between GUVs and SUVs.

In order to assess the mixing behaviour of systems with different phospholipid headgroup, phospholipids with same tail (16:0) were selected. The micro-DSC thermograms of SUVs with binary composition prepared at 1:1 molar ratio of DPPC:DPPE, DPPC:DPPE and DPPE:DPPE are reported in Fig.3.5.

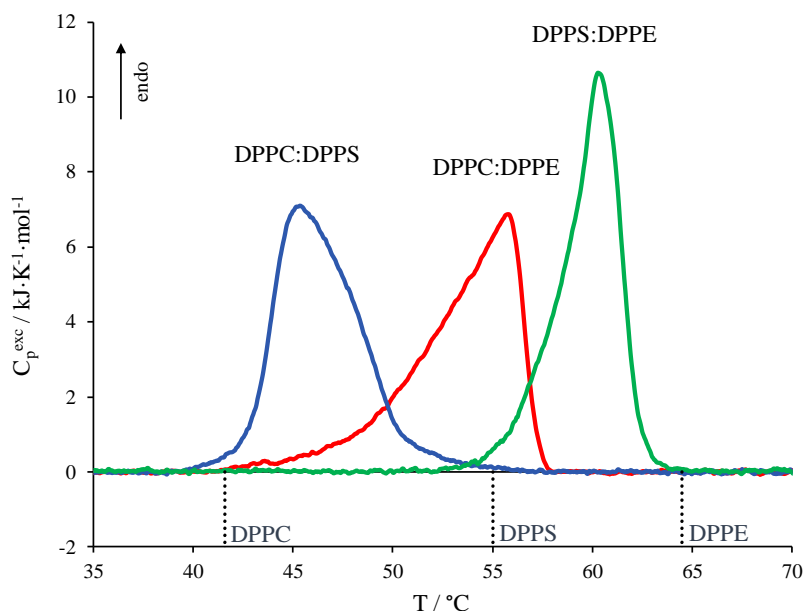


Figure 3.5: Micro-DSC thermograms for vesicles obtained by 1:1 DPPC:DPPE, DPPC:DPPE and DPPE:DPPE mixtures. The dotted vertical lines mark the T_{max} of pure DPPC, DPPE and DPPE MLBs (left to right).

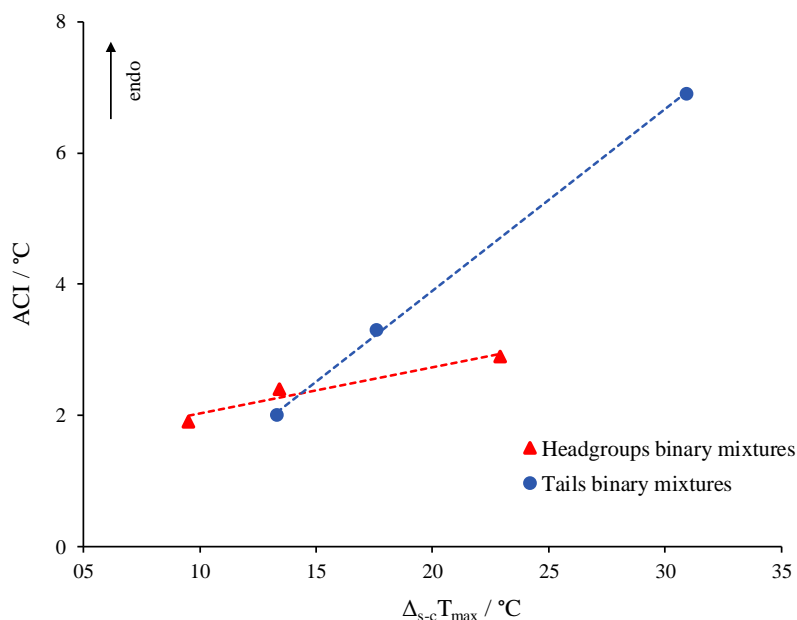


Figure 3.6: Graphical representation of the influence of the gap between the T_{max} values of the respective single-component systems, $\Delta_{s-c}T_{max}$, on thermograms breadth represented by ACI when generated by differences in headgroups or acyl chain length.

We observed broad profiles typical of unilamellar vesicles with mixed composition, corresponding to a less cooperative main gel-to-liquid crystalline phase transition. In each case the transition range was located between the transition T_{max} of the respective single-component dispersions (Bach and Wachtel, 1989; Galvagnion et al., 2016; Mabrey and Sturtevant, 1976; McMullen et al., 1999) (also indicated in the figure by the vertical dotted lines). Analogously to what we observed for phospholipid mixtures with different tails length, the mixtures of equivalent phospholipids which only differ for the headgroup somehow followed a similar behaviour in terms of thermodynamic compatibility. Indeed, the absence of evident shoulders and the position of such profiles indicate that phospholipids with different headgroups, such as choline, ethanolamine and serine are thermodynamically compatible, *i.e.* miscible, despite the difference in phospholipid headgroups' size and charge.

The breadth of the peaks can be quantified through the ACI values (Table 3.1), whose correlation with the gap between the T_{max} values of the respective single-component systems, $\Delta_{s-c}T_{max}$, is highlighted in Fig.3.6. We observed that the loss of cooperativity described by the ACI values well follows the $\Delta_{s-c}T_{max}$ gap analogously to what occurs for the phospholipid tails effect. However, the trends highlighted in Fig.3.6 revealed that the differences in tails length are able to produce a more severe dispersion of the membrane's thermodynamic phases.

The overall enthalpies, the peak maximum temperature values, T_{max} , and the transition average temperature, \bar{T} , obtained are collected in Table 3.1.

The thermograms of the three headgroups binary mixtures were strongly asymmetric and for such dispersed and asymmetric profiles the \bar{T} is more representative than the T_{max} since the overall phase distribution is considered. The $|\bar{T} - T_{max}|$ value obtained by data reported in Table 3.1 was 1.1°C for DPPC:DPPS, 2.5°C for DPPC:DPPE, 0.8°C for DPPS:DPPE and can be considered as an asymmetry index.

The \bar{T} values were very close to the expected temperatures, $T_{expected}$, obtained by simply combining the T_{max} of the respective single-component systems. Furthermore, the overall enthalpies observed resulted to be additive to those observed for the single-components. This highlighted that there is not any relevant extra enthalpic contribution due to interaction between different headgroups, hence revealing that the thermotropic behaviour of these vesicles is mainly entropically driven. Similar additivity effects and entropically driven phenomena were observed for differences in tail lengths.

In order to confirm the proportionality of the effects highlighted in all 1:1 saturated phospholipids binary systems, two model membranes with ternary compositions were obtained as SUVs by combining the same phospholipid used so far and reflecting the proportions observed in the ISGs (MacDonald et al., 2015): a phospholipid tails ternary membrane as 7 DPPC : 2 DSPC : 1 DMPC molar ratio and a phospholipid headgroups ternary membrane as

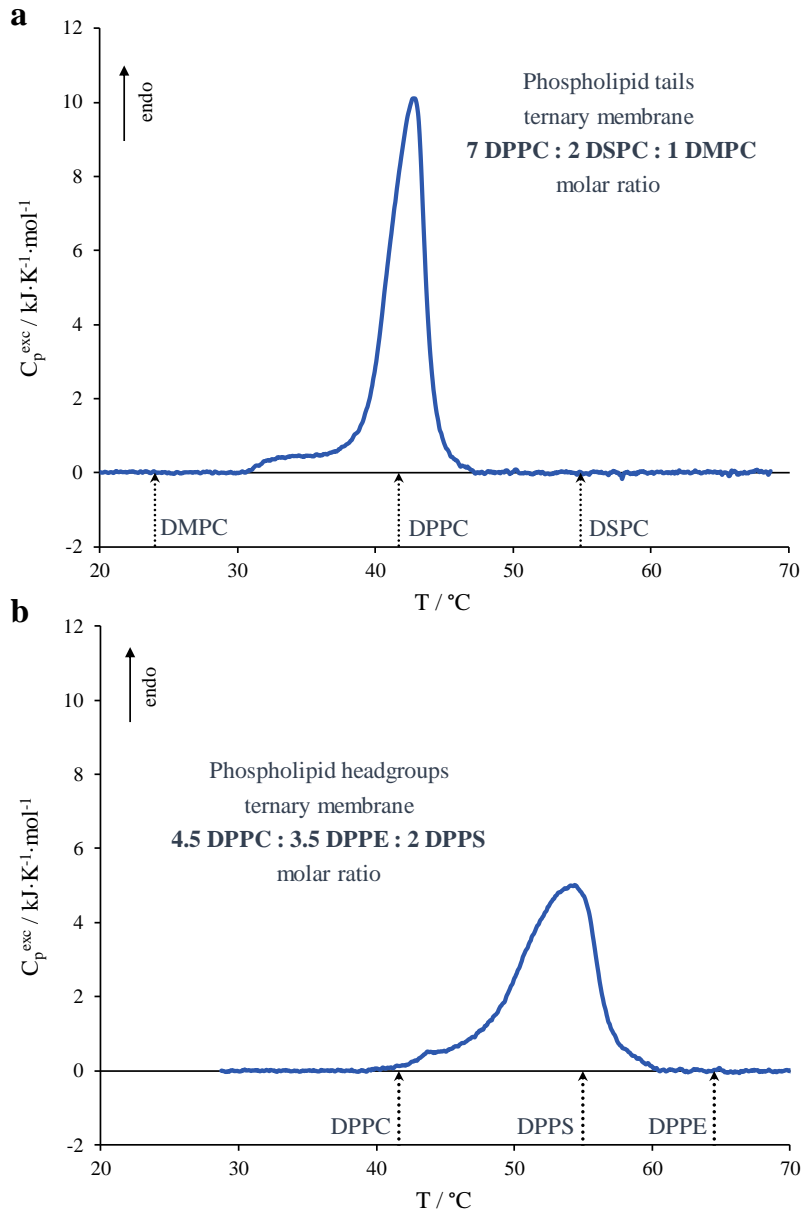


Figure 3.7: a) Micro-DSC thermograms for the phospholipid tails ternary membrane as 7 DPPC : 2 DSPC : 1 DMPC molar ratio. The dotted vertical arrows mark the T_{max} of pure DMPC, DPPC and DSPC MLBs (left to right). b) Micro-DSC thermogram for vesicles obtained as 4.5 DPPC : 3.5 DPPE : 2 DPPS. The dotted vertical arrows mark the T_{max} of pure DPPC, DPPS and DPPE MLBs (left to right).

Table 3.2: Thermodynamic parameters evaluated from micro-DSC investigations for phospholipid tails and headgroups ternary systems and for a tails quaternary system. The parameters were compared with the arithmetical values calculated from single-component systems. The second cycle heating curves were used to obtain the main transition enthalpy (ΔH°), the peak maximum temperature (T_{max}), the transition average temperature (\bar{T}) and the Average Cooperativity Index (ACI).

	Expected		Experimental			
	ΔH° kJ·mol ⁻¹	$T_{expected}$ °C	ΔH° kJ·mol ⁻¹	T_{max} °C	\bar{T} °C	ACI °C
Tails ternary membrane	36	42.5	37 ± 2	42.8 ± 0.3	41.5 ± 0.3	2.5 ± 0.2
Headgroups ternary membrane	36	52.3	36 ± 2	54.5 ± 0.2	52.4 ± 0.1	3.3 ± 0.1
Tails quaternary membrane	32	-	33 ± 2	41.7 ± 0.3	39.6 ± 0.3	3.0 ± 0.2

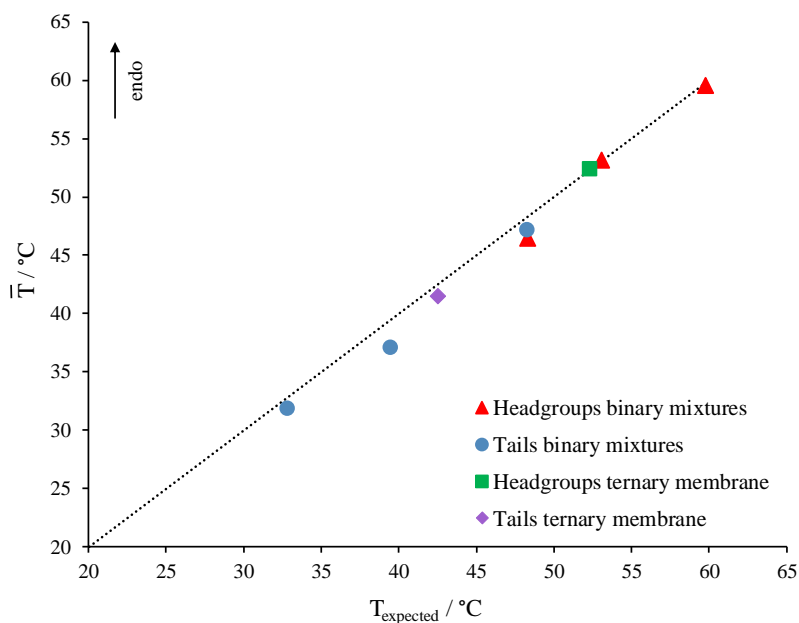


Figure 3.8: Graphical representation of the transition average temperature, \bar{T} , of several representative model membranes versus the temperature expected by combining the T_{max} of the respective single-component systems, $T_{expected}$.

4.5 DPPC : 3.5 DPPE : 2 DPPS molar ratio. Their calorimetric profiles are represented by the curves in Fig.3.7.

As for the tails ternary membrane in Fig.3.7a, the composition represented the 50% of the headgroups and an average of 75% of the tails in real ISGs (MacDonald et al., 2015). We observed a thermogram that resembles the profile exhibited by the binary systems in Fig.3.4. Indeed, we observed a main peak with a slightly higher maximum temperature (42.8°C) than the T_{max} of the major component (DPPC), which reflects the presence of a little amount of DSPC, as well as the small “step” at the beginning of the curve, which reflects the presence of DMPC. Indeed, the temperature range of the initial part of the curve corresponds with the DPPC:DMPC mixed phases reported in Fig.3.4. The \bar{T} value obtained was ($41.5 \pm 0.3^{\circ}\text{C}$) was comparable to the $T_{expected}$ (42.5°C) obtained from the constituents' T_{max} .

As for the headgroups ternary membrane in Fig.3.7b, the composition reflected the 80% of the headgroups and an average of 35% of the tails in real ISGs (MacDonald et al., 2015). An asymmetric peak was observed for which the \bar{T} value ($52.4 \pm 0.1^{\circ}\text{C}$) was matching to the $T_{expected}$ (52.3°C) obtained from the constituents' T_{max} .

The enthalpies observed for both the ternary membranes are reported in Table 3.2 and are in line with those expected from the references' enthalpies following the components proportions. The comparison between the experimental and the expected enthalpies indicated that the pretransitions are prevented in such complex systems and once again confirmed the entropic nature of the mixing phenomena that influence the thermodynamic stability of these membranes since the overall enthalpy resulted to be still additive.

The overall picture in terms of correlation between the \bar{T} and $T_{expected}$ is represented by Fig.3.8. We observed an almost linear correlation between the observed \bar{T} and the $T_{expected}$. According to these results, we may argue that the trends of \bar{T} and enthalpic stability proportionally follow the constituents' contributions in case of phospholipids with saturated acyl chains, indicating high thermodynamic compatibility of such species. Furthermore, the strong

proportionality shown highlights that predictions on the position of the thermodynamic profiles are allowed and deviations might be used to detect other type of interactions due to different composition and/or to external agents than the expected phospholipid packing.

3.3.3. Effects of unsaturated phospholipid acyl chains

In order to focus on the influence of the phospholipid tails' unsaturation, a quaternary membrane was prepared by including the 5% of an unsaturated component, DOPC, into the phospholipid tails ternary membrane. A composition as 6.7 DPPC : 1.8 DSPC : 1.0 DMPC : 0.5 DOPC molar ratio was achieved and the corresponding micro-DSC trace is shown in Fig.3.9 together with the above-described tails ternary system for the sake of comparison. Analogously to the tails ternary membrane, such a composition reflected the

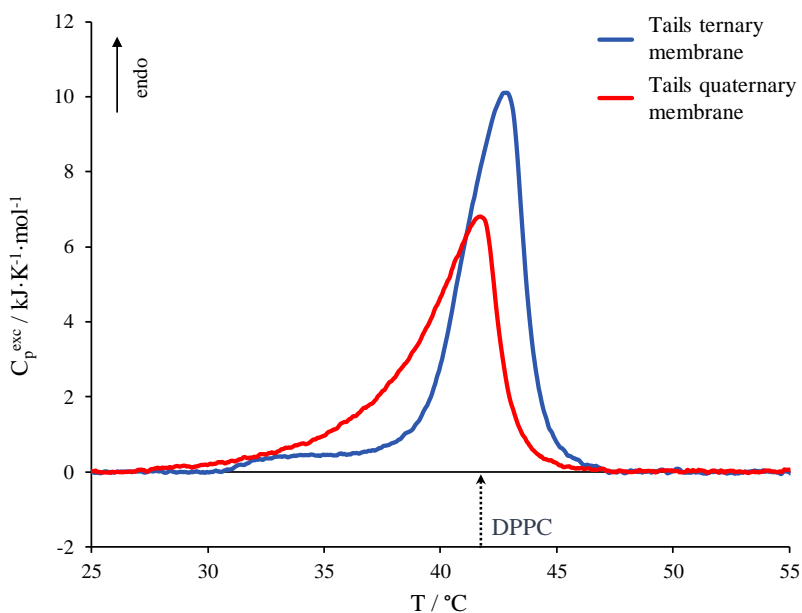


Figure 3.9: Micro-DSC thermograms for the tails ternary membrane as 7 DPPC : 2 DSPC : 1 DMPC molar ratio (blue curve) and the tails quaternary membrane obtained by the addition of the 5% of DOPC to the ternary membrane achieving a 6.7 DPPC : 1.8 DSPC : 1.0 DMPC : 0.5 DOPC molar ratio (red curve). The dotted vertical arrow marks the T_m of pure DPPC MLBs.

components proportions and represented the 50% of the headgroups and an average of 75% of the tails in real ISGs (MacDonald et al., 2015), reflecting the phospholipid ratio of the real membrane.

The quaternary membrane's thermogram appeared asymmetric and broader than the ternary one, showing a more homogeneous phases distribution as a consequence of the addition of unsaturations and fully covering the initial step of the ternary membrane's profile. Moreover, the T_{max} is slight shifted towards lower temperatures (41.7°C).

The enthalpy value is reported in Table 3.2 together with all the other thermodynamic parameters. We observed that the introduction of an unsaturated component has a strong influence (also considering the small amount added) as regards both the phases distribution that become broader and more homogenous and the entropic effect that compromise the overall thermodynamic stability. Such effects are often related to the concept of "membrane flexibility" that is well known to play an important role in the biological frame.

3.3.4. *Hierarchy of thermodynamic contributions*

The thermodynamic information obtained so far allowed us to depict a scenario describing a hierarchy of the observed entropic contributions on the thermodynamic stability of model and/or real cell membranes. The overall information indicated that the strength of the effects can be catalogued as

$$\text{membrane curvature} < \text{phospholipid headgroup} < \\ < \text{phospholipid tail length} < \text{phospholipid tail unsaturation}.$$

In particular: membrane curvature effects become negligible for multicomponent systems prepared as SUVs and/or as vesicles with a bigger size; headgroups and tails length produce effects for which the enthalpy and the \bar{T} proportionally follow the single-component's contributions and the loss

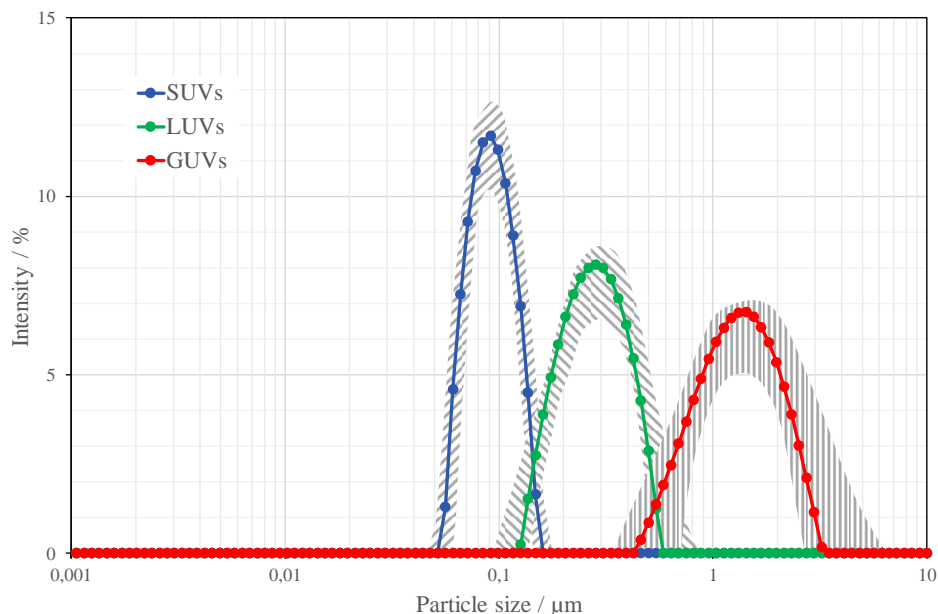


Figure 3.10: DLS data obtained at 25°C for 1:1 DPPC:DMPC vesicles prepared as GUVs (red), LUVs (green) and SUVs (blue) are reported as an example of size distribution. The size distributions recorded for other various liposomal preparations were within the variability regions indicated as grey lines.

of overall cooperativity depends on the transition temperature gap between the constituents (this last effect is less pronounced for headgroups than tails length differences); the presence of phospholipid tail unsaturation is the factor that produces the most severe effect on membrane thermotropic behaviour by generally destabilizing it both in terms of enthalpy, transition temperature and cooperativity.

In principle, by knowing such a hierarchy of interaction, simpler *ad hoc* model membranes that reflect the behaviour of more complex ones might be prepared.

3.3.5. Spectroscopic characterization

DLS measurements were performed in order to verify if the size of the extruded vesicles was in agreement with the polycarbonate filters'

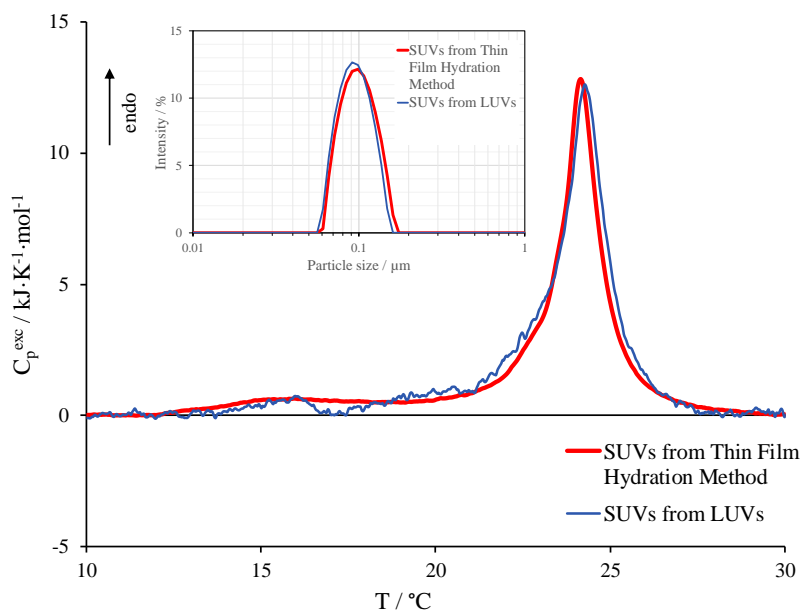


Figure 3.11: Comparison between micro-DSC thermograms for DMPC SUVs obtained by thin film hydration method (red curve, 2.5mM) and DMPC SUVs obtained by extruding LUVs (blue curve, ~0.3mM). The box reports the comparison between the respective size distribution obtained by DLS.

specifications and to verify that the GUVs sizes were of the order of 1 μ m or higher.

Fig.3.10 reports the range of the size distributions for the GUVs, LUVs and SUVs suspensions investigated in this work. We observed that the particular formulations do not severely affect the extrusion efficiency.

Combined DLS/micro-DSC measurements were also performed in order to demonstrate that the two different protocols adopted for the preparation unilamellar liposomes (one for GUVs/LUVs (Moscho et al., 1996) and one for SUVs (Laouini et al., 2012)) are equivalent and do not produce relevant differences in vesicle morphology and calorimetric profile. With this purpose, DMPC SUVs samples were also prepared by extruding LUVs suspensions, which came from GUVs, through 100nm polycarbonate membranes. Fig.3.11 shows the comparison of micro-DSC thermograms for SUVs obtained through

the two different methods. Similar profiles were observed confirming the above assertion and that small size differences observed are not significant in terms of micro-DSC profiles. As mentioned above, the SUVs extruded from LUVs signal is noisier due to the lower lipid concentration dictated by the preparation method.

3.4. References

- Bach, D., Wachtel, E., 1989. Thermotropic properties of mixtures of negatively charged phospholipids with cholesterol in the presence and absence of Li⁺ or Ca²⁺ ions. *Biochim. Biophys. Acta - Biomembr.* 979, 11–19.
- Bacia, K., Schwille, P., Kurzchalia, T., 2005. From The Cover: Sterol structure determines the separation of phases and the curvature of the liquid-ordered phase in model membranes. *Proc. Natl. Acad. Sci.* 102, 3272–3277.
- Bagatolli, L.A., Gratton, E., 2000. A Correlation between Lipid Domain Shape and Binary Phospholipid Mixture Composition in Free Standing Bilayers: A Two-Photon Fluorescence Microscopy Study. *Biophys. J.* 79, 434–447.
- Barone, G., Del Vecchio, P., Fessas, D., Giancola, C., Graziano, G., 1992. THESEUS: A new software package for the handling and analysis of thermal denaturation data of biological macromolecules. *J. Therm. Anal.* 38, 2779–2790.
- Biltonen, R.L., Lichtenberg, D., 1993. The use of differential scanning calorimetry as a tool to characterize liposome preparations. *Chem. Phys. Lipids* 64, 129–142.
- Brzustowicz, M.R., Brunger, A.T., 2005. X-ray scattering from unilamellar lipid vesicles. *J. Appl. Crystallogr.* 38, 126–131.
- Galvagnion, C., Brown, J.W.P., Ouberai, M.M., Flagmeier, P., Vendruscolo, M., Buell, A.K., Sparr, E., Dobson, C.M., 2016. Chemical properties of lipids

- strongly affect the kinetics of the membrane-induced aggregation of α -synuclein. *Proc. Natl. Acad. Sci.* 113, 7065–7070.
- Gardikis, K., Hatziantoniou, S., Signorelli, M., Pusceddu, M., Micha-Screttas, M., Schiraldi, A., Demetzos, C., Fessas, D., 2010. Thermodynamic and structural characterization of Liposomal-Locked in-Dendrimers as drug carriers. *Colloids Surfaces B Biointerfaces* 81, 11–19.
- Heimburg, T., 1998. Mechanical aspects of membrane thermodynamics. Estimation of the mechanical properties of lipid membranes close to the chain melting transition from calorimetry. *Biochim. Biophys. Acta - Biomembr.* 1415, 147–162.
- Heimburg, T., 2000. A Model for the Lipid Pretransition: Coupling of Ripple Formation with the Chain-Melting Transition. *Biophys. J.* 78, 1154–1165.
- Ising, E., 1924. “Report on the theory of ferromagnetism.” *Beitrag zur Theorie des Ferromagnetismus* 253–258.
- Ivanova, V.P., Heimburg, T., 2001. Histogram method to obtain heat capacities in lipid monolayers, curved bilayers, and membranes containing peptides. *Phys. Rev. E* 63, 041914.
- Koynova, R., Caffrey, M., 1998. Phases and phase transitions of the phosphatidylcholines. *Biochim. Biophys. Acta - Rev. Biomembr.* 1376, 91–145.
- Laouini, A., Jaafar-Maalej, C., Limayem-Blouza, I., Sfar, S., Charcosset, C., Fessi, H., 2012. Preparation, Characterization and Applications of Liposomes: State of the Art. *J. Colloid Sci. Biotechnol.* 1, 147–168.
- Losada-Pérez, P., Mertens, N., de Medio-Vasconcelos, B., Slenders, E., Leys, J., Peeters, M., van Grinsven, B., Gruber, J., Glorieux, C., Pfeiffer, H., Wagner, P., Thoen, J., 2015. Phase Transitions of Binary Lipid Mixtures: A Combined Study by Adiabatic Scanning Calorimetry and Quartz Crystal

- Microbalance with Dissipation Monitoring. *Adv. Condens. Matter Phys.* 2015, 1–14.
- Mabrey, S., Sturtevant, J.M., 1976. Investigation of phase transitions of lipids and lipid mixtures by sensitivity differential scanning calorimetry. *Proc. Natl. Acad. Sci.* 73, 3862–3866.
- MacDonald, M.J., Ade, L., Ntambi, J.M., Ansari, I.-U.H., Stoker, S.W., 2015. Characterization of Phospholipids in Insulin Secretory Granules and Mitochondria in Pancreatic Beta Cells and Their Changes with Glucose Stimulation. *J. Biol. Chem.* 290, 11075–11092.
- MacDonald, R.C., MacDonald, R.I., Menco, B.P.M., Takeshita, K., Subbarao, N.K., Hu, L., 1991. Small-volume extrusion apparatus for preparation of large, unilamellar vesicles. *Biochim. Biophys. Acta - Biomembr.* 1061, 297–303.
- Marrink, S.J., Mark, A.E., 2003. Molecular Dynamics Simulation of the Formation, Structure, and Dynamics of Small Phospholipid Vesicles. *J. Am. Chem. Soc.* 125, 15233–15242.
- McMahon, H.T., Gallop, J.L., 2005. Membrane curvature and mechanisms of dynamic cell membrane remodelling. *Nature* 438, 590–596.
- McMullen, T.P.W., Lewis, R.N.A.H., McElhaney, R.N., 1999. Calorimetric and spectroscopic studies of the effects of cholesterol on the thermotropic phase behavior and organization of a homologous series of linear saturated phosphatidylethanolamine bilayers. *Biochim. Biophys. Acta - Biomembr.* 1416, 119–134.
- Moscho, A., Orwar, O., Chiu, D.T., Modi, B.P., Zare, R.N., 1996. Rapid preparation of giant unilamellar vesicles. *Proc. Natl. Acad. Sci.* 93, 11443–11447.

- Mouritsen, O.G., 2011. Lipids, curvature, and nano-medicine. *Eur. J. Lipid Sci. Technol.* 113, 1174–1187.
- Parthasarathy, R., Groves, J.T., 2007. Curvature and spatial organization in biological membranes. *Soft Matter* 3, 24–33.
- Prince, A., Sandhu, P., Kumar, P., Dash, E., Sharma, S., Arakha, M., Jha, S., Akhter, Y., Saleem, M., 2016. Lipid-II Independent Antimicrobial Mechanism of Nisin Depends on Its Crowding and Degree of Oligomerization. *Sci. Rep.* 6, 1–15.
- Riske, K.A., Barroso, R.P., Vequi-Suplicy, C.C., Germano, R., Henriques, V.B., Lamy, M.T., 2009. Lipid bilayer pre-transition as the beginning of the melting process. *Biochim. Biophys. Acta - Biomembr.* 1788, 954–963.
- Risselada, H.J., Marrink, S.J., 2009. Curvature effects on lipid packing and dynamics in liposomes revealed by coarse grained molecular dynamics simulations. *Phys. Chem. Chem. Phys.* 11, 2056.
- Saitta, F., Signorelli, M., Fessas, D., 2019. Dissecting the effects of free fatty acids on the thermodynamic stability of complex model membranes mimicking insulin secretory granules. *Colloids Surfaces B Biointerfaces* 176, 167–175.
- Sciacca, M.F.M., Carbone, V., Pappalardo, M., Milardi, D., La Rosa, C., Grasso, D.M., 2009. Interaction of human amylin with phosphatidylcholine and phosphatidylserine membranes. *Mol. Cryst. Liq. Cryst.* 500, 73–81.
- Stewart, J.C.M., 1980. Colorimetric determination of phospholipids with ammonium ferrothiocyanate. *Anal. Biochem.* 104, 10–14.
- Tonnesen, A., Christensen, S.M., Tkach, V., Stamou, D., 2014. Geometrical Membrane Curvature as an Allosteric Regulator of Membrane Protein Structure and Function. *Biophys. J.* 106, 201–209.

ISG-representative model membranes

The addition of sphingomyelins and lysophosphatidylcholines together with a more complete fatty acids distribution characterizing the phospholipid bilayer of the Insulin Secretory Granules to the model membranes of the previous chapter allowed the achievement of a fourteen-components model membrane that reflected the 80% of phospholipids present in ISGs. In this chapter a thermodynamic exploitation of such membrane performed through micro-DSC technique is presented aiming to assess the synergic contributions to the stability of a mixed complex system very close to real membranes. The further inclusion of cholesterol was finally considered for the achievement of the final ISG-like membrane.

In spite of the high complexity of lipid organization processes occurring in cell membranes, the thermotropic behaviour observed for both the cholesterol-free and cholesterol-containing ISG-like vesicles were highly comparable to real cell membrane DSC profiles reported in the literature.

4.1. Introduction

Cells and vesicles functionalities are not only dependent on protein-based mechanisms. Indeed, lipid composition of phospholipid membranes severely affect their thermodynamic stability, which in turn is able to influence

membrane proteins' functionality (Heimburg et al., 1999; Samuli Ollila et al., 2007; Zhang et al., 2003).

Lipid vesicles are exemplary model systems able to provide simulations of cell membranes, such as organelles and vesicles involved in cell trafficking. Clearly it is hard to perfectly mime a real biological membrane because of the presence of membrane proteins and of a distribution across the inner and the outer leaflets that is not only regulated by protein-independent processes as thermodynamic rearrangements (Boesze-Battaglia and Schimmel, 1997; Risselada and Marrink, 2009; Yeagle and Young, 1986), but also directly by proteins action (Daleke, 2003; Heimburg et al., 1999; Römer et al., 2010; Sezgin et al., 2017). However, despite the numerous studies on model membranes carried out mainly through calorimetric, spectroscopic and imaging techniques, such model systems were characterized by an extremely simple composition which does not keep into consideration the complexity and the asymmetry of the real bilayers (Rothman and Lenard, 1977). In this frame, simulating peculiarities and composition complexity of a real cell membrane might be a key point for the correct interpretation of membrane-based mechanisms in cells since each factor might produce modifications in membrane thermodynamics, which in turn might lead to functionality modifications.

In this work, a thermodynamic study of Small Unilamellar Vesicles (SUVs) with complex composition at physiological pH by using the micro-DSC technique was performed. 16:0 LysoPC and sphingomyelins (egg sphingomyelin was used in this case) were introduced to the model membranes of the previous chapter reproducing the 80% of the headgroups and an average of 35% of the tails in real ISGs (MacDonald et al., 2015). In order to integrate the acyl chain distribution, vesicles were therefore obtained by mixing fourteen different lipids, achieving a composition which represents the 80% of the headgroups and an average of 80% of the tails in real ISGs. The inclusion of cholesterol was finally considered for the achievement of final ISG-like membrane.

4.2. Materials and methods

4.2.1. Materials

1,2-distearoyl-sn-glycero-3-phosphocholine (DSPC), 1,2-dipalmitoyl-sn-glycero-3-phosphocholine (DPPC), 1,2-dimyristoyl-sn-glycero-3-phosphocholine (DMPC), 1,2-dioleoyl-sn-glycero-3-phosphocholine (DOPC), 1,2-distearoyl-sn-glycero-3-phosphoethanolamine (DSPE), 1,2-dipalmitoyl-sn-glycero-3-phosphoethanolamine (DPPE), 1,2-dioleoyl-sn-glycero-3-phosphoethanolamine (DOPE), 1,2-distearoyl-sn-glycero-3-phospho-L-serine (DSPS, sodium salt), 1,2-dipalmitoyl-sn-glycero-3-phospho-L-serine (DPPS, sodium salt), 1,2-dioleoyl-sn-glycero-3-phospho-L-serine (DOPS, sodium salt), 1-palmitoyl-2-hydroxy-sn-glycero-3-phosphocholine (16:0 LPC), 1-behenoyl-2-hydroxy-sn-glycero-3-phosphocholine (22:0 LPC), 1-oleoyl-2-hydroxy-sn-glycero-3-phosphocholine (18:1 LPC), egg sphingomyelin (EggSM, Chicken) and cholesterol powders were purchased from Avanti Polar Lipids (purity certified by the supplier >99%) and used without further purification, whereas the other chemicals were obtained from Sigma-Aldrich. All solvents were of analytical grade.

4.2.2. Selection of vesicles constituents

The components mentioned above reflect the ISGs' fatty acid distribution (MacDonald et al., 2015) with the exception of EggSM that was preferred for practical reasons instead of the combination of synthetic sphingomyelins. EggSM was selected among other natural sphingomyelins, such as BrainSM and MilkSM, because of the higher similarity of the fatty acid distribution to those reported for the ISGs, according to the supplier's information.

4.2.3. Liposomes preparation

Small Unilamellar Vesicles (SUVs) were prepared through thin-film hydration (Laouini et al., 2012). An amount of about 20mg lipids were dissolved in

chloroform:methanol 3:1 in a round-bottomed flask. Lipids were dried under a stream of dry nitrogen gas and evaporated to dryness through rotary evaporation (Heidolph Laborota 4000 efficient, WB eco, Schwabach, Germany) at 45°C. The films were kept under vacuum for at least 3 hours to remove solvent traces and then aged overnight at 4°C. For the hydration, 10mM phosphate buffer (pH 7.4) at a temperature above the gel-to-liquid-crystal transition of the lipid system was added up to a 10mg/mL lipid concentration. After the complete dispersion of the lipid films, the obtained mixtures were slowly stirred in water bath, at the same temperature chosen for the buffer, for about an hour until the induction of a homogenous suspension. The MLVs dispersions obtained were extruded through polycarbonate filters (pore size of 100nm) mounted on a heated mini-extruder (Avanti Polar Lipids, Alabaster, AL, USA) fitted with two 1mL gastight syringes (Hamilton, Reno, NV, USA) in order to obtain SUVs suspensions. An odd number of passages, usually 41, was performed to avoid any contamination by liposomes that might have not passed through the filters, as suggested elsewhere (MacDonald et al., 1991).

As mentioned in the previous chapter, DLS data indicated that the described procedure produces SUVs with a size distribution around the nominal provided by the supplier (*i.e.* 100nm) and small deviations are not sufficient to influence the micro-DSC thermograms. For this reason, this characterization was not repeated here.

4.2.4. Thermal analysis measurements

Detailed information and specifications about the applied calorimetric method (micro-DSC) have been already reported in section 3.2.4. Please refer to that section.

As a brief recall, a Setaram micro-DSCIII (Setaram Instrumentation, Caluire, France) operating with 1mL hermetically closed pans was employed at 0.5°C/min scanning rate. SUVs samples were diluted up to 2.5mM

phospholipid concentration and the final phospholipid concentration for all kind of vesicles was checked by the Stewart assay (Stewart, 1980). Raw data were worked out with the dedicated software "THESEUS" (Barone et al, 1992) for obtaining the excess specific heat trace, $C_p^{exc}(T)$, with respect to the low temperature lipids state.

Since more complex systems were here considered, the application of two heating/cooling cycles to vesicle dispersions was not sufficient for the achievement of equilibrium phases. Lipid phases in metastable equilibria and kinetic phenomena may arise if the liposomal composition is more complex. In this case, six heating/cooling cycles might be necessary for the achievement of thermograms reproducibility. In all cases, the last cycle thermograms were considered for analysis of the thermotropic transitions shown in figures.

In order to quantitatively compare and discuss the transition cooperativity between different systems, the transition average temperature, \bar{T} , and the average cooperativity index, ACI , defined in section 3.2.4 were adopted. Briefly, the transition average temperature, \bar{T} , is defined as

$$\bar{T} = \int_{T_0}^{T_f} T \cdot f(T) dT$$

being T_0 and T_f the initial and final limit of the observable peak, respectively, and the frequency function $f(T)$ is the normalized calorimetric peak distribution

$$f(T) = \frac{C_p^{exc}(T)}{\Delta H^{\circ}},$$

whereas the average cooperativity index, ACI , is defined as

$$ACI = \sqrt{\int_{T_0}^{T_f} (T - \bar{T})^2 \cdot f(T) dT}.$$

Moreover, the $|\bar{T} - T_{max}|$ difference represents a peak asymmetry index.

4.3. Results and discussion

4.3.1. From five to fourteen-components vesicles

Considering the phospholipid headgroups ternary model membrane described in section 3.3.2 and in Fig.3.7, the stepwise analysis of the contribution to the membrane thermodynamic stability was continued by the investigation of new components that slightly differ from the above-mentioned in terms of molecular geometry and chemical structure: lysophosphatidylcholines and sphingomyelin. Indeed, lysophosphatidylcholines have a peculiar conical shape because of the loss of one of the two acyl chains existing in a phospholipid, which instead has a cylindrical shape, whereas an acyl chain and the glycerol of phospholipids are replaced by a sphingosine molecule in sphingomyelins. In order to highlight such peculiarities, we chose to keep using lipids with same tail length (16:0) for the preparation of such a model membrane. Specifically, 16:0 LPC was selected among lysophosphatidylcholines, whereas sphingomyelins were represented by EggSM. As for the last component, EggSM was selected for practical reasons (see section 4.2.2) and because its fatty acids distribution mainly consists in 16:0 chains (86%) according to the supplier's information.

A five-components model membrane that reflected the major macro-categories constituting the ISGs' bilayer (phosphatidylcholines, phosphatidylethanolamines, phosphatidylserines, sphingomyelins and lysophosphatidylcholines) was therefore prepared by including 16:0 LPC and EggSM to the headgroups ternary membrane, achieving a composition equal to 2.80 DPPC : 2.15 DPPE : 1.40 DPPS : 2.40 16:0LPC : 1.25 EggSM molar ratio (MacDonald et al., 2015) (Fig.4.1a). The composition of such a preparation reflects the 80% of the headgroups and an average of 35% of the tails in real ISGs.

The micro-DSC profile of the resulting five-components model membrane is reported in Fig.4.2 and the relative thermodynamic parameters are reported in Table 4.1. We observed an asymmetric and biphasic profile, index of phase

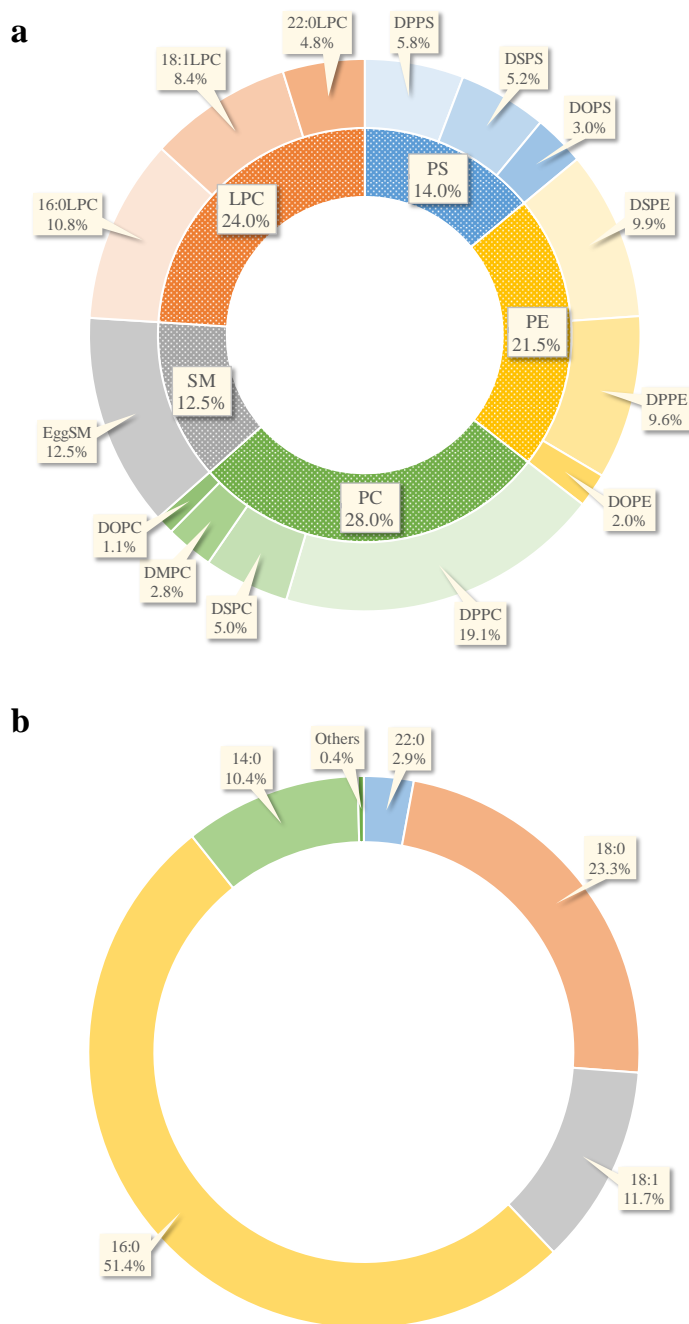


Figure 4.1: Diagrams representing a) the composition of the five-components membrane (inner cycle) and the fourteen-components model membrane mimicking the ISG phospholipid bilayer (outer cycle) and b) the detailed percentages highlighting the acyl chains involved in the fourteen-components vesicles.

separation. The introduction of the two new components in ISG's proportions produced a destabilizing entropic effect with a loss of overall cooperativity (see ACI) and the transition range was shifted toward lower temperatures ($\bar{T} = 47.2 \pm 0.3^\circ\text{C}$) with respect to the headgroups ternary membrane. On the other hand, a slight increase in overall transition enthalpy was observed. Taking into consideration that a phase separation was observed, we may argue that some packing interactions might maybe be enhanced within the more stable phase, justifying the increase of transition enthalpy.

Despite sphingomyelin is reported in the literature to generate phase separation (Filippov et al., 2006; Untrach and Graham, 1977; Wang and Silvius, 2003) and also some information is known on 16:0 LPC effects (Lu et al., 1997, 2001; Van Echteld et al., 1980), specifically attributing the observed effects to one of these two components is beyond the scope of this thesis, since an even more in-depth thermodynamic dissection of the contributions becomes more difficult when molecules that disturb the regular packing of the

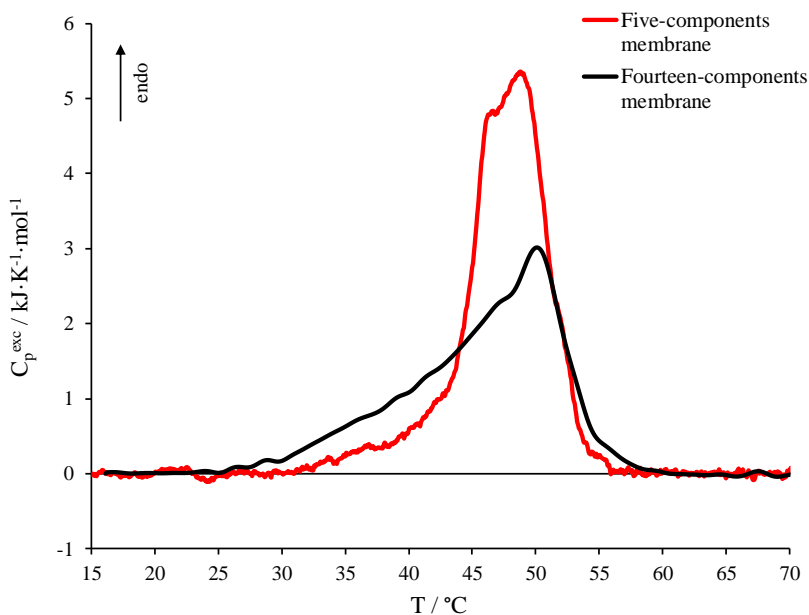


Figure 4.2: Micro-DSC thermograms for the five-components model membrane (red curve) and the fourteen-components membrane (black curve) prepared with compositions as in Fig.4.1.

Table 4.1: Thermodynamic parameters evaluated from micro-DSC investigations for several complex systems mimicking the ISGs' phospholipid bilayer. The last cycle heating curves were used to obtain the main transition enthalpy (ΔH°), the peak maximum temperature (T_{max}), the transition average temperature (\bar{T}) and the Average Cooperativity Index (ACI).

	ΔH° kJ·mol ⁻¹	T_{max} °C	\bar{T} °C	ACI °C
Five-components membrane	42 ± 2	48.5 ± 0.5	47.2 ± 0.3	3.8 ± 0.2
Fourteen-components membrane	35 ± 2	50.4 ± 0.5	45.5 ± 0.3	6.3 ± 0.2
+10% CHOL	23 ± 2	44.8 ± 0.3	43.2 ± 0.3	5.7 ± 0.2
+20% CHOL	18 ± 2	46.4 ± 0.3	43.7 ± 0.3	6.0 ± 0.2

hydrophobic chains within the bilayer are present, e.g. unsaturated acyl chains, cholesterol (Shigematsu et al., 2014; Wolf et al., 2001), etc.

This part of stepwise evaluation discussed so far (including the previous chapter) was focused on the evaluation of the single contributions to the stability of phospholipid bilayers and was achieved by keeping the phospholipid headgroups the same when investigating the tails effects and the phospholipid tails length constant for the assessment of the influence of different headgroups.

In order to conclusively simulate the ISGs lipid bilayers at our best, integrating all the contributions, the preparation of a fourteen-components model membrane was achieved by proportionally selecting the most abundant acyl chains for each macro-category that inspired the five-components system. Details of this membrane composition are reported in Fig.4.1. This system is very close to the phospholipid composition of the real ISG and achieves the 80% of representativity in terms of both headgroups and acyl chains (MacDonald et al., 2015). However, despite one of the most noteworthy components of most of the real cell membranes including ISGs is cholesterol, it was omitted in this preparation to allow a specific analysis of phospholipid

interactions and will be considered in the next section in order to separately verify and discriminate its effects on the overall system.

The micro-DSC profile of the fourteen-components vesicles is reported in Fig.4.2. We observed that the introduction of acyl chains differences severely enhanced the calorimetric profile asymmetry and the loss of cooperativity compared to the one obtained for the five-components membrane (ACI values of $6.3 \pm 0.2^\circ\text{C}$ vs $3.8 \pm 0.2^\circ\text{C}$ for the five components). Moreover, the overall transition range was slightly extended toward both lower and higher temperatures, whereas the transition enthalpy significantly decreased. On the other hand, the phase separation previously seen for the five-components membrane seemed to be preserved. All these effects are coherent with the information's achieved so far, *i.e.* the higher composition complexity justifies the cooperativity loss, whereas the cooperativity and enthalpy loss are in line with the presence of about 11.7% of oleoyl chains since unsaturated acyl chains are known to destabilize the membrane stability from both an entropic

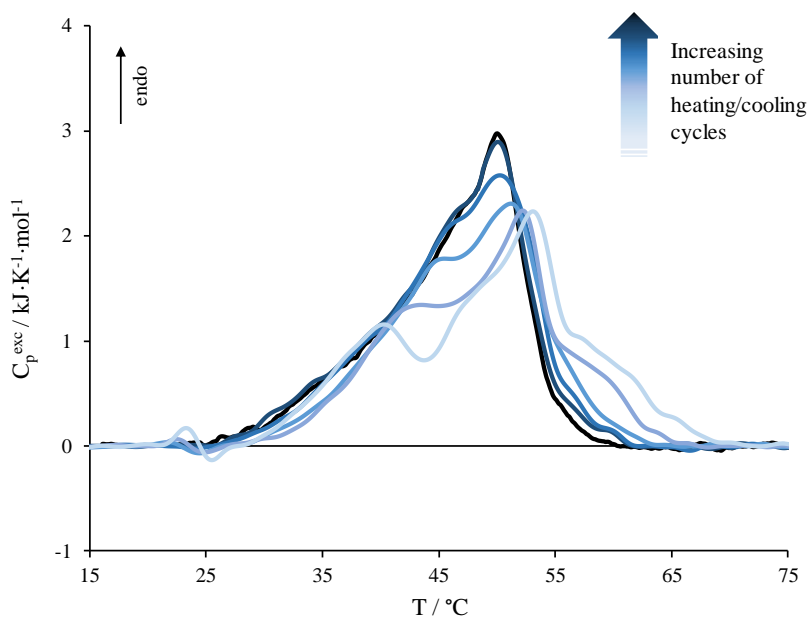


Figure 4.3: Micro-DSC thermograms for the fourteen-components membrane obtained through the application of six heating/cooling cycles. The traces colour becomes darker as the number of heating/cooling cycle increases.

and an enthalpic point of view as shown in section 3.3.3. The slight extension of the overall transition range to higher temperature than the five-components membrane may be ascribable to the presence of 23.3% of stearyl chains.

It is noteworthy emphasising that, as mentioned in section 4.2.4, the calorimetric profiles obtained for such complex vesicles underwent more than two heating/cooling cycles for the achievement of reproducibility. Thermograms deriving from consecutive cycles revealed impressive kinetic reorganization phenomena of the constituents and are reported in Fig.4.3 for the fourteen-components vesicles as an example. The first heating scan (reported as the lightest blue trace) produced a much broader signal than the final one (reported as a black trace). Moreover, we observed the presence a heterogeneous phase distribution that clearly reflected the composition complexity of the fourteen-components membrane. The calorimetric profile of this membrane gradually became narrower as consecutive ramps were applied, revealing the reorganization of lipid phases within the vesicles. The sixth heating scan was considered as thermodynamically meaningful, analogously to what was done for all the other high-complexity membranes.

4.3.2. *ISG-like membrane: influence of cholesterol*

To conclude such a stepwise investigation, the action of cholesterol in membrane thermotropic behaviour was considered, achieving the preparation of two fifteen-components membranes by the addition of cholesterol at different percentages (10% and 20%).

The relative thermograms are shown in Fig.4.4 and compared with the cholesterol-free fourteen-components vesicles. We observed a strong destabilizing effect with a progressive enthalpy depletion that depended on cholesterol amount, whereas the overall transition range remained almost the same. In particular, with the inclusion of 10% of cholesterol we observed a depletion of the signal in correspondence with the most stable phases, revealing a selective action of cholesterol to major affect the most ordered

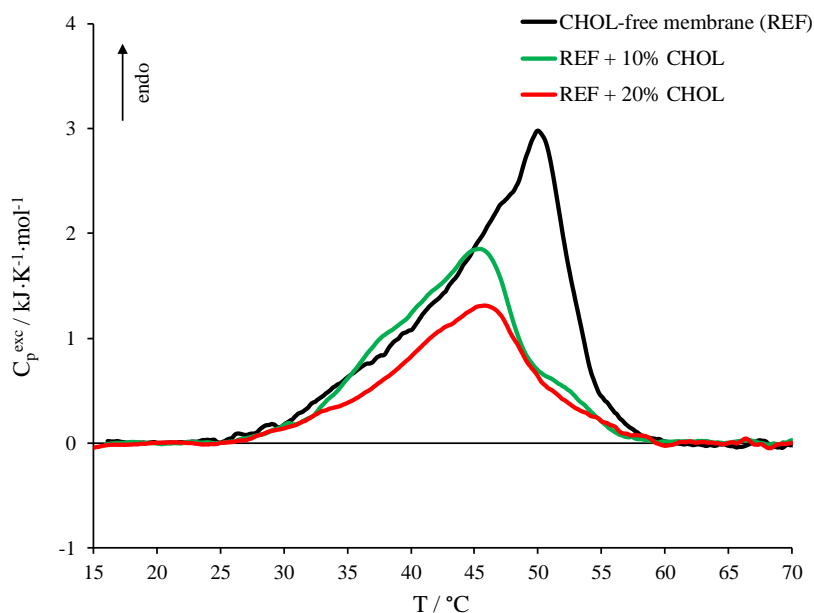


Figure 4.4: Micro-DSC thermograms obtained for a cholesterol-free fourteen-components membrane (black curve) and membranes with the addition of 10% and 20% of cholesterol (green and red curves, respectively).

and/or stable regions (McMullen and McElhaney, 1997). However, the increase of the perturbing molecule concentration up to 20% also influenced the less stable lipid population.

In conclusion, cholesterol inclusion led to a membrane with big destabilized part. Roughly, if we assume an average enthalpic contribution, the ratio of the observed enthalpies against the cholesterol-free membrane indicated systems with about 30% and 50% of phospholipids in a disordered state for 10% and 20% cholesterol addition, respectively, and the phase distribution of the remaining part was spread in a large transition range (from about 25°C to 50 °C).

This scenario is very close to reality, *i.e.* compatible with the literature based on the fluid-mosaic model (Nicolson, 2014) and reflected the versatility of real membranes, which can explore both fluid and ordered regions in order

to fulfil the necessity dictated by the several intermembrane proteins and cellular mechanisms.

In this chapter, we investigated the intrinsic membrane thermodynamics being aware that the *in vivo* cell membranes the phospholipid composition and distribution across the inner and the outer leaflets are not only regulated by protein-independent processes as thermodynamic rearrangements (Boesze-Battaglia and Schimmel, 1997; Risselada and Marrink, 2009; Yeagle and Young, 1986), but may also directly depend on proteins action (Daleke, 2003; Heimburg et al., 1999; Römer et al., 2010; Sezgin et al., 2017).

However, in spite of the high complexity of lipid organization processes occurring in cell membranes, literature data show that the thermotropic behaviour detected by DSC for both real cholesterol-free and cholesterol-containing cell membrane (de Kruffy et al., 1972; Mackey et al., 1991) is very close to the ones obtained for the cholesterol-free (*i.e.* the fourteen-components vesicles) and fifteen-components ISG-like membranes here presented, which therefore are able to well reflect the behaviour real cell membranes. As well, such good a representation of a real membrane also indicates that the peculiar membrane lipid composition used in this chapter do not compromise the general conclusions here presented about the membrane thermodynamics, the influence of cholesterol and the effects of other perturbing agents as free fatty acids (FFAs). FFAs influence on membrane thermodynamic stability will be object of the next chapter.

4.4. References

- Barone, G., Del Vecchio, P., Fessas, D., Giancola, C., Graziano, G., 1992. THESEUS: A new software package for the handling and analysis of thermal denaturation data of biological macromolecules. *J. Therm. Anal.* 38, 2779–2790.

- Boesze-Battaglia, K., Schimmel, R., 1997. Cell membrane lipid composition and distribution: implications for cell function and lessons learned from photoreceptors and platelets. *J. Exp. Biol.* 200, 2927–2936.
- Daleke, D.L., 2003. Regulation of transbilayer plasma membrane phospholipid asymmetry. *J. Lipid Res.* 44, 233–242.
- de Kruijff, B., Demel, R.A., dan Deenen, L.L.M., 1972. The effect of cholesterol and epicholesterol incorporation on the permeability and on the phase transition of intact *Acholeplasma laidlawii* cell membranes and derived liposomes. *Biochim. Biophys. Acta - Biomembr.* 255, 331–347.
- Filippov, A., Orädd, G., Lindblom, G., 2006. Sphingomyelin Structure Influences the Lateral Diffusion and Raft Formation in Lipid Bilayers. *Biophys. J.* 90, 2086–2092.
- Heimburg, T., Angerstein, B., Marsh, D., 1999. Binding of Peripheral Proteins to Mixed Lipid Membranes: Effect of Lipid Demixing upon Binding. *Biophys. J.* 76, 2575–2586.
- Laouini, A., Jaafar-Maalej, C., Limayem-Blouza, I., Sfar, S., Charcosset, C., Fessi, H., 2012. Preparation, Characterization and Applications of Liposomes: State of the Art. *J. Colloid Sci. Biotechnol.* 1, 147–168.
- Lu, J.-Z., Hao, Y.-H., Chen, J.-W., 2001. Effect of Cholesterol on the Formation of an Interdigitated Gel Phase in Lysophosphatidylcholine and Phosphatidylcholine Binary Mixtures. *J. Biochem.* 129, 891–898.
- Lu, J., Xu, Y., Chen, J., Huang, F., 1997. Effect of lysophosphatidylcholine on behavior and structure of phosphatidylcholine liposomes. *Sci. China Ser. C Life Sci.* 40, 622–629.
- MacDonald, M.J., Ade, L., Ntambi, J.M., Ansari, I.-U.H., Stoker, S.W., 2015. Characterization of Phospholipids in Insulin Secretory Granules and

- Mitochondria in Pancreatic Beta Cells and Their Changes with Glucose Stimulation. *J. Biol. Chem.* 290, 11075–11092.
- MacDonald, R.C., MacDonald, R.I., Menco, B.P.M., Takeshita, K., Subbarao, N.K., Hu, L., 1991. Small-volume extrusion apparatus for preparation of large, unilamellar vesicles. *Biochim. Biophys. Acta - Biomembr.* 1061, 297–303.
- Mackey, B.M., Miles, C.A., Parsons, S.E., Seymour, D.A., 1991. Thermal denaturation of whole cells and cell components of *Escherichia coli* examined by differential scanning calorimetry. *J. Gen. Microbiol.* 137, 2361–2374.
- McMullen, T.P.W., McElhaney, R.N., 1997. Differential Scanning Calorimetric Studies of the Interaction of Cholesterol with Distearoyl and Dielaidoyl Molecular Species of Phosphatidylcholine, Phosphatidylethanolamine, and Phosphatidylserine. *Biochemistry* 36, 4979–4986.
- Nicolson, G.L., 2014. The Fluid–Mosaic Model of Membrane Structure: Still relevant to understanding the structure, function and dynamics of biological membranes after more than 40years. *Biochim. Biophys. Acta - Biomembr.* 1838, 1451–1466.
- Risselada, H.J., Marrink, S.J., 2009. Curvature effects on lipid packing and dynamics in liposomes revealed by coarse grained molecular dynamics simulations. *Phys. Chem. Chem. Phys.* 11, 2056.
- Römer, W., Pontani, L.-L., Sorre, B., Rentero, C., Berland, L., Chambon, V., Lamaze, C., Bassereau, P., Sykes, C., Gaus, K., Johannes, L., 2010. Actin Dynamics Drive Membrane Reorganization and Scission in Clathrin-Independent Endocytosis. *Cell* 140, 540–553.
- Rothman, J.E., Lenard, J., 1977. Membrane Asymmetry. *Science* 195, 743–753.

- Samuli Ollila, O.H., Róg, T., Karttunen, M., Vattulainen, I., 2007. Role of sterol type on lateral pressure profiles of lipid membranes affecting membrane protein functionality: Comparison between cholesterol, desmosterol, 7-dehydrocholesterol and ketosterol. *J. Struct. Biol.* 159, 311–323.
- Sezgin, E., Levental, I., Mayor, S., Eggeling, C., 2017. The mystery of membrane organization: composition, regulation and roles of lipid rafts. *Nat. Rev. Mol. Cell Biol.* 18, 361–374.
- Shigematsu, T., Koshiyama, K., Wada, S., 2014. Molecular dynamics simulations of pore formation in stretched phospholipid/cholesterol bilayers. *Chem. Phys. Lipids* 183, 43–49.
- Stewart, J.C.M., 1980. Colorimetric determination of phospholipids with ammonium ferrothiocyanate. *Anal. Biochem.* 104, 10–14.
- Untrach, S.H., Graham, G., 1977. Molecular interactions between lecithin and sphingomyelin. Temperature-and composition-dependent phase separation. *J. Biol. Chem.* 252, 4449–4457.
- Van Echteld, C.J.A., De Kruijff, B., De Gier, J., 1980. Differential miscibility properties of various phosphatidylcholine/lysophosphatidylcholine mixtures. *Biochim. Biophys. Acta - Biomembr.* 595, 71–81.
- Wang, T.-Y., Silvius, J.R., 2003. Sphingolipid Partitioning into Ordered Domains in Cholesterol-Free and Cholesterol-Containing Lipid Bilayers. *Biophys. J.* 84, 367–378.
- Wolf, C., Koumanov, K., Tenchov, B., Quinn, P.J., 2001. Cholesterol favors phase separation of sphingomyelin. *Biophys. Chem.* 89, 163–172.
- Yeagle, P.L., Young, J.E., 1986. Factors contributing to the distribution of cholesterol among phospholipid vesicles. *J. Biol. Chem.* 261, 8175–8181.

Zhang, W., Bogdanov, M., Pi, J., Pittard, A.J., Dowhan, W., 2003. Reversible Topological Organization within a Polytopic Membrane Protein Is Governed by a Change in Membrane Phospholipid Composition. *J. Biol. Chem.* 278, 50128–50135.

Free fatty acids effects on lipid membranes

This chapter describes a micro-DSC study of the influence of several free fatty acids (FFAs) on some of the lipid membranes prepared throughout the stepwise investigation of the factors contributing to the cell membrane thermotropic behaviour reported in the previous chapters. The effects of two saturated FFAs (stearic and palmitic acids) and two monounsaturated ones (the *cis*-unsaturated oleic acid and the *trans*-unsaturated elaidic acid) were assessed by adding different percentages to both simple and multi-components vesicles also to highlight the role played by the phospholipid composition in FFAs action.

5.1. Introduction

Low levels of Free Fatty Acids (FFAs) are naturally present in biological membranes (around 0.3-10% of total lipids) (O'Connor et al., 1999) as well as in plasma. Indeed, FFAs have been shown to be involved in several membrane-mediated cellular processes as membrane-bound enzyme activity (Schmalzing and Kutschera, 1982), lipid-assisted protein transport across the bilayer (La Rosa et al., 2016), fusion of lipid vesicles and cells (Creutz, 1981) and/or alteration of the microdomains of cell phospholipid bilayers as well as their physical properties (Ibarguren et al., 2014; Klausner et al., 1980). Moreover, they also act as signalling molecules for several cell mechanisms

(Brash, 2001; Desbois and Smith, 2010; Kenny et al., 2009; Khan et al., 1995; Ruzin and Novick, 2000), for instance insulin secretion (Itoh et al., 2003). Of course, the effect of FFAs on membranes and other cellular processes is dependent on their structural and chemical nature (Davidsen et al., 2002; Funari et al., 2003; Høyrup et al., 2001; Koynova and Tenchov, 2001).

Nevertheless, altered FFAs levels are generally associated to pathological states. For instance, they are recurrent in diabetic and/or obese subjects and plasma FFAs concentration is generally high in both with levels that tend to be increasingly higher with the increase of weight (Björntorp et al., 1969). Specifically for Type 2 Diabetes Mellitus (T2DM), studies regarding the possible involvement of FFAs in the onset and/or progression of the disease are widely reported in the literature, referring both to their possible involvement in altered metabolic pathways (El-Assaad et al., 2003; Maedler et al., 2001) and to the direct action of FFAs on membranes (Milardi et al., 2014). Moreover, the action of FFAs has also been hypothesized to play a role in the interaction of amylin, an amyloidogenic protein, with cell membranes (La Rosa et al., 2016) likely leading to the pancreatic β -cells failure by apoptosis (Westermarck et al., 2011).

Several studies are reported to highlight the FFAs-membrane interaction mainly using spectroscopic, imaging, molecular dynamics and/or theoretical approaches (Kurniawan et al., 2017; Prades et al., 2003; Zavodnik et al., 1997), but, to our knowledge, only few works are devoted to a thermodynamic characterization of the role of the FFAs on the overall membrane stability. Moreover, most of these studies, including the calorimetric approach (Ortiz and Gómez-Fernández, 1987; Schullery et al., 1981), describe model systems whose, for instance, do not resemble the complexity of the composition of real biological vesicles (Rothman and Lenard, 1977).

In this chapter a calorimetric study of the influence of some FFAs on membrane stability is displayed discriminating vesicles' compositional aspects by means of model membranes with progressive complexity aimed to simulate a real membrane, namely the phospholipid bilayer of the Insulin Secretory

Granules (ISGs). Specifically, four FFAs that differ from each other in terms of acyl chain length and presence of *cis*-/*trans*-unsaturations, such as palmitic, stearic, oleic and elaidic acids, were selected. The influence of the addition of different amounts of FFAs to systems with different level of compositional complexity allowed the evaluation of effects deriving from the FFAs' chemical nature and their magnitude on such detailed membranes as the real ones.

5.2. Materials and methods

5.2.1. Materials

1,2-distearoyl-sn-glycero-3-phosphocholine (DSPC), 1,2-dipalmitoyl-sn-glycero-3-phosphocholine (DPPC), 1,2-dimyristoyl-sn-glycero-3-phosphocholine (DMPC), 1,2-dioleoyl-sn-glycero-3-phosphocholine (DOPC), 1,2-distearoyl-sn-glycero-3-phosphoethanolamine (DSPE), 1,2-dipalmitoyl-sn-glycero-3-phosphoethanolamine (DPPE), 1,2-dioleoyl-sn-glycero-3-phosphoethanolamine (DOPE), 1,2-distearoyl-sn-glycero-3-phospho-L-serine (DSPS, sodium salt), 1,2-dipalmitoyl-sn-glycero-3-phospho-L-serine (DPPS, sodium salt), 1,2-dioleoyl-sn-glycero-3-phospho-L-serine (DOPS, sodium salt), 1-palmitoyl-2-hydroxy-sn-glycero-3-phosphocholine (16:0 LPC), 1-behenoyl-2-hydroxy-sn-glycero-3-phosphocholine (22:0 LPC), 1-oleoyl-2-hydroxy-sn-glycero-3-phosphocholine (18:1 LPC), egg sphingomyelin (EggSM, Chicken) and cholesterol powders were purchased from Avanti Polar Lipids (purity certified by the supplier >99%) whereas palmitic acid (PA), stearic acid (SA), oleic acid (OA) and elaidic acid (EA) as well as the other chemicals, were obtained from Sigma-Aldrich. The lipids were of the highest available purity ($\geq 99\%$) and were used without further purification. All solvents were of analytical grade.

5.2.2. Liposomes preparation

Small Unilamellar Vesicles (SUVs) were prepared as described in section 4.2.3 and FFAs were mixed with phospholipids prior to dissolve them in

chloroform:methanol 3:1. Lipid mixtures that did not contain the serine headgroup were dissolved in chloroform.

5.2.3. Spectroscopic characterization

The hydrodynamic diameter of some liposomal formulations was measured by Dynamic Light Scattering (DLS). Amounts of 100 μ L of SUVs preparations were diluted in buffer up to 3mL after the annealing of the dispersions. Measurements were performed at 25°C through a light-scattering instrument (Litesizer™ 500, Anton Paar, Graz, Austria) in side-scatter mode.

5.2.4. Thermal analysis measurements

Detailed information and specifications about the applied calorimetric method (micro-DSC) have been already reported in section 3.2.4 and 4.2.4. Please refer to those sections.

As a brief recall, a Setaram micro-DSCIII (Setaram Instrumentation, Caluire, France) operating with 1mL hermetically closed pans was employed at 0.5°C/min scanning rate. SUVs samples were diluted up to 2.5mM phospholipid concentration and the final phospholipid concentration for all kind of vesicles was checked by the Stewart assay (Stewart, 1980). Raw data were worked out with the dedicated software “THESEUS” (Barone et al, 1992) for obtaining the excess specific heat trace, $C_p^{exc}(T)$, with respect to the low temperature lipids state.

5.3. Results and discussion

5.3.1. Spectroscopic characterization

DLS measurements were performed in order to verify if the addition of FFAs was able to cause discrepancies in vesicles size distributions.

Fig.5.1 reports the range of the size distributions for the several FFAs-containing liposomal suspensions investigated in this chapter. We observed

that the particular formulations do not severely affect the model membranes size distribution.

5.3.2. FFAs on simple model membranes

In order to dissect the effects of different FFAs on the thermodynamic stability of model cell membranes, experiments on relatively simple vesicles were performed. For this reason, the phospholipid tails ternary and quaternary model membranes already described in sections 3.3.2 and 3.3.3 and shown in Fig.3.9 were preliminary considered.

The calorimetric profiles of such systems including different amounts of palmitic, stearic and oleic acids were recorded and are shown in Fig.5.2, Fig.5.3 and Fig.5.4. The relevant thermodynamic parameters are reported in Table 5.1.

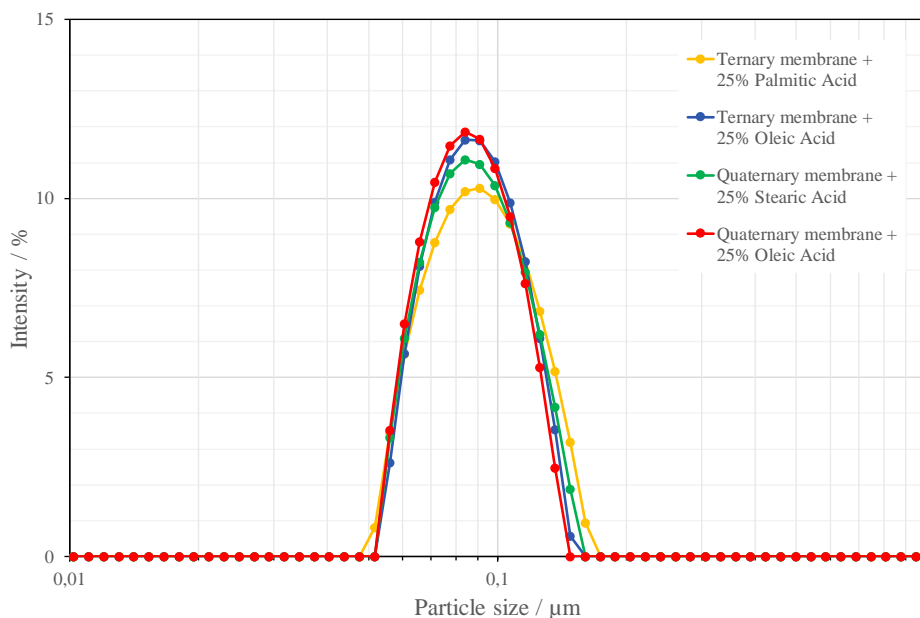


Figure 5.1: DLS data obtained at 25°C for some SUVs prepared as completely saturated tails ternary membrane and unsaturated quaternary membrane (already described in sections 3.3.2 and 3.3.3) containing the 25% of several FFAs as palmitic, stearic and oleic acids.

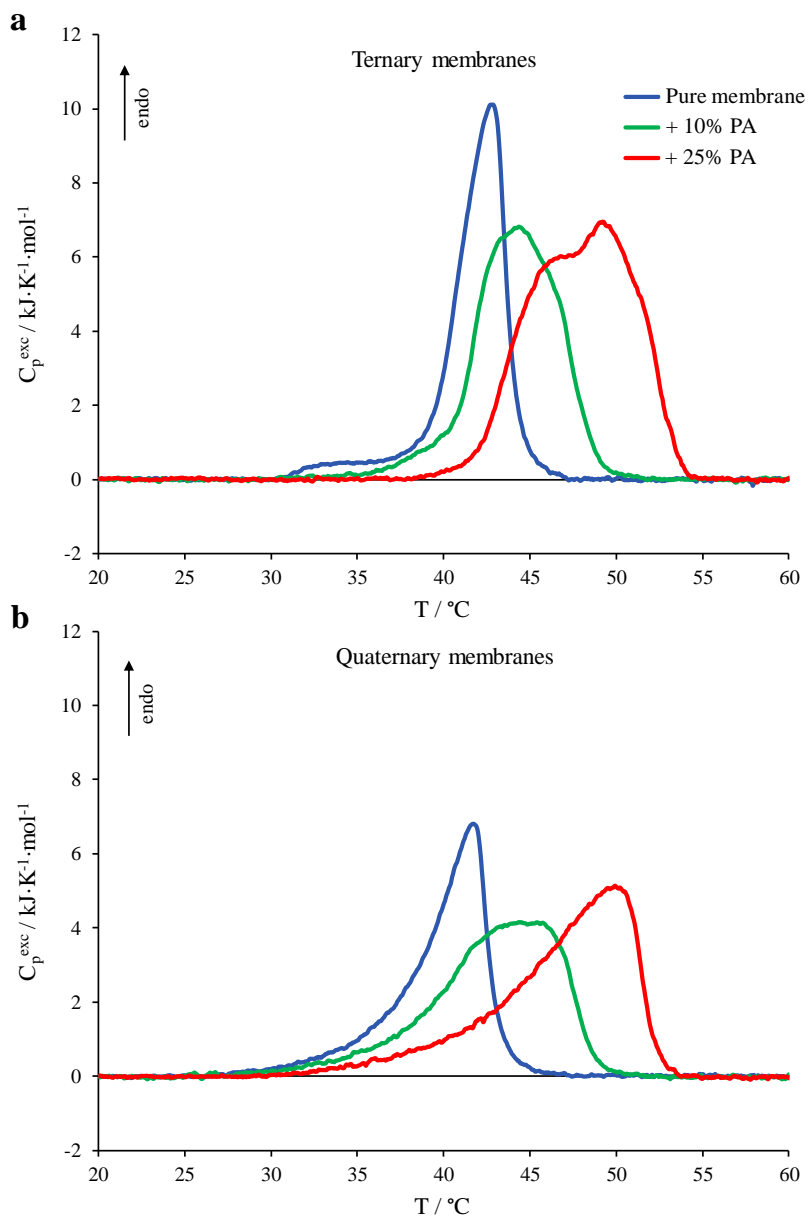


Figure 5.2: Micro-DSC profiles for pure vesicles (blue curves) and vesicles with the addition of the 10% (green curves) and the 25% (red curves) of palmitic acid (PA). Thermograms are reported for both the a) ternary and b) quaternary tails membrane already described in sections 3.3.2 and 3.3.3.

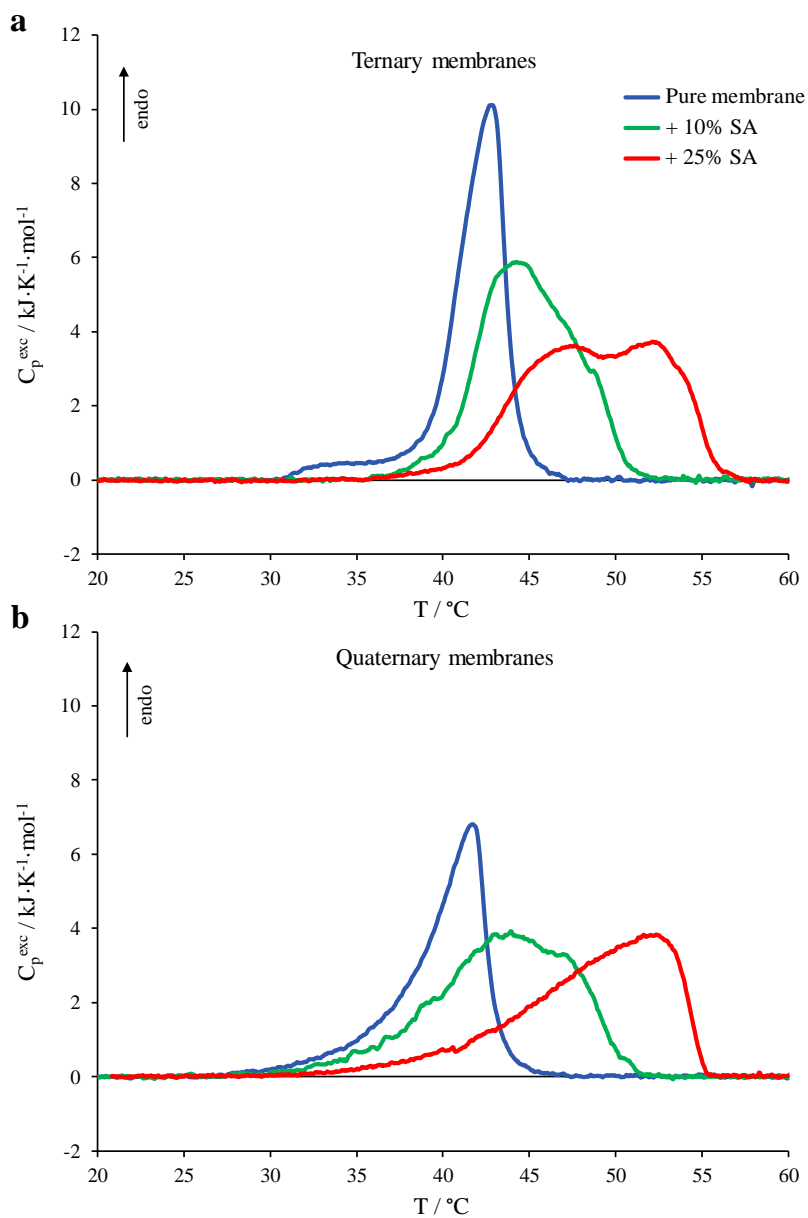


Figure 5.3: Micro-DSC profiles for pure vesicles (blue curves) and vesicles with the addition of the 10% (green curves) and the 25% (red curves) of stearic acid (SA). Thermograms are reported for both the a) ternary and b) quaternary tails membrane already described in sections 3.3.2 and 3.3.3.

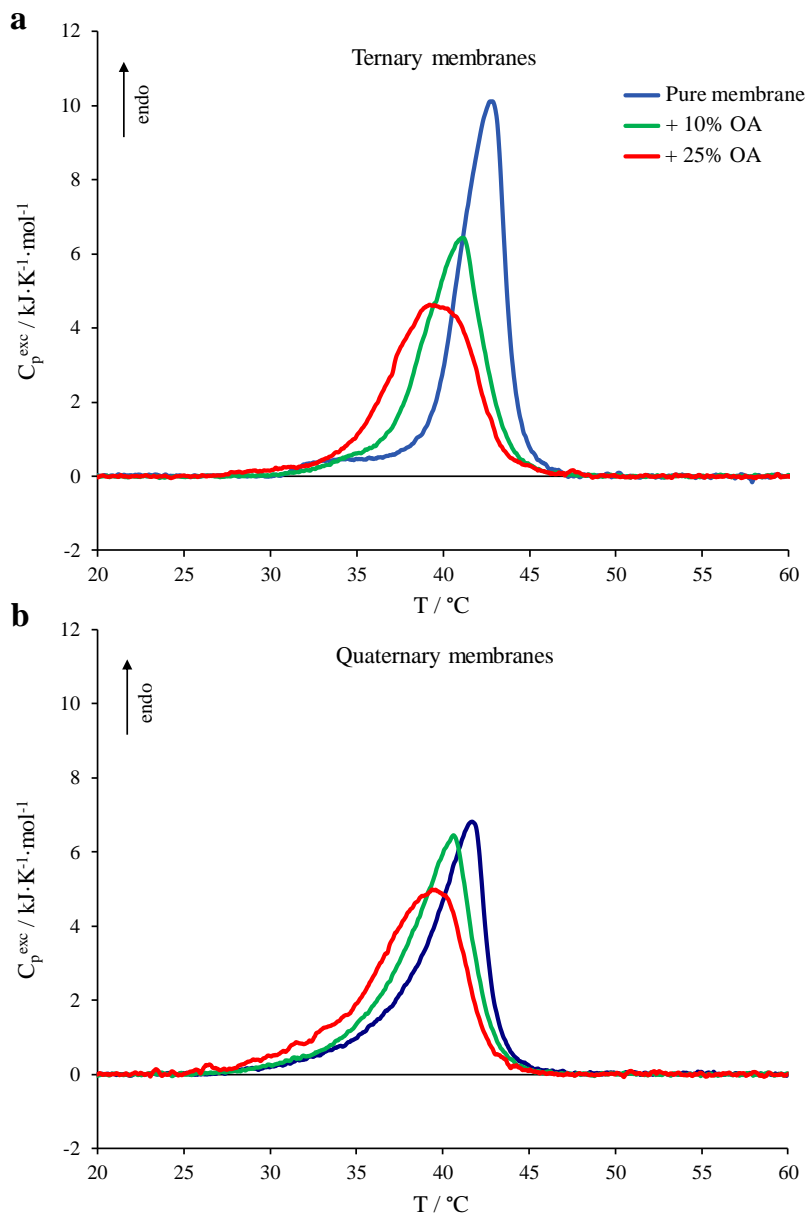


Figure 5.4: Micro-DSC profiles for pure vesicles (blue curves) and vesicles with the addition of the 10% (green curves) and the 25% (red curves) of oleic acid (OA). Thermograms are reported for both the a) ternary and b) quaternary tails membrane already described in sections 3.3.2 and 3.3.3.

Table 5.1: Thermodynamic parameters evaluated from micro-DSC investigations for several systems including different FFAs within the phospholipid bilayer. The last cycle heating curves were used to obtain the main transition enthalpy (ΔH°), the peak maximum temperature (T_{max}), the transition average temperature (\bar{T}) and the Average Cooperativity Index (ACI).

	Calculated	Experimental			
	ΔH° kJ·mol ⁻¹	ΔH° kJ·mol ⁻¹	T_{max} °C	\bar{T} °C	ACI °C
<i>FFAs on simple model membranes</i>					
Pure Ternary					
Membrane	36	37 ± 2	42.8 ± 0.3	41.5 ± 0.3	2.5 ± 0.2
+10% Palmitic Ac.		42 ± 2	44.4 ± 0.3	44.0 ± 0.3	2.7 ± 0.2
+25% Palmitic Ac.		55 ± 2	49.3 ± 0.3	47.9 ± 0.3	2.8 ± 0.2
+10% Stearic Ac.		41 ± 2	44.3 ± 0.3	44.9 ± 0.3	2.7 ± 0.2
+25% Stearic Ac.		41 ± 2	52.2 ± 0.3	48.7 ± 0.3	3.9 ± 0.2
+10% Oleic Ac.		30 ± 2	41.1 ± 0.3	40.1 ± 0.3	2.4 ± 0.2
+25% Oleic Ac.		30 ± 2	39.2 ± 0.3	38.9 ± 0.3	2.9 ± 0.2
Pure Quaternary					
Membrane	32	33 ± 2	41.7 ± 0.3	39.6 ± 0.3	3.0 ± 0.2
+10% Palmitic Ac.		38 ± 2	44.4 ± 0.3	42.6 ± 0.3	3.9 ± 0.2
+25% Palmitic Ac.		41 ± 2	49.9 ± 0.3	46.4 ± 0.3	4.2 ± 0.2
+10% Stearic Ac.		39 ± 2	43.9 ± 0.3	43.1 ± 0.3	4.1 ± 0.2
+25% Stearic Ac.		38 ± 2	52.3 ± 0.3	48.2 ± 0.3	4.6 ± 0.2
+10% Oleic Ac.		33 ± 2	40.6 ± 0.3	38.8 ± 0.3	3.0 ± 0.2
+25% Oleic Ac.		34 ± 2	39.4 ± 0.3	37.7 ± 0.3	3.4 ± 0.2
<i>FFAs on ISG-like membranes</i>					
CHOL-free fourteen-					
comp. membrane		35 ± 2	50.4 ± 0.5	45.5 ± 0.3	6.3 ± 0.2
+20% Stearic Ac.		43 ± 2	54.3 ± 0.3	52.3 ± 0.3	6.2 ± 0.2
ISG-like					
membrane		23 ± 2	44.8 ± 0.3	43.2 ± 0.3	5.7 ± 0.2
+20% Stearic Ac.		34 ± 2	52.1 ± 0.3	48.4 ± 0.3	6.6 ± 0.2
+20% Oleic Ac.		15 ± 2	42.6 ± 0.3	38.0 ± 0.3	5.8 ± 0.2
+20% Elaidic Ac.		29 ± 2	45.7 ± 0.3	43.5 ± 0.3	5.2 ± 0.2

As regards the saturated FFAs, both palmitic and stearic acids exhibited very strong stabilizing effects and evident amplification of phase separations where at least two main domains may be identified. The magnitude of the overall effect depended on the FFA percentage added and seemed to drive to the enrichment of the more stable domain's population. In both cases, these effects seemed more pronounced in the case of the quaternary membrane maybe as a consequence of an enhanced membrane "flexibility".

For both the ternary and quaternary membranes a slight enthalpic increment was observed (Table 5.1) and seemed to reach a saturation level, with the exception of palmitic acid (whose carbon chain is as long as the DPPC tails) in the ternary membrane. Indeed, for such a system the enthalpic contribution followed the amount of added FFAs and gradually became relevant. Taking into consideration the molar composition of the membrane, which is rich in DPPC (70%), we may argue that the interaction between FFAs having the same length of the major constituent's tails with the membrane components is somehow favourite in a relatively ordered system. Conversely, in the case of the more "perturbed" quaternary membrane these effects were attenuated and the enthalpic contribution to the overall stabilization remained modest regardless of the FFAs percentage, again assigning a predominant role to the entropic effects that dictate the thermodynamic stability.

On the other hand, the presence of an unsaturated FFA as oleic acid caused reverse effects, *i.e.* an overall thermodynamic destabilization of both membranes.

The overall picture is represented in Fig.5.5 in terms of shift of the transition average temperature, \bar{T} , of such systems with respect to the pure membranes values. This comparison shows that in first approximation the main effects are common to these membranes. In particular, in the case of saturated FFAs the stabilizing effects depend on the number of carbon units (chain's length) and are more pronounced in less stable membranes, for instance the quaternary one. By contrast, in the case of unsaturated FFAs the destabilizing effects are more pronounced in more stable membranes, such as the ternary one.

In any case, we observed an overall loss of transition cooperativity (Table 5.1) and the effects were dependent of the amount of FFAs included, *i.e.* no saturation of such mainly entropic effects were observed in the concentration range investigated. However, regardless of the added FFA, the cooperativity of the quaternary membrane's thermodynamic profiles is lower than the ternary membrane's ones because of the higher level of disorder of the lipid packing.

5.3.3. FFAs on ISG-like membranes

Although the percentage of cholesterol within cell membranes may reach the 40-50% (Tsuchiya et al., 2010; Yeagle, 1985), the study of the action of external agents as FFAs was carried out by selecting a fifteen-components membrane containing only 10% cholesterol as reference final membrane in

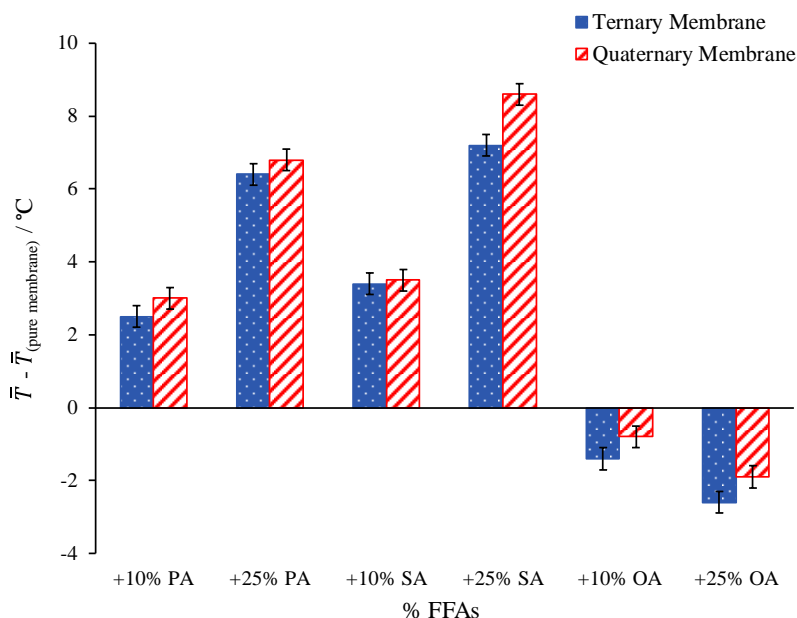


Figure 5.5: Histogram representation showing the effects of 10% and 25% of palmitic acid (PA), stearic acid (SA) and oleic acid (OA) on ternary (blue full bars) and quaternary (red lined bars) model membranes in terms of transition average temperature \bar{T} .

order to keep the micro-DSC signals well detectable. Indeed, reaching too elevated amounts of cholesterol would have affected the thermograms because of the low signal-to-noise ratio. In any case, Table 4.1 showed that the higher the cholesterol amount, the lower the differences on the thermotropic behaviour of the vesicles. Therefore, we will refer to the fourteen-components vesicles containing 10% of cholesterol as reference *ISG-like membrane*.

The effect of 20% addition stearic and oleic acids on cell membrane thermodynamics is reported in Fig.5.6a and the relevant thermodynamic parameters are reported in Table 5.1. At a first glance, Fig.5.6a shows stabilizing effects for the saturated FFA (stearic acid, green curve) and destabilizing effects for the unsaturated FFA (oleic acid, blue curve), revealing a similar scenario obtained in the previous section for less complex membranes. Such respective stabilization and destabilization were also observed in terms of enthalpic contribution (Table 5.1). Since these observations are in line with those described in the previous discussion, we may conclude that the way in which the FFAs influence the vesicles thermotropic behaviour is almost of the same nature regardless of the membrane lipid composition. Main composition-dependent differences may only be revealed in terms of magnitude of stabilization or destabilization of the membrane thermodynamics.

To complete the pattern depicted so far, the study the influence of a *trans*-unsaturated FFA as the elaidic acid on the ISG-like membrane was included and the resulting micro-DSC profile is reported as red trace in Fig.5.6b. A different effect of elaidic acid with respect to the corresponded *cis*-unsaturated FFA (oleic acid) was observed, *i.e.* a mainly enthalpic stabilization effect. This behaviour is in line with the conclusions for which, if we consider that the presence of a *trans* double bond makes such FFA linear, we expect it to be packable within the vesicle hydrophobic core analogously to stearic acid.

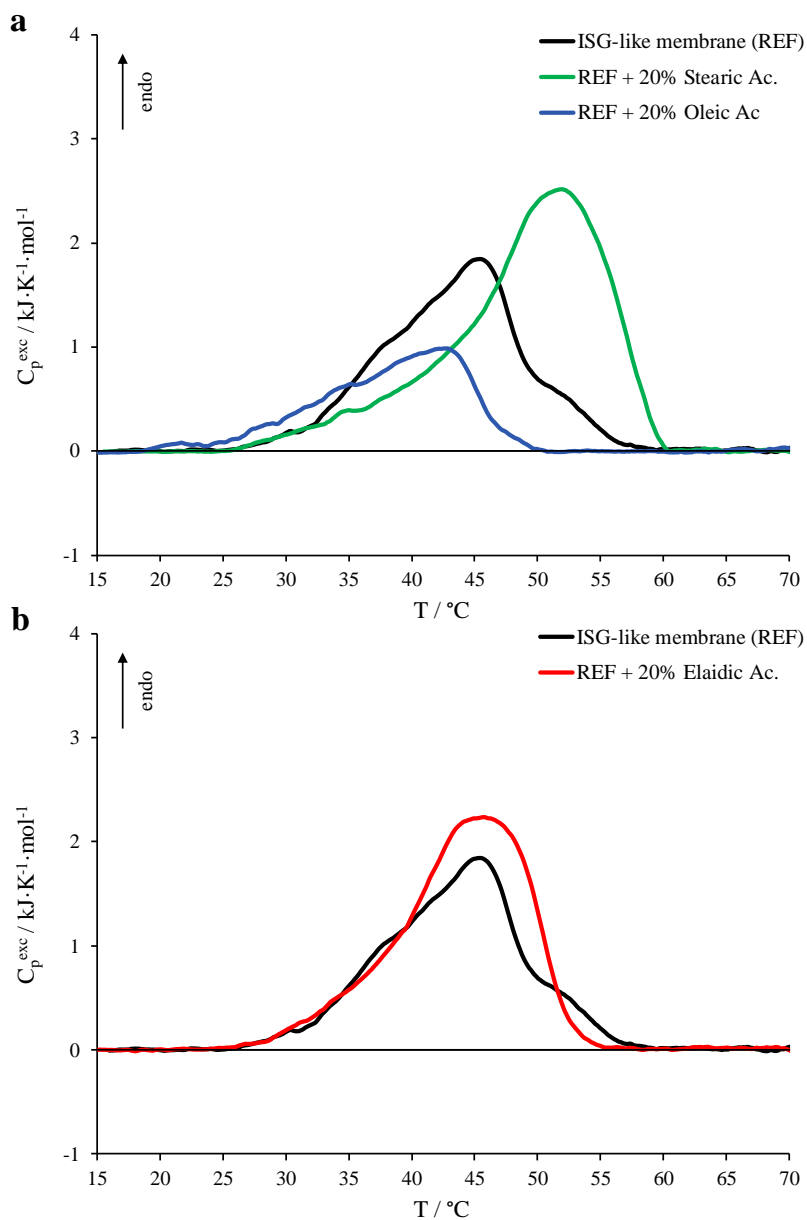


Figure 5.6: Micro-DSC profiles for the ISG-like vesicles (black curve) and vesicles with the addition of 20% FFAs. Thermograms are reported for membranes including stearic acid (green curve) and oleic acid (blue curve) in panel a, whereas elaidic acid (red curve) is shown in panel b.

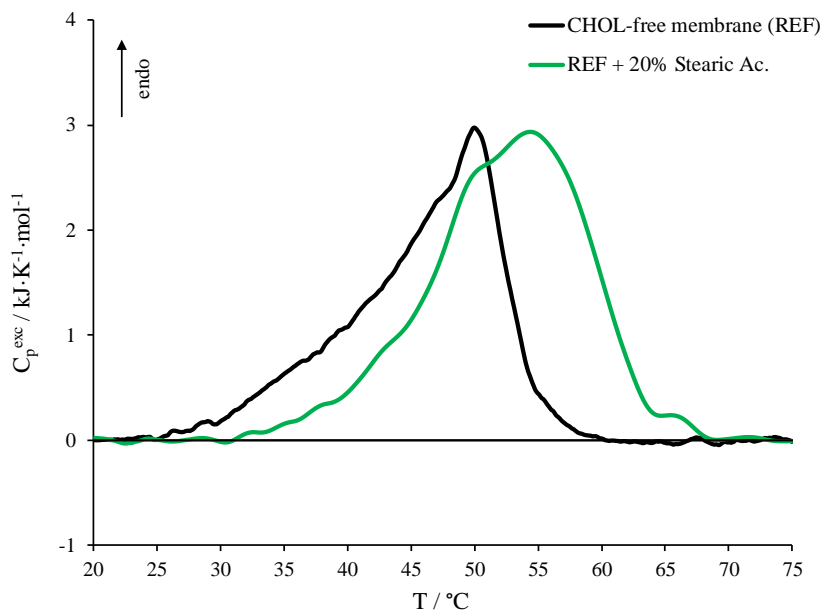


Figure 5.7: Micro-DSC thermograms for the cholesterol-free fourteen-components membrane (black curve) and vesicles with the addition of 20% of stearic acid (green curve).

However, despite the common stabilization, the effect was minor as regard both the enthalpic and the entropic contributions, suggesting peculiarities in the incorporation of elaidic acid such as the fact that it does not strongly affect the lipid packing of the bilayer, which is responsible for the specific profile of the gel-to-liquid crystalline phase transition.

On the other hand, as suggested by the literature (Kishi et al., 2018), we may infer that most of elaidic acid molecules were included in cholesterol-rich domains and only a small amount of FFA contributed to the overall phospholipidic transition ΔH° . The hypothesised selectivity of elaidic acid for cholesterol may be explained by considering the possibility of the establishment of CH- π interactions between the trans double bond and the -CH groups of the rigid tetracyclic ring structure (Fantini and Barrantes, 2013;

Nishio et al., 1995) facilitated by the acid's linear structure differently from oleic acid which is less prone to be packed and/or segregated.

Further interpretations about the influence of FFAs on membrane stability were obtained through experiments on the cholesterol-free fourteen-components vesicles including 20% of stearic acid. Fig.5.7 reports the micro-DSC thermograms for the cholesterol-free fourteen-components membrane alone and in presence of 20% of FFA and the respective thermodynamic parameters are reported in Table 5.1. We observed that the addition of stearic acid to the fourteen-components membrane led to the expected effects on the basis of the forenamed results, *i.e.* it produced an overall thermodynamic stabilization of the bilayer both in terms of enthalpic and entropic contributions. If we compare the enthalpic increment deriving from the addition of stearic acid to both the cholesterol-free and the cholesterol-containing vesicles (the REF curves in Fig.5.7 and Fig.5.6a, respectively), the cholesterol-free membrane experienced a ΔH^p increase of +22.9% (+8 kJ/mol), whereas a ΔH^p increase of +47.8% (+11 kJ/mol) was detected for the cholesterol-containing ISG-like membrane. In other words, stearic acid had a stronger effect on the cholesterol-containing membrane. Since the enthalpic increment corresponds to the establishment of extra chain-chain interaction, we may infer that stearic acid is able to reorganize the lipid phase so much to steal phospholipids from the cholesterol-rich phases, since such the transition of such phospholipid was abolished by the presence of cholesterol.

As for the entropic effects, the effects of lipid reorganization were bigger in terms of range transition with the addition of stearic acid to the cholesterol-free membrane as evidenced by the \bar{T} reported in Table 5.1, whereas ACI values show that stearic acid affected the breadth of the ISG-like membrane much more than the cholesterol-free membrane.

5.4. References

- Barone, G., Del Vecchio, P., Fessas, D., Giancola, C., Graziano, G., 1992. THESEUS: A new software package for the handling and analysis of thermal denaturation data of biological macromolecules. *J. Therm. Anal.* 38, 2779–2790.
- Brash, A.R., 2001. Arachidonic acid as a bioactive molecule. *J. Clin. Invest.* 107, 1339–1345.
- Creutz, C.E., 1981. cis-Unsaturated fatty acids induce the fusion of chromaffin granules aggregated by synexin. *J. Cell Biol.* 91, 247–256.
- Davidsen, J., Mouritsen, O.G., Jørgensen, K., 2002. Synergistic permeability enhancing effect of lysophospholipids and fatty acids on lipid membranes. *Biochim. Biophys. Acta - Biomembr.* 1564, 256–262.
- Desbois, A.P., Smith, V.J., 2010. Antibacterial free fatty acids: activities, mechanisms of action and biotechnological potential. *Appl. Microbiol. Biotechnol.* 85, 1629–1642.
- El-Assaad, W., Buteau, J., Peyot, M.-L., Nolan, C., Roudit, R., Hardy, S., Joly, E., Dbaibo, G., Rosenberg, L., Prentki, M., 2003. Saturated Fatty Acids Synergize with Elevated Glucose to Cause Pancreatic β -Cell Death. *Endocrinology* 144, 4154–4163.
- Fantini, J., Barrantes, F.J., 2013. How cholesterol interacts with membrane proteins: an exploration of cholesterol-binding sites including CRAC, CARC, and tilted domains. *Front. Physiol.* 4, 1–9.
- Funari, S.S., Barceló, F., Escribá, P. V., 2003. Effects of oleic acid and its congeners, elaidic and stearic acids, on the structural properties of phosphatidylethanolamine membranes. *J. Lipid Res.* 44, 567–575.

- Høyrup, P., Davidsen, J., Jørgensen, K., 2001. Lipid Membrane Partitioning of Lysolipids and Fatty Acids: Effects of Membrane Phase Structure and Detergent Chain Length. *J. Phys. Chem. B* 105, 2649–2657.
- Ibarguren, M., López, D.J., Escribá, P. V., 2014. The effect of natural and synthetic fatty acids on membrane structure, microdomain organization, cellular functions and human health. *Biochim. Biophys. Acta - Biomembr.* 1838, 1518–1528.
- Itoh, Y., Kawamata, Y., Harada, M., Kobayashi, M., Fujii, R., Fukusumi, S., Ogi, K., Hosoya, M., Tanaka, Y., Uejima, H., Tanaka, H., Maruyama, M., Satoh, R., Okubo, S., Kizawa, H., Komatsu, H., Matsumura, F., Noguchi, Y., Shinohara, T., Hinuma, S., Fujisawa, Y., Fujino, M., 2003. Free fatty acids regulate insulin secretion from pancreatic β cells through GPR40. *Nature* 422, 173–176.
- Kenny, J.G., Ward, D., Josefsson, E., Jonsson, I.-M., Hinds, J., Rees, H.H., Lindsay, J.A., Tarkowski, A., Horsburgh, M.J., 2009. The *Staphylococcus aureus* Response to Unsaturated Long Chain Free Fatty Acids: Survival Mechanisms and Virulence Implications. *PLoS One* 4, e4344.
- Khan, W.A., Blobe, G.C., Hannun, Y.A., 1995. Arachidonic acid and free fatty acids as second messengers and the role of protein kinase C. *Cell. Signal.* 7, 171–184.
- Kishi, S., Fujiwara-Tani, R., Luo, Y., Kawahara, I., Goto, K., Fujii, K., Ohmori, H., Nakashima, C., Sasaki, T., Kuniyasu, H., 2018. Pro-metastatic signaling of the trans fatty acid elaidic acid is associated with lipid rafts. *Oncol. Lett.* 15, 4423–4426.
- Klausner, R.D., Kleinfeld, A.M., Hoover, R.L., Karnovsky, M.J., 1980. Lipid domains in membranes. Evidence derived from structural perturbations induced by free fatty acids and lifetime heterogeneity analysis. *J. Biol. Chem.* 255, 1286–1295.

- Koynova, R., Tenchov, B., 2001. Interactions of surfactants and fatty acids with lipids. *Curr. Opin. Colloid Interface Sci.* 6, 277–286.
- Kurniawan, J., Suga, K., Kuhl, T.L., 2017. Interaction forces and membrane charge tunability: Oleic acid containing membranes in different pH conditions. *Biochim. Biophys. Acta - Biomembr.* 1859, 211–217.
- La Rosa, C., Scalisi, S., Lolicato, F., Pannuzzo, M., Raudino, A., 2016. Lipid-assisted protein transport: A diffusion-reaction model supported by kinetic experiments and molecular dynamics simulations. *J. Chem. Phys.* 144, 184901.
- Maedler, K., Spinas, G.A., Dyntar, D., Moritz, W., Kaiser, N., Donath, M.Y., 2001. Distinct Effects of Saturated and Monounsaturated Fatty Acids on β -Cell Turnover and Function. *Diabetes* 50, 69–76.
- Milardi, D., Sciacca, M.F.M., Randazzo, L., Raudino, A., La Rosa, C., 2014. The Role of Calcium, Lipid Membranes and Islet Amyloid Polypeptide in the Onset of Type 2 Diabetes: Innocent Bystanders or Partners in a Crime? *Front. Endocrinol. (Lausanne)*. 5, 1–4.
- Nishio, M., Umezawa, Y., Hirota, M., Takeuchi, Y., 1995. The CH/ π interaction: significance in molecular recognition. *Tetrahedron* 51, 8665–8701.
- O'Connor, L.J., Nicholas, T., Levin, R.M., 1999. Subcellular Distribution of Free Fatty Acids, Phospholipids, and Endogenous Lipase Activity of Rabbit Urinary Bladder Smooth Muscle and Mucosa. In: *Advances in Bladder Research*. Springer, Boston, MA, pp. 265–273.
- Ortiz, A., Gómez-Fernández, J.C., 1987. A differential scanning calorimetry study of the interaction of free fatty acids with phospholipid membranes. *Chem. Phys. Lipids* 45, 75–91.

- Prades, J., Funari, S.S., Escribá, P. V., Barceló, F., 2003. Effects of unsaturated fatty acids and triacylglycerols on phosphatidylethanolamine membrane structure. *J. Lipid Res.* 44, 1720–1727.
- Rothman, J.E., Lenard, J., 1977. Membrane Asymmetry. *Science* (80-). 195, 743–753.
- Ruzin, A., Novick, R.P., 2000. Equivalence of Lauric Acid and Glycerol Monolaurate as Inhibitors of Signal Transduction in *Staphylococcus aureus*. *J. Bacteriol.* 182, 2668–2671.
- Schmalzing, G., Kutschera, P., 1982. Modulation of ATPase activities of human erythrocyte membranes by free fatty acids or phospholipase A2. *J. Membr. Biol.* 69, 65–76.
- Schullery, S.E., Seder, T.A., Weinstein, D.A., Bryant, D.A., 1981. Differential thermal analysis of dipalmitoylphosphatidylcholine-fatty acid mixtures. *Biochemistry* 20, 6818–6824.
- Stewart, J.C.M., 1980. Colorimetric determination of phospholipids with ammonium ferrothiocyanate. *Anal. Biochem.* 104, 10–14.
- Tsuchiya, M., Hosaka, M., Moriguchi, T., Zhang, S., Suda, M., Yokota-Hashimoto, H., Shinozuka, K., Takeuchi, T., 2010. Cholesterol Biosynthesis Pathway Intermediates and Inhibitors Regulate Glucose-Stimulated Insulin Secretion and Secretory Granule Formation in Pancreatic β -Cells. *Endocrinology* 151, 4705–4716.
- Westermarck, P., Andersson, A., Westermarck, G.T., 2011. Islet Amyloid Polypeptide, Islet Amyloid, and Diabetes Mellitus. *Physiol. Rev.* 91, 795–826.
- Yeagle, P.L., 1985. Cholesterol and the cell membrane. *Biochim. Biophys. Acta - Rev. Biomembr.* 822, 267–287.

Zavodnik, I., Zaborowski, A., Niekurzak, A., Bryszewska, M., 1997. Effect of free fatty acids on erythrocyte morphology and membrane fluidity. *IUBMB Life* 42, 123–133.

Peptide-membrane interaction

The previous chapters showed the stepwise characterization of highly complex ISG-like membranes together with the investigation of the influence of several free fatty acids (FFAs) on such vesicles. A noteworthy result is that the general conclusions presented about the membrane thermodynamics are general and may be applied to many other biological systems. Such evidence might allow one to design simpler *ad hoc* vesicles that retrace the desired lipid bilayers' thermodynamics in order to better focus on specific interactions of external agents with model membranes.

The design of a simpler *ad hoc* model membrane and its interaction with nisin, a pore-forming peptide, will be object of this chapter, also highlighting the FFAs influence on peptide-membrane interaction.

6.1. Introduction

Antimicrobial peptides (AMPs) represent efficient tools against pathogenic bacteria. Their action is mainly based on the deformation of cell membranes through several mechanisms as a detergent-like solubilisation process upon the parallel aggregation of peptide molecules to the membrane plane (Shai, 1999), as well as the formation of toroidal pores or barrel-stave upon perpendicular oligomeric assembly of the peptide (Boheim, 1974; Leontiadou et al., 2006; Melo et al., 2009).

Nisin, a cationic peptide with 34 amino acid residues, is an important AMP and belongs to class I pore-forming bacteriocins. Its antimicrobial action mainly consists in the interruption of bacteria's cell-wall biosynthesis through the specific interaction with lipid II, a membrane-anchored cell-wall precursor essential for bacterial cell-wall biosynthesis, and in the generation of pores in cell membranes (Breukink et al., 1999; Hasper et al., 2006; van Heusden et al., 2002). However, the direct interaction between nisin and phospholipids is equally able to deform the bacterial cell membranes through a lipid II-independent mechanism when at high peptide concentration regime (Prince et al., 2016).

The significant consideration attracted by nisin during the last years is due to its application as food preservative and as antibiotic in health care (Pandit et al., 2017; Severina et al., 1998). Several technologies have also been optimized in order to enhance the efficacy of the peptide, leading for instance to new formulations consisting in liposome-encapsulated nisin or bioconjugation with nanoparticles (da Silva Malheiros et al., 2010; Laridi et al., 2003; Pandit et al., 2017; Were et al., 2004).

The large use of nisin in food technologies and in biomedical field, the pore-forming activity of this peptide and the relative simplicity of the structures involved in the action against cell membranes make nisin a good candidate as model peptide the study of the interaction between proteins and the cell membranes' lipid component (Taylor et al., 2005).

In this frame, this chapter reports a calorimetric and spectroscopic study of the pore-forming peptide nisin-membrane interaction in FFAs-free and FFAs-containing model membranes. Considering the thermodynamic information reached in the previous chapters, a simplified model membrane that resembled the micro-DSC profile of the ISG-like membrane (see chapter 4) was designed and prepared by combining specific percentages of DMPC, DPPS and DOPC, hence obtaining a simpler system even maintaining a realistic calorimetric profile in terms of cooperativity and enthalpy of the gel-to-liquid crystalline phase transition. Nisin-membrane interaction was

investigated on the simplified membrane through micro-DSC, fluorescence spectroscopy and DLS at physiological pH (pH 7.4), also evaluating the effects of six different FFAs on membrane stability, namely two saturated FFAs (palmitic acid and stearic acid), two monounsaturated FFAs (the *cis*-unsaturated oleic acid and the *trans*-unsaturated elaidic acid) and two polyunsaturated FFAs (the ω -6 linoleic acid and the ω -3 docosahexaenoic acid or DHA) in order to highlight the weight of the presence of various FFAs on protein-cell membrane interaction.

6.2. Materials and methods

6.2.1. Materials

1,2-dimyristoyl-sn-glycero-3-phosphocholine (DMPC), 1,2-dioleoyl-sn-glycero-3-phosphocholine (DOPC) and 1,2-dipalmitoyl-sn-glycero-3-phospho-L-serine (DPPS, sodium salt) powders were purchased from Avanti Polar Lipids (purity certified by the supplier >99%) whereas palmitic acid (PA), stearic acid (SA), oleic acid (OA), elaidic acid (EA), linoleic acid (LA) and docosahexaenoic acid (DHA), as well as Nisin from *Lactococcus lactis* (lyophilized powder containing ~2.5% w/w nisin), SP Sepharose Fast Flow and the other chemicals were obtained from Sigma-Aldrich. The lipids were of the highest available purity ($\geq 99\%$) and were used without further purification. All solvents were of analytical grade.

6.2.2. Liposomes preparation

Small Unilamellar Vesicles (SUVs) were prepared as described in section 4.2.3 and FFAs were mixed with phospholipids prior to dissolve them in chloroform:methanol 3:1.

The final phospholipid concentration was checked by the Stewart assay (Stewart, 1980).

6.2.3. Nisin purification and stock solutions preparation

Commercial nisin (lyophilized powder containing ~2.5% w/w nisin) was purified according to a procedure already reported in the literature (Abts et al., 2011). Nisin was dissolved 1.3g/100mL in 50mM lactic acid pH 3. The nisin solution was filtered through 0.45 μ m pores and applied to a 5mL SP Sepharose fast flow cation exchange column (GE Healthcare). After a washing step with 50mL 600mM NaCl, purified Nisin was eluted from the column using 50mL 800mM NaCl. To remove NaCl, protein in the elution fractions was precipitated with 20% (v/v) trichloroacetic acid (TCA) overnight at 4°C. Precipitated protein was washed two times with ice-cold acetone to remove residual TCA and then lyophilized. The purity level was assessed to be >99% by HPLC.

Nisin stock solutions were daily prepared by dissolving the appropriate protein amounts in 10mM phosphate buffer (pH 7.4). In order to help the protein solubilization, nisin solutions were subjected to a mild sonication until clear samples were obtained.

6.2.4. Thermal analysis measurements

Detailed information and specifications about the applied calorimetric method (micro-DSC) have been already reported in section 3.2.4. Please refer to that section.

As a brief recall, a Setaram micro-DSCIII (Setaram Instrumentation, Caluire, France) operating with 1mL hermetically closed pans was employed at 0.5°C/min scanning rate. The adequate amounts of SUVs dispersions and nisin stock solution were mixed and diluted in 10mM phosphate buffer (pH 7.4) just before launching the measurement achieving 2.5mM and 30 μ M concentrations for phospholipids and nisin, respectively. The final phospholipid concentration was checked by the Stewart assay (Stewart, 1980). Raw data were worked out with the dedicated software "THESEUS" (Barone et al, 1992) for obtaining the excess specific heat trace, $C_p^{exc}(T)$, with

respect to the low temperature lipids state. Four heating-cooling cycles were applied to each sample. All transitions were reversible and the last cycle heating curves were considered to evaluate the parameters of the thermotropic transitions observed.

6.2.5. Spectroscopic characterization

6.2.5.1. Fluorescence spectroscopy

Fluorescence anisotropy measurements were performed with a PerkinElmer LS-55 spectrofluorometer (PerkinElmer, Waltham, MA, USA). To monitor the fluidity of phospholipid bilayers, the apolar diphenylhexatriene (DPH) was used as fluorescent probe and was incorporated within the hydrophobic region of the vesicle bilayer (Lentz et al., 1976). The excitation and emission wavelengths were 348 nm and 426 nm, respectively (Shinitzky and Barenholz, 1974, 1978; Tanfani et al., 1989). The slit width of the excitation monochromator was 4nm, whereas the slit width of the emission monochromator was 2.5nm. Increasing volumes of nisin solution were added to the liposomal suspensions giving rise to a final volume of 800 μ L per sample with 500 μ M phospholipid concentration and 0, 10, 20, 30, 40, 60 μ M of nisin. Fluorescent probes were singly added up to 1 μ M (500:1 phospholipid/fluorescent probe molar ratio). Treated samples were well mixed and incubated in dark under continuous stirring for two hours at 37°C before measurement. The temperature of the cuvette holder was controlled (Thermo Fisher Scientific, Haake SC 100, Waltham, MA, USA) and the experiments in isothermal conditions were carried out at 37°C in order to reflect the physiological temperature, whereas the experiments in temperature scan were performed within the range from 10°C to 64°C with temperature steps of 3°C, allowing the samples to equilibrate prior the reading of fluorescence anisotropy values. The polarization values, r , were calculated by the fluorescence data manager programme using Jablonski's equation:

$$r = \frac{(I_{VV} - GI_{VH})}{(I_{VV} + 2GI_{VH})}$$

where I_{VV} and I_{VH} are the vertical and horizontal fluorescence intensities, respectively, to the vertical polarization of the excitation light beam. The factor $G = I_{HV}/I_{HH}$ (grating correction factor) corrects the polarizing effects of the monochromator.

6.2.5.2. Dynamic light scattering

The hydrodynamic diameter of some liposomal formulations was measured at 25°C through a light-scattering instrument (Zetasizer Nano-ZS, Malvern Panalytical Ltd, Malvern, UK) in back-scatter mode. Vesicle dispersions were obtained with the same protocol used for fluorescence measurement and the final concentration was 500µM.

6.3. Results and discussion

6.3.1. Model membrane design

In order to make investigations on the interaction of model cell membranes with other external agents easier, a simplified model membrane that retrace the ISG lipid bilayers' thermodynamics was designed on the basis of the hierarchy of contributions to cell membrane thermodynamic stability (chapter 3) and of the calorimetric profile obtained for the ISG-like membrane (sections 4.3.1 and 4.3.2). Since the ISG-like vesicles (*i.e.* the fourteen-components system with the addition of 10% of cholesterol) displayed a gel-to-liquid crystalline phase transition ranging from about 25°C to 60°C, we selected DMPC ($T_{max} = 24.0 \pm 0.2^\circ\text{C}$, from section 3.3.1) and DPPS ($T_{max} \approx 55^\circ\text{C}$) (Bach and Wachtel, 1989; Galvagnion et al., 2016) as main phospholipids for the simplified vesicle modelling in order to also consider the presence of at least two different tail lengths as well as two different headgroups.

The micro-DSC thermograms for vesicles prepared at 3:2 molar ratio of DMPC:DPPS is reported in Fig.6.1 as a black trace. We observed a mainly

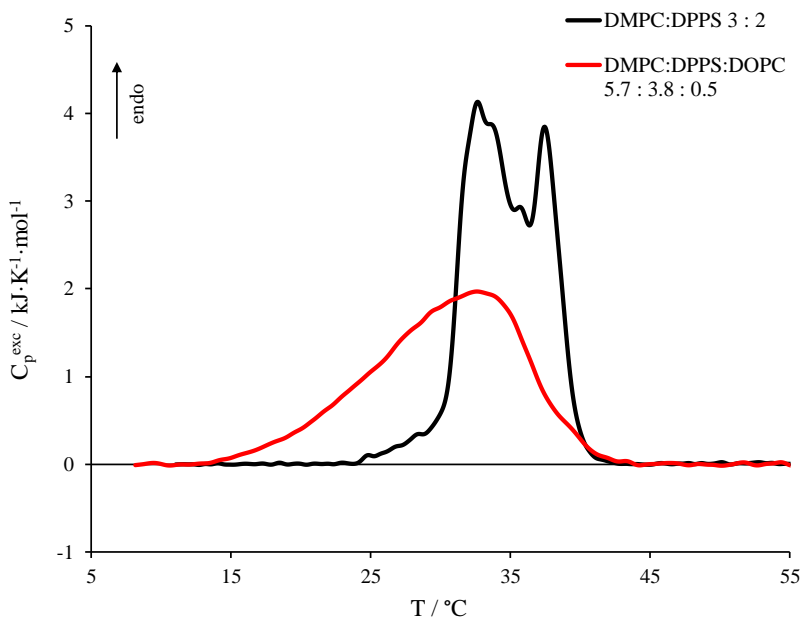


Figure 6.1: Micro-DSC profiles for DMPC:DPPS 3:2 vesicles (black curve) and vesicles obtained by the addition of 5% of DOPC to the DMPC:DPPS 3:2 system achieving a 5.7 DMPC : 3.8 DPPS : 0.5 DOPC molar ratio (red curve).

biphasic profile reflecting a high heterogeneousness of the lipid phases due to the low miscibility of the constituents. However, as expected from the composition-dependent proportionality of the entropic contribution to the transition, the profile is located within the transition T_{max} of the respective single-component dispersions and the transition average temperature, \bar{T} , is comparable to the expected value calculated by considering the used phospholipid molar ratio ($34.5 \pm 0.1^\circ\text{C}$ and 36.4°C , respectively), as reported in Table 6.1. Furthermore, the average cooperativity index, ACI; for this system ($2.8 \pm 0.1^\circ\text{C}$) was in accordance with the correlation of ACI values against the gap between the T_{max} values of the respective single-component systems, $\Delta_{s-c}T_{max}$, highlighted in Fig. 3.6 for both the 1:1 tails and headgroups binary systems (chapter 3). Indeed, the obtained ACI value for the 3:2 DMPC:DPPS mixture, *i.e.*, a system with a $\Delta_{s-c}T_{max}$ of $\sim 31^\circ\text{C}$ and whose

Table 6.1: Thermodynamic parameters evaluated from micro-DSC thermograms obtained from the modelling of a simplified model membrane. The parameters were compared with the arithmetical values calculated from single-component systems. The last cycle heating curves were used to obtain the main transition enthalpy (ΔH°), the peak maximum temperature (T_{max}), the transition average temperature (\bar{T}) and the Average Cooperativity Index (ACI).

	Expected		Experimental			
	ΔH°	$T_{expected}$	ΔH°	T_{max}	\bar{T}	ACI
	$\text{kJ}\cdot\text{mol}^{-1}$	$^\circ\text{C}$	$\text{kJ}\cdot\text{mol}^{-1}$	$^\circ\text{C}$	$^\circ\text{C}$	$^\circ\text{C}$
DMPC:DPPS 3:2	30	36.4	30 ± 2	32.6 ± 0.1	34.5 ± 0.1	2.8 ± 0.1
DMPC:DPPS:						
DOPC 5.7:3.8:0.5	29	-	26 ± 2	32.6 ± 0.6	30.1 ± 0.1	5.3 ± 0.1

phospholipids differ both in tails and headgroups, was lower than the expected ones from the respective 1:1 binary mixtures, since those lipid proportions reflect an extreme mixing condition.

As for the enthalpic contribution to the transition (Table 6.1), the overall enthalpy observed resulted to be still additive compared to those of the single-components. Hence, the absence of relevant extra enthalpic contribution once again confirmed that the thermotropic behaviour of these vesicles is mainly entropically driven.

In order to enhance the homogeneousness of the lipid phase as well as of the DSC profile and to include unsaturated phospholipid tails, the 5% of DOPC was added to the 3:2 DMPC:DPPS systems achieving a 5.7 DMPC : 3.8 DPPS : 0.5 DOPC molar ratio. The respective micro-DSC profile is shown in Fig.6.1 as a red trace and the relevant thermodynamic parameters are reported in Table 6.1. We observed an asymmetric and a much broader thermogram as revealed by the marked increase of the ACI value up to $5.3 \pm 0.1^\circ\text{C}$, showing a more homogeneous phases distribution as a consequence of the addition of unsaturations. Moreover, the \bar{T} was considerably shifted towards lower temperatures ($30.1 \pm 0.1^\circ\text{C}$), as well as the overall transition enthalpy decreased.

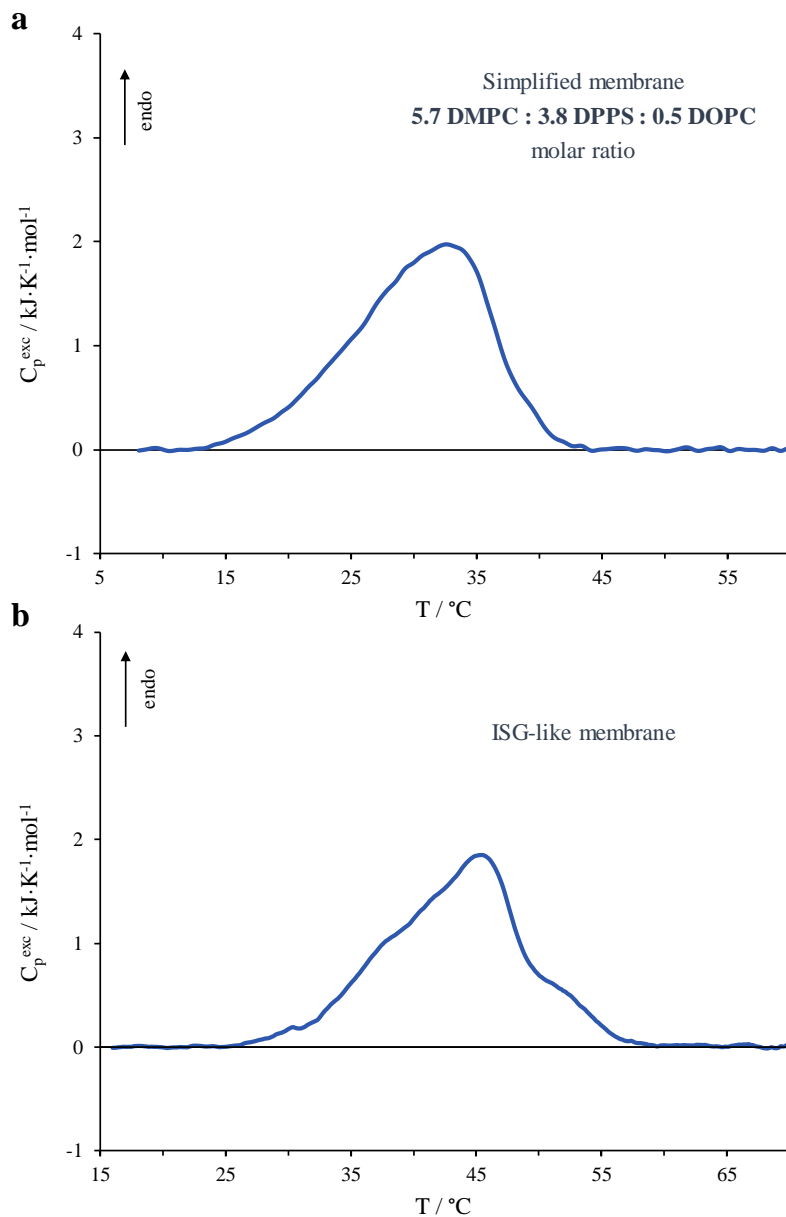


Figure 6.2: a) Micro-DSC thermograms for the new simplified membrane as 5.7 DMPC : 3.8 DPPS : 0.5 DOPC molar ratio. b) Micro-DSC thermogram for the ISG-like membrane described in section 4.3.2, i.e. the fourteen-components system with the addition of 10% of cholesterol.

To sum up, the choice of considering DMPC and DPPS as 3:2 molar ratio for modelling the new membrane allowed to design a membrane with a reasonable ratio between neutral and negatively charged phospholipids (MacDonald et al., 2015; Rothman and Lenard, 1977) and with a such tail length difference to produce a significant peak breadth after the addition of only 5% of DOPC. Moreover, the micro-DSC profile obtained for the new membrane is highly comparable to the one exhibited by the ISG-like membrane (*i.e.* the fourteen-components system with the addition of 10% of cholesterol in section 4.3.2) (Fig.6.2), hence maintaining a realistic calorimetric profile in terms of cooperativity and enthalpy of the gel-to-liquid crystalline phase transition. The only exception regards the temperature range covered which was at higher temperatures for the ISG-like membrane because of the presence of harder phospholipids than DPPS and DMPC. In any case, the low temperature range covered by the new vesicles allowed us to consider a more flexible lipid bilayer resembling more the behaviour of real cell membranes at physiological temperature (de Kruffy et al., 1972). We will refer to such a new model membrane as “simplified membrane” in the next sections.

6.3.2. *Differential scanning calorimetry and fluorescence spectroscopy*

The micro-DSC thermograms obtained for the simplified membrane (5.7 DMPC : 3.8 DPPS : 0.5 DOPC) alone and in presence of 30 μ M of nisin are shown in Fig.6.3, whereas the relevant thermodynamic parameter are reported in Table 6.2. The choice of 30 μ M of nisin concentration represented an optimization of micro-DSC experiments and was a compromise between selecting the highest nisin:phospholipid ratio and avoiding side effects due to the too high nisin concentration. We observed that the presence of 30 μ M of nisin, which corresponded to a nisin:phospholipid molar ratio of 1:100, led to a moderate stabilizing effect from both an enthalpic and an entropic point of view, although the transition covered the same temperature range than

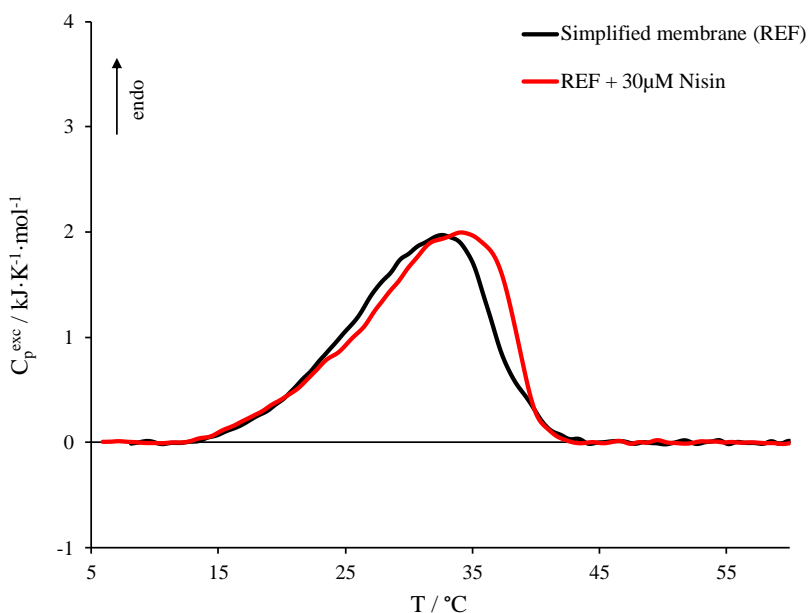


Figure 6.3: Micro-DSC profiles for the simplified membrane alone (black curve, corresponding to the profile in Fig.6.2a) and in presence of 30 μM nisin (red curve). Nisin:phospholipid molar ratio was 1:100.

without peptide. The slight stabilization of the high-stability lipid phases might suggest that the insertion of peptide within the bilayer is able to produce phase segregations as well as a general lipid reorganization.

In order to evaluate the influence of various FFAs on the interaction between nisin and the model membrane, the micro-DSC thermograms for vesicles containing six different FFAs were first recorded and are reported in Fig.6.4. The considered FFAs were two saturated fatty acids as palmitic acid and stearic acid, two monounsaturated FFAs as the *cis*-unsaturated oleic acid and the *trans*-unsaturated elaidic acid, and two polyunsaturated FFAs as the ω -6 linoleic acid and the ω -3 docosahexaenoic acid (DHA).

We observed that the addition of 20% of palmitic and stearic acids generated more severe membrane stabilization if compared to the effect deriving from elaidic acid, totally in accordance with the results of the previous

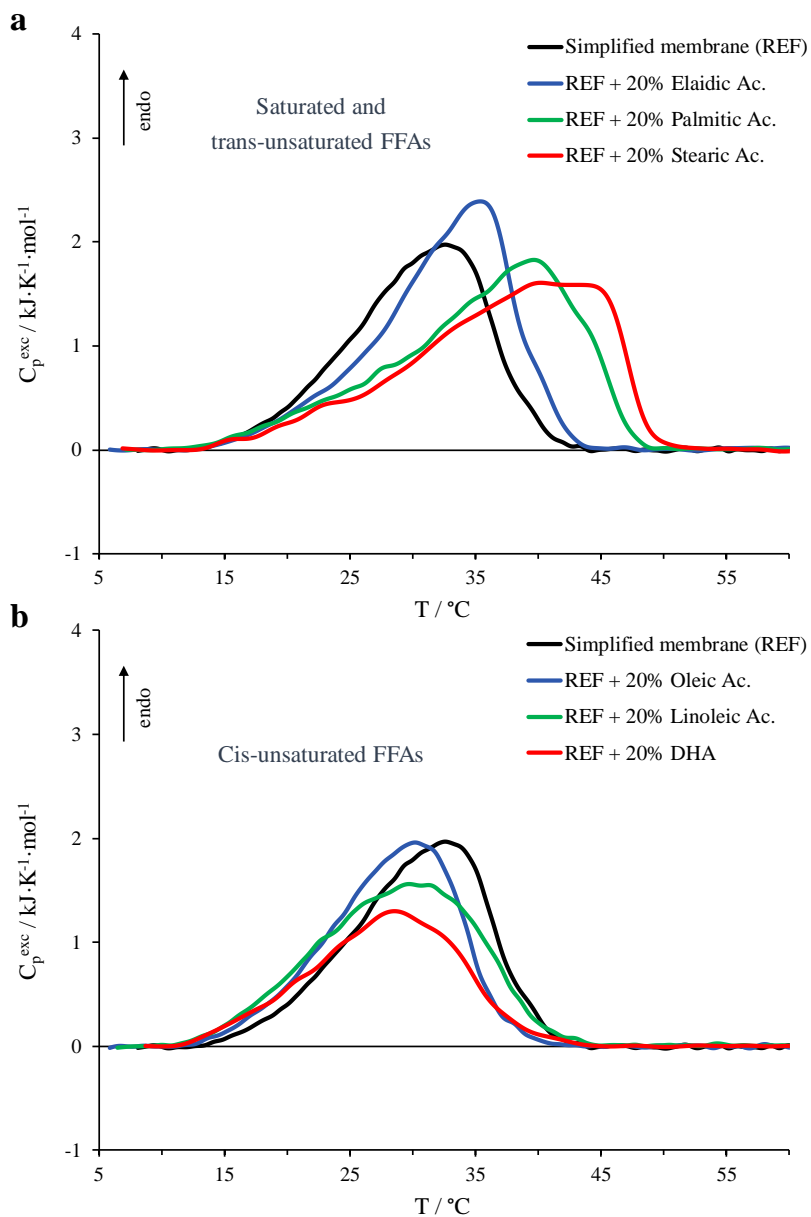


Figure 6.4: Micro-DSC profiles for the simplified vesicles (black curve) and vesicles with the addition of 20% FFAs. Thermograms are reported for membranes including saturated and trans-unsaturated FFAs in panel a, whereas the cis-unsaturated FFAs are shown in panel b.

Table 6.2: Thermodynamic parameters evaluated from micro-DSC investigations for several FFAs-containing simplified vesicles alone and in presence of 30 μ M nisin. The last cycle heating curves were used to obtain the main transition enthalpy (ΔH°), the peak maximum temperature (T_{max}), the transition average temperature (\bar{T}) and the Average Cooperativity Index (ACI). The transition average temperature (\bar{T}) was also compared to the temperature at the sigmoid flex point (T_{flex}) obtained from fluorescence spectroscopy measurements. The labels reported on the table indicate palmitic acid (PA), stearic acid (SA), elaidic acid (EA), oleic acid (OA), linoleic acid (LA) and docosahexaenoic acid (DHA).

	Calorimetry				Spectroscopy
	ΔH° kJ·mol ⁻¹	T_{max} °C	\bar{T} °C	ACI °C	T_{flex} °C
Simplified					
membrane (REF)	26 ± 2	32.6 ± 0.6	30.1 ± 0.1	5.3 ± 0.1	30.8 ± 0.4
REF + Nisin	28 ± 2	34.3 ± 0.5	30.7 ± 0.1	5.6 ± 0.1	-
REF + PA	30 ± 2	39.5 ± 0.4	34.9 ± 0.2	7.3 ± 0.2	37.1 ± 0.6
REF + PA + Nisin	35 ± 2	39.3 ± 0.7	34.4 ± 0.2	7.1 ± 0.2	-
REF + SA	30 ± 2	39.9 ± 0.6	36.6 ± 0.2	7.6 ± 0.2	38.1 ± 0.7
REF + SA + Nisin	28 ± 2	41.5 ± 0.2	36.6 ± 0.2	7.4 ± 0.2	-
REF + EA	30 ± 2	35.0 ± 0.6	31.9 ± 0.2	5.5 ± 0.2	33.8 ± 0.7
REF + EA + Nisin	28 ± 2	36.0 ± 0.2	32.7 ± 0.2	5.7 ± 0.2	-
REF + OA	24 ± 2	30.6 ± 0.6	28.1 ± 0.2	5.1 ± 0.2	28.8 ± 0.6
REF + OA + Nisin	27 ± 2	29.6 ± 0.5	29.1 ± 0.2	5.7 ± 0.2	-
REF + LA	25 ± 2	29.9 ± 0.4	28.5 ± 0.2	6.1 ± 0.2	27.7 ± 0.5
REF + LA + Nisin	20 ± 2	26.8 ± 0.5	25.8 ± 0.2	5.7 ± 0.2	-
REF + DHA	18 ± 2	28.3 ± 0.9	27.6 ± 0.2	5.9 ± 0.2	25.9 ± 1.5
REF + DHA + Nisin	29 ± 2	32.0 ± 0.5	29.3 ± 0.2	5.9 ± 0.2	-

chapter. Moreover, the effect of 20% of all the *cis*-unsaturated FFAs led to a moderate destabilization of the membrane thermodynamic stability whose magnitude depended on the number of C=C double bonds (Table 6.2). Specifically, linoleic acid enhanced the lipid phases distribution also towards higher temperatures than oleic acid as revealed by the ACI value, whereas the high irregularity of DHA's molecular structure was reflected in a strong

decrease of the enthalpic contribution to the gel-to-liquid crystalline phase transition.

The already established information about the behaviour of FFAs-containing vesicles achieved by micro-DSC was also confirmed by fluorescence spectroscopy. Fig.6.5 shows, as an example, the micro-DSC gel-to-liquid crystalline phase transition obtained for linoleic acid and the superimposition of the sigmoidal trend of fluorescence anisotropy values, r , against temperature. We observed that the fall of the anisotropy values well matched the temperature region interested by the phase transition since the probe's fluorescence anisotropy reflects the levels of order and packing of phospholipid acyl chains. Moreover, the sigmoid flex point was comparable to the \bar{T} obtained from the calorimetric curve. Indeed, the flex point theoretically

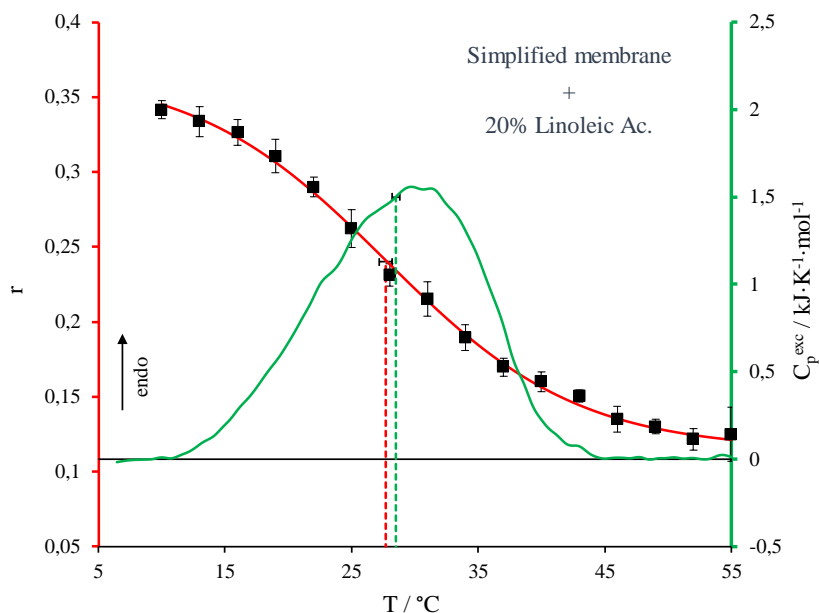


Figure 6.5: Example of superimposition of fluorescence anisotropy (r) of DPH in simplified vesicles containing 20% of linoleic acid (red trace) to the respective micro-DSC profile (green trace). The dashed lines indicate the \bar{T} for the calorimetric curve (green line) and the flex point of the sigmoid obtained from fluorescence anisotropy (red line). Probe:lipid molar ratio was 1:500.

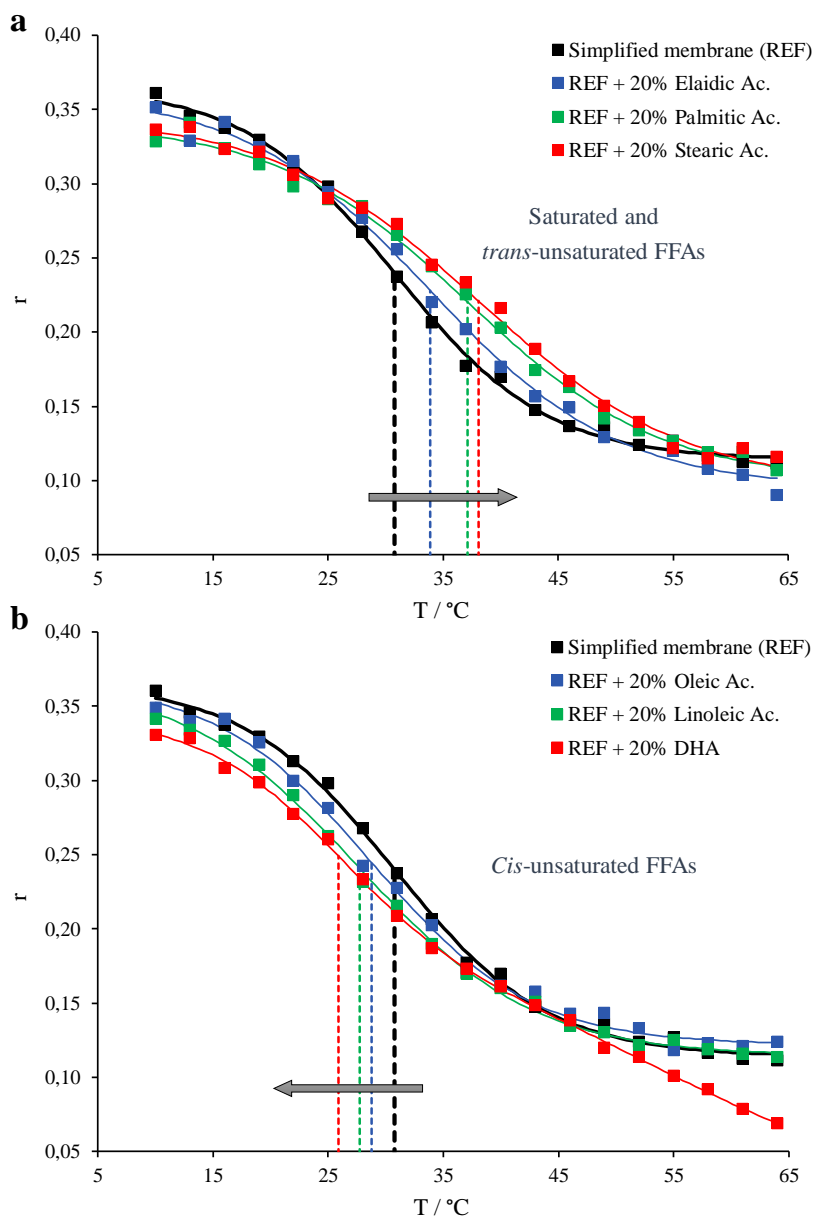


Figure 6.6: Fluorescence anisotropy (r) of DPH in simplified vesicles containing 20% of FFAs. The FFAs-free reference system is shown as black squares, whereas the FFAs considered are a) elaidic acid (blue squares), palmitic acid (green squares) and stearic acid (red squares), and b) oleic acid (blue squares), linoleic acid (green squares) and DHA (red squares). The dashed lines indicate the flex point of the sigmoidal fits with the respective colours. Probe:lipid molar ratio was 1:500.

corresponds to a 50% degree of progress of the process, thus indicating an average temperature of the transition.

The sigmoidal trends of the fluorescence anisotropy values obtained for the simplified membrane containing saturated and *trans*-unsaturated FFAs compared to the simplified membrane alone are reported in Fig.6.6a, whereas Fig.6.6b shows the trends for vesicles containing the *cis*-unsaturated FFAs. We observed that the flex points of the several sigmoids followed the same trend of the \bar{T} derived from micro-DSC measurements. Specifically, the sigmoids for vesicles containing stearic and palmitic acids are shifted toward higher temperatures than elaidic acid, whilst the flex points for vesicles containing oleic acid, linoleic acid and DHA were increasingly shifted toward lower temperatures depending on the number of unsaturated C=C bonds.

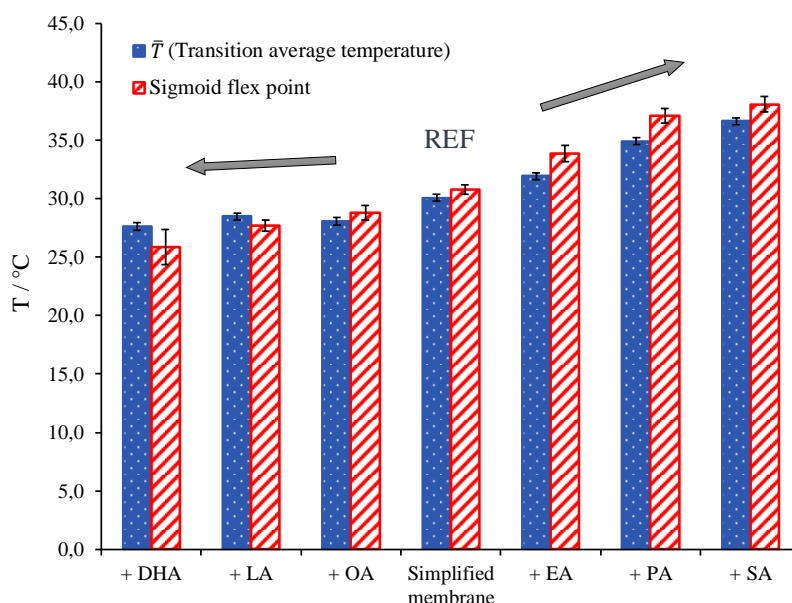


Figure 6.7: Histogram representation showing the \bar{T} values from micro-DSC curves (dotted blue bars) and the flex point of the sigmoids from fluorescence anisotropy (lined red bars) obtained for the simplified membrane alone and containing the 20% of various FFAs. The labels reported on the histogram indicate docosahexaenoic acid (DHA), linoleic acid (LA), oleic acid (OA), elaidic acid (EA), palmitic acid (PA) and stearic acid (SA)

Fig.6.7 reports a comparison between the \bar{T} values from micro-DSC curves (dotted blue bars) and the flex point of the sigmoids from fluorescence anisotropy (lined red bars) obtained for the simplified membrane alone and containing the 20% of various FFAs. As already mentioned above for vesicles containing linoleic acid (Fig.6.5), the flex points obtained from spectroscopic experiments were in accordance with the \bar{T} values of the calorimetric ones, confirming once again the type of effect produced by FFAs with different chemical structure. The slight differences between the two values may be ascribable to the lower sensitivity of the spectroscopic technique for the detection of lipid phase transitions than the calorimetric one, made also worse by the experimental conditions since the heating ramp for fluorescence measurements was obtained by applying fixed temperature steps of 3°C each.

The influence of 30µM nisin on the various vesicles is reported in Fig.6.8. At a first glance, we observed that all the systems underwent a lipid reorganization upon interacting with the peptide. Vesicles containing elaidic and stearic acid were the least affected by nisin in terms of entropic contributions as revealed by \bar{T} and ACI values in Table 6.2, even exhibiting a small transition enthalpy loss. On the other hand, vesicles containing linoleic acid exhibited a strong destabilization from both an enthalpic and entropic point of view. Instead, the remaining systems, containing DHA, oleic and palmitic acids, were characterized by a more or less strong entropic and enthalpic stabilization of the transition.

In an attempt to comment the thermotropic behaviour of such system, we may divide the description into two parts. As regards the vesicles containing *cis*-unsaturated FFAs, we may hypothesize that, if with oleic acid a slight membrane stabilization occurred, in presence of linoleic acid the destabilizing effects deriving from the presence of the FFA is too high to prevent any stabilization. In other words, a compensation between the stabilizing effect due to nisin interaction and the destabilization deriving from the unsaturated acyl chains. This hypothesized effect should have been maximum in DHA-containing vesicles. However, their micro-DSC profile obtained in presence of

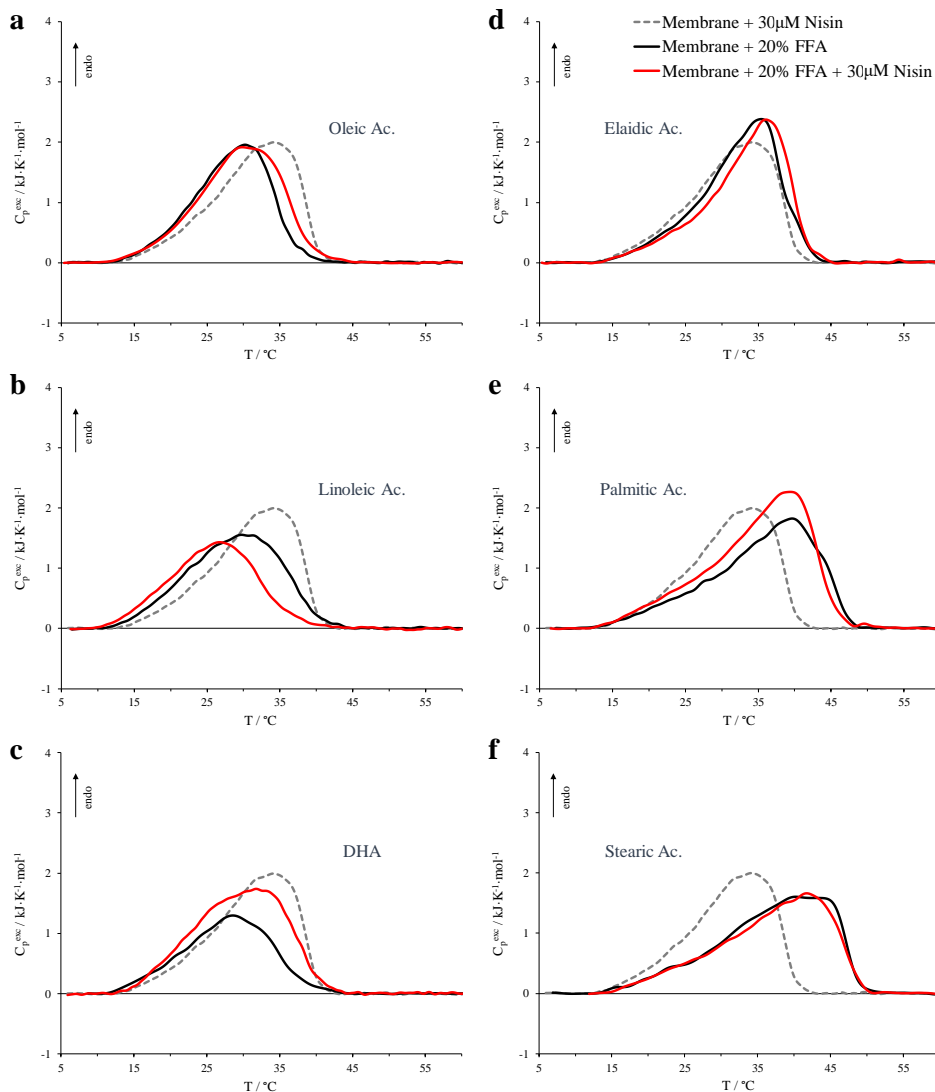


Figure 6.8: Micro-DSC profiles for the simplified membrane containing 20% of different FFAs (black curves) and for the same vesicles in presence of 30µM nisin (red curves). The profile of the FFAs-free simplified membrane in presence of 30µM nisin (corresponding to the red curve in Fig.6.3) is also represented as reference by the dashed grey trace. Nisin:phospholipid molar ratio was 1:100.

nisin (red curve in Fig.6.8c) is clearly characterized by a high-stability lipid region that seems to move close to the profile obtained for the FFAs-free simplified membrane in presence of nisin (dashed grey curve in Fig.6.8c). This aspect, also supported by the enthalpy values in Table 6.2, together with the

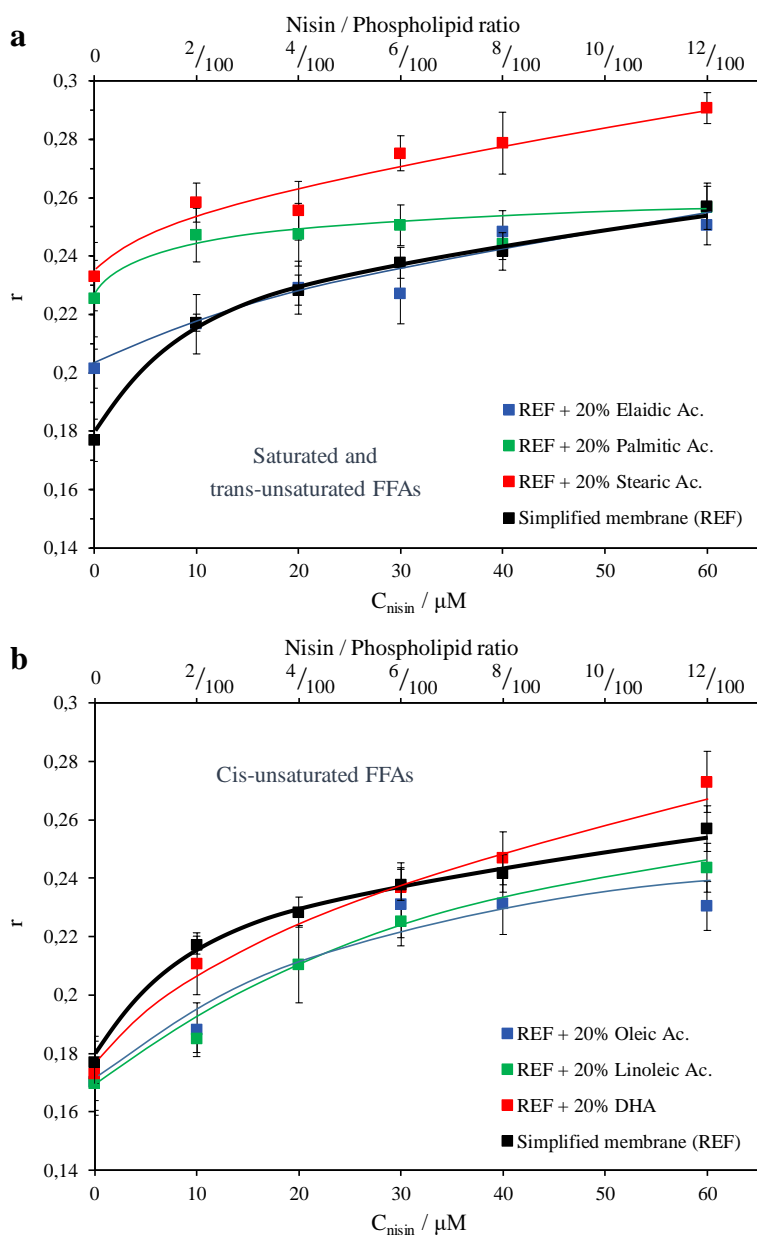


Figure 6.9: Fluorescence anisotropy (r) of DPH in simplified vesicles containing 20% of FFAs and exposed to several nisin concentrations. The respective nisin/phospholipid ratios are displayed on the upper x-axis. The FFAs-free reference system is shown as black squares, whereas the FFAs considered are a) elaidic acid (blue squares), palmitic acid (green squares) and stearic acid (red squares), and b) oleic acid (blue squares), linoleic acid (green squares) and DHA (red squares). The curves indicate tentative fits of the trends with the respective colours. Probe:lipid molar ratio was 1:500.

high DHA's molecular irregularity because of the six *cis*- double bonds might suggest a partial ejection of DHA molecules from the phospholipid bilayer, whereas nisin molecules still tends to enhance the vesicles thermodynamic stability.

As for the *trans*-unsaturated and saturated FFAs, the effect of nisin was almost the same for all with the exception of the strong enthalpic stabilizing effect for vesicles containing palmitic acid. We may consider that this last system is the only one that contains FFAs molecules with an acyl chain that perfectly matches the tails length of one phospholipid constituent of the membrane, *i.e.* DPPS tails. As already seen for the effect of palmitic acid on completely saturated ternary membrane and unsaturated quaternary membrane (section 5.3.2), increasing amounts of palmitic acid in membrane containing dipalmitoyl phospholipids lead to both an entropic and enthalpic stabilization of the systems. Therefore, we may argue that, in our case, nisin molecules promoted a segregation of palmitic acid within DPPS-rich regions, thus enhancing lipid chains interactions and increasing the enthalpic contribution to the phase transition.

In order to evaluate the effect of higher nisin concentrations on the FFAs-free and FFAs-containing systems, fluorescence anisotropy measurements were performed exploring several nisin/phospholipid molar ratios (Fig.6.9). We observed that increasing nisin concentrations produced progressively high fluorescence anisotropy values for all the systems, *i.e.* a gradual enhancement of the overall lipid packing level. However, such effects tended to reach a saturation because of the very high concentration of the peptide if compared to the phospholipid one.

6.3.3. *Dynamic light scattering*

In order to achieve additional information on the interaction between the FFAs-containing vesicles and the pore-forming nisin, DLS experiments were performed and some examples of the size distributions are shown in Fig.6.10,

Table 6.3: Physicochemical characteristics obtained from DLS measurements for several vesicles (containing 20% of FFAs) alone or in presence of 10 μ M nisin (nisin:phospholipid ratio was 1:50). The reported parameters are z-Average diameter (Z_{ave}) with standard deviation (SD^1) and the polydispersity index (PDI) with standard deviation (SD^2). The labels reported on the table indicate palmitic acid (PA), stearic acid (SA), elaidic acid (EA), oleic acid (OA), linoleic acid (LA) and docosahexaenoic acid (DHA).

		Z_{ave} nm	SD^1 nm	PDI	SD^2
Simplified membrane (REF)	alone	84.2	0.6	0.279	0.007
	with nisin	1950	44	0.141	0.038
REF + PA	alone	103.0	0.9	0.444	0.010
	with nisin	6786	298	0.501	0.060
REF + SA	alone	126.9	1.2	0.588	0.011
	with nisin	3266	53	0.137	0.116
REF + EA	alone	87.5	0.9	0.325	0.002
	with nisin	1761	79	0.315	0.028
REF + OA	alone	67.4	0.2	0.103	0.005
	with nisin	2055	351	0.695	0.356
REF + LA	alone	69.4	0.2	0.074	0.004
	with nisin	298.8	0.6	0.508	0.005
REF + DHA	alone	75.2	0.1	0.070	0.028
	with nisin	176.4	1.1	0.296	0.026

Fig.6.11 and Fig.6.12. Moreover, the relevant parameters obtained from DLS measurements are collected in Table 6.3.

As shown by the table and figures, all the systems displayed compatible size distributions to the liposome extrusion protocol adopted for their preparation when analysed without nisin, *i.e.* z-average diameters around the polycarbonate membrane pores size of 100nm. However, after the addition of nisin up to a nisin:phospholipid molar ratio of 1:50, most of the systems

exhibited a severe increase of the size that may suggest the formation of aggregates. Two exceptions were represented by vesicles containing linoleic acid and DHA (Fig.6.11 and Fig.6.12, respectively). Indeed, we did not observe any relevant variation in size distribution, whereas small increments in z-average diameter were observed for both (Table 6.3). It is noteworthy highlighting that these two systems showed peculiarities in micro-DSC profiles in compared to the others, revealing a connection with the behaviour displayed.

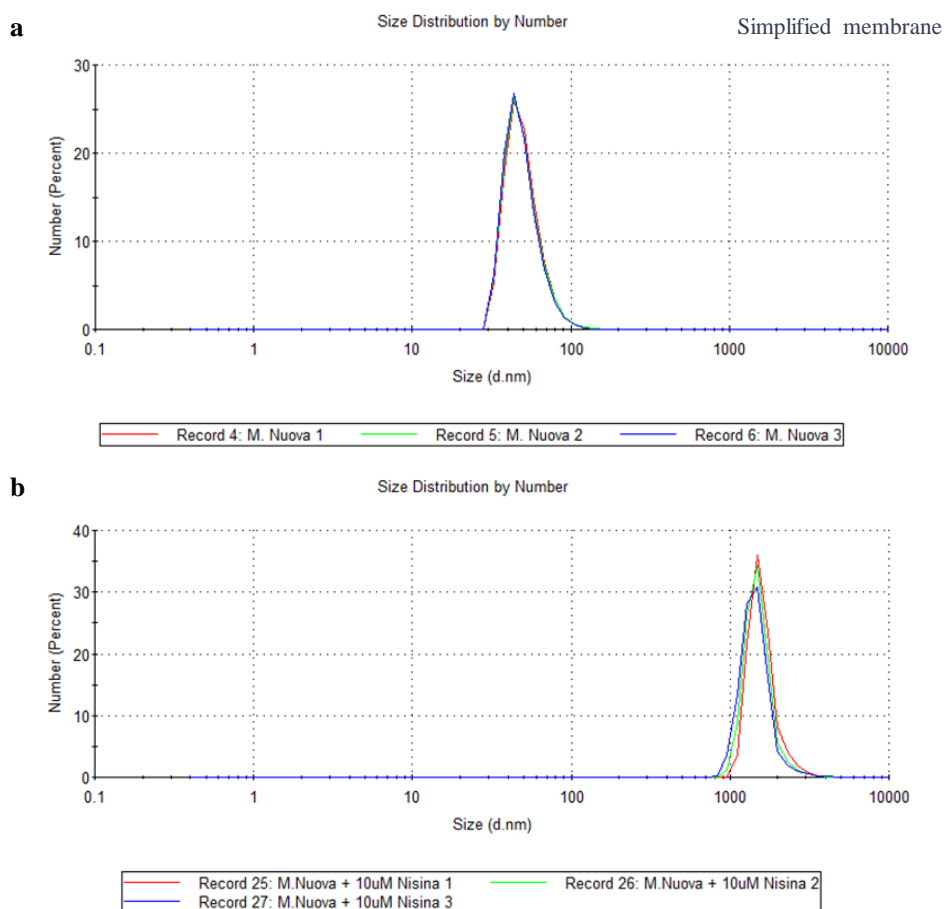


Figure 6.10: DLS profiles for the simplified membrane alone and in presence of $10\mu\text{M}$ nisin (nisin:phospholipid was 1:50).

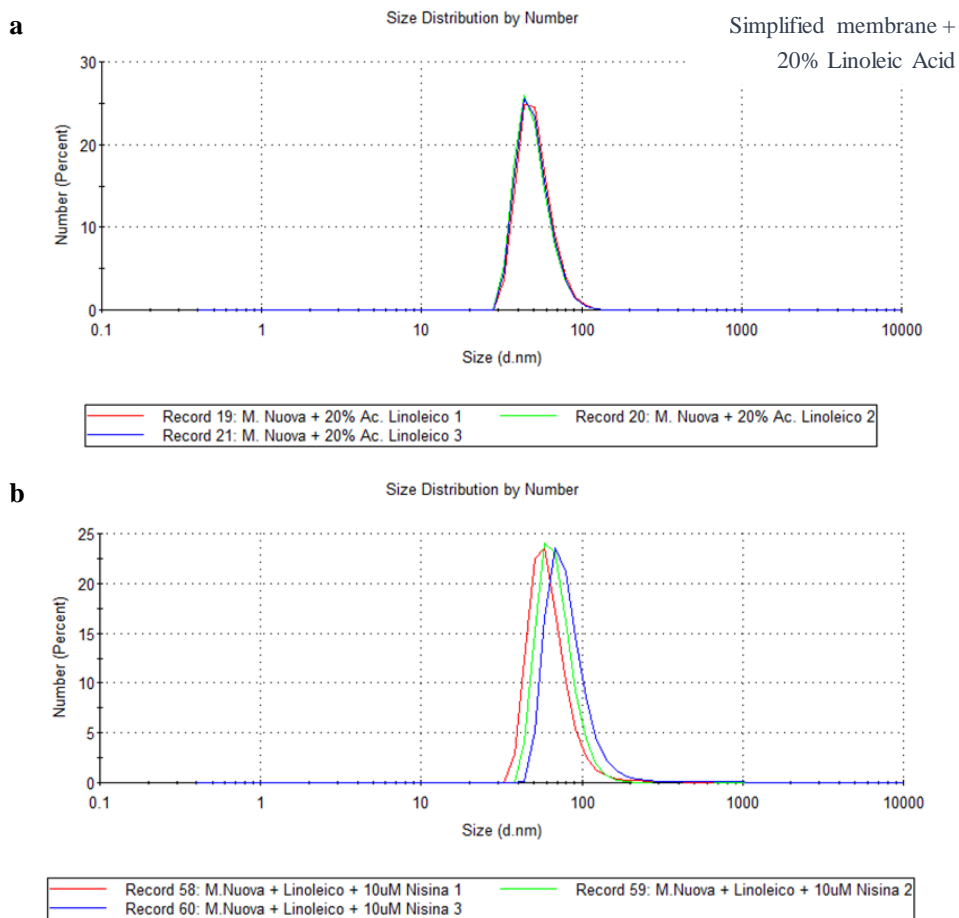


Figure 6.11: DLS profiles for the simplified membrane + 20% linoleic acid alone and in presence of 10 μ M nisin (nisin:phospholipid was 1:50).

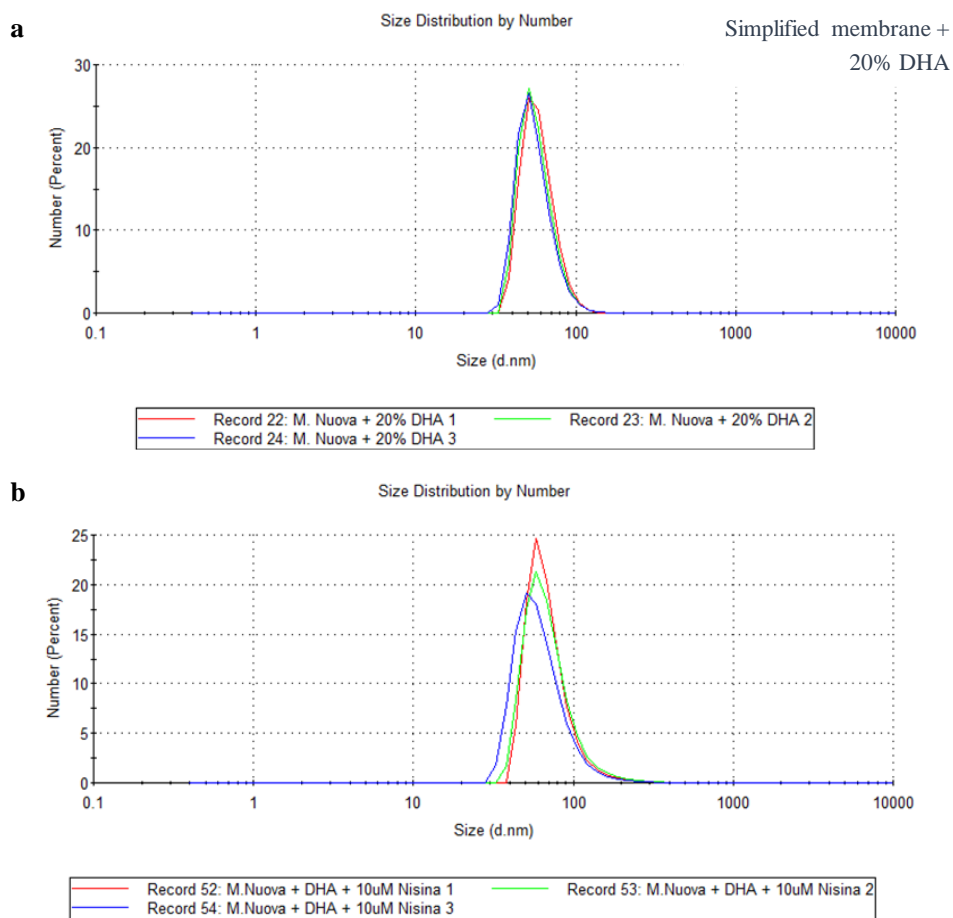


Figure 6.12: DLS profiles for the simplified membrane + 20% DHA alone and in presence of 10 μ M nisin (nisin:phospholipid was 1:50).

6.4. References

- Abts, A., Mavaro, A., Stindt, J., Bakkes, P.J., Metzger, S., Driessen, A.J.M., Smits, S.H.J., Schmitt, L., 2011. Easy and Rapid Purification of Highly Active Nisin. *Int. J. Pept.* 2011, 1–9.
- Bach, D., Wachtel, E., 1989. Thermotropic properties of mixtures of negatively charged phospholipids with cholesterol in the presence and absence of Li⁺ or Ca²⁺ ions. *Biochim. Biophys. Acta - Biomembr.* 979, 11–19.
- Barone, G., Del Vecchio, P., Fessas, D., Giancola, C., Graziano, G., 1992. THESEUS: A new software package for the handling and analysis of thermal denaturation data of biological macromolecules. *J. Therm. Anal.* 38, 2779–2790.
- Boheim, G., 1974. Statistical analysis of alamethicin channels in black lipid membranes. *J. Membr. Biol.* 19, 277–303.
- Breukink, E., Wiedemann, I., van Kraaij, C., Kuipers, O.P., Sahl, H.G., de Kruijff, B., 1999. Use of the cell wall precursor lipid II by a pore-forming peptide antibiotic. *Science* 286, 2361–4.
- da Silva Malheiros, P., Daroit, D.J., da Silveira, N.P., Brandelli, A., 2010. Effect of nanovesicle-encapsulated nisin on growth of *Listeria monocytogenes* in milk. *Food Microbiol.* 27, 175–178.
- de Kruijff, B., Demel, R.A., dan Deenen, L.L.M., 1972. The effect of cholesterol and epicholesterol incorporation on the permeability and on the phase transition of intact *Acholeplasma laidlawii* cell membranes and derived liposomes. *Biochim. Biophys. Acta - Biomembr.* 255, 331–347.
- Galvagnion, C., Brown, J.W.P., Ouberai, M.M., Flagmeier, P., Vendruscolo, M., Buell, A.K., Sparr, E., Dobson, C.M., 2016. Chemical properties of lipids strongly affect the kinetics of the membrane-induced aggregation of α -synuclein. *Proc. Natl. Acad. Sci.* 113, 7065–7070.

- Hasper, H.E., Kramer, N.E., Smith, J.L., Hillman, J.D., Zachariah, C., Kuipers, O.P., de Kruijff, B., Breukink, E., 2006. An Alternative Bactericidal Mechanism of Action for Lantibiotic Peptides That Target Lipid II. *Science* 313, 1636–1637.
- Laridi, R., Kheadr, E.E., Benech, R.O., Vuilleumard, J.C., Lacroix, C., Fliss, I., 2003. Liposome encapsulated nisin Z: optimization, stability and release during milk fermentation. *Int. Dairy J.* 13, 325–336.
- Lentz, B.R., Barenholz, Y., Thompson, T.E., 1976. Fluorescence depolarization studies of phase transitions and fluidity in phospholipid bilayers. 1. Single component phosphatidylcholine liposomes. *Biochemistry* 15, 4521–4528.
- Leontiadou, H., Mark, A.E., Marrink, S.J., 2006. Antimicrobial Peptides in Action. *J. Am. Chem. Soc.* 128, 12156–12161.
- MacDonald, M.J., Ade, L., Ntambi, J.M., Ansari, I.-U.H., Stoker, S.W., 2015. Characterization of Phospholipids in Insulin Secretory Granules and Mitochondria in Pancreatic Beta Cells and Their Changes with Glucose Stimulation. *J. Biol. Chem.* 290, 11075–11092.
- Melo, M.N., Ferre, R., Castanho, M.A.R.B., 2009. Antimicrobial peptides: linking partition, activity and high membrane-bound concentrations. *Nat. Rev. Microbiol.* 7, 245–250.
- Pandit, R., Rai, M., Santos, C.A., 2017. Enhanced antimicrobial activity of the food-protecting nisin peptide by bioconjugation with silver nanoparticles. *Environ. Chem. Lett.* 15, 443–452.
- Prince, A., Sandhu, P., Ror, P., Dash, E., Sharma, S., Arakha, M., Jha, S., Akhter, Y., Saleem, M., 2016. Lipid-II Independent Antimicrobial Mechanism of Nisin Depends On Its Crowding And Degree Of Oligomerization. *Sci. Rep.* 6, 37908.

- Rothman, J.E., Lenard, J., 1977. Membrane Asymmetry. *Science* 195, 743–753.
- Severina, E., Severin, A., Tomasz, A., 1998. Antibacterial efficacy of nisin against multidrug-resistant Gram-positive pathogens. *J. Antimicrob. Chemother.* 41, 341–347.
- Shai, Y., 1999. Mechanism of the binding, insertion and destabilization of phospholipid bilayer membranes by α -helical antimicrobial and cell non-selective membrane-lytic peptides. *Biochim. Biophys. Acta - Biomembr.* 1462, 55–70.
- Shinitzky, M., Barenholz, Y., 1974. Dynamics of the hydrocarbon layer in liposomes of lecithin and sphingomyelin containing dicetylphosphate. *J. Biol. Chem.* 249, 2652–2657.
- Shinitzky, M., Barenholz, Y., 1978. Fluidity parameters of lipid regions determined by fluorescence polarization. *Biochim. Biophys. Acta - Rev. Biomembr.* 515, 367–394.
- Stewart, J.C.M., 1980. Colorimetric determination of phospholipids with ammonium ferrothiocyanate. *Anal. Biochem.* 104, 10–14.
- Tanfani, F., Curatola, G., Bertoli, E., 1989. Steady-state fluorescence anisotropy and multifrequency phase fluorometry on oxidized phosphatidylcholine vesicles. *Chem. Phys. Lipids* 50, 1–9.
- Taylor, T.M., Davidson, P.M., Bruce, B.D., Weiss, J., 2005. Ultrasonic Spectroscopy and Differential Scanning Calorimetry of Liposomal-Encapsulated Nisin. *J. Agric. Food Chem.* 53, 8722–8728.
- van Heusden, H.E., de Kruijff, B., Breukink, E., 2002. Lipid II Induces a Transmembrane Orientation of the Pore-Forming Peptide Lantibiotic Nisin. *Biochemistry* 41, 12171–12178.

Were, L.M., Bruce, B., Davidson, P.M., Weiss, J., 2004. Encapsulation of Nisin and Lysozyme in Liposomes Enhances Efficacy against *Listeria monocytogenes*. *J. Food Prot.* 67, 922–927.

General conclusions

The experimental evidences of this thesis, which followed a stepwise approach as regard the membranes complexity, permitted to discriminate the basic effects that dictate the membrane thermodynamic stability and the influence of the FFAs inclusion.

We may conclude that the main factors that dictate the overall thermodynamic stability of cell membranes' phospholipid bilayers mainly act through entropic effects. Specifically, curvature effects are relevant among single-component unilamellar vesicles, but become of minor importance in more complex systems, also just including binary composition membranes. The overall stability of mixed membranes depends on the relative molar ratio of the saturated phospholipids and the constituents' contributions are somehow "additive", *i.e.* they are proportional to the lipid composition. However, the loss of cooperativity of the gel-to-liquid crystalline phase transition due to differences in headgroups is less pronounced than that produced by differences in tails length, which in turn are able to produce a more severe dispersion of the membrane's thermodynamic phases. Instead, the presence of unsaturated phospholipids, even in minor amounts, has a relevant overall destabilizing effect and enhance the homogeneousness on the phases distribution. Nevertheless, as for the other components, as sphingomyelin, lysophospholipids, as well as for the above-mentioned unsaturated acyl chains, the description of their influence is less simple since

they are able to generate visible entropic and enthalpic destabilization but their effects do not follow the linear trend highlighted by the saturated phospholipids. However, it emerged that in multi-components systems all the effects are mediated, limiting the presence of severe phase separations.

The preparation of a fourteen-components model membrane was achieved by proportionally selecting the most abundant acyl chains for each macro-category constituting the ISG's membrane, namely phosphatidylcholines, phosphatidylethanolamines, phosphatidylserines, sphingomyelins and lysophosphatidylcholines. This system was very close to the phospholipid composition of the real ISG reaching the 80% of representativeness in terms of both headgroups and acyl chains. The inclusion of cholesterol led to a strong membrane order loss ("fluidification"). Specifically, the effect of cholesterol depended on the added amount, revealing a preferable action on the most stable phases, whereas the less stable phases were impaired at higher cholesterol percentages.

As for the FFAs influence, the presence of saturated fatty acids (stearic and palmitic acids) mainly produced an entropic strong stabilizing effect as well as an enthalpic contribution, whilst a *trans*-unsaturated acid was able to produce only moderate stabilizing effects mainly of enthalpic nature. By contrast, the *cis*-unsaturated FFAs (oleic, linoleic and docosahexaenoic acids) produced an overall destabilization of the membranes that depended on the level of unsaturation of the acyl chain. Nevertheless, we figured out that the observed stabilizing or destabilizing effects occurred regardless of the membrane lipid composition and any possible difference might only regard the magnitude of the effect.

The conclusions accomplished with the calorimetric technique as for the effects deriving from the addition of various FFAs to model membranes were also confirmed by means of fluorescence spectroscopy. Moreover, the flex points obtained from the sigmoidal trends of DPH probe's fluorescence anisotropy against temperature were well comparable to the transition average temperature (\bar{T}) got from micro-DSC thermograms, thus indicating

that the sigmoids' flex point are indicative of an average temperature of the transition.

Despite a real cell membrane is much more complex because of other non-lipid constituents as proteins and/or environmental conditions, etc., comparison with literature data indicate that these peculiarities seem to not compromise the general conclusions here presented about the membrane thermodynamics, influence of cholesterol and effects of FFAs. Furthermore, all the thermodynamic information achieved so far, allowed to predict the calorimetric profile of model membrane, hence to design a simplified model membrane resembling the transition cooperativity and enthalpy of the ISG-like one's.

As regards the model membrane-nisin interaction, we may conclude that both the FFAs-free and most of FFAs-containing model membranes were affected by moderate lipid reorganization. The exception to this behaviour were represented by linoleic acid, for which entropic and enthalpic destabilizations occurred, and DHA, which instead exhibited an evident stabilization. Such exceptions were somehow reflected by DLS experiments as well. Indeed, the size distributions of all these last systems were shifted towards higher size values in presence of nisin, suggesting the formation of aggregates, whereas vesicles containing linoleic acid and DHA did not display relevant size variation.

Implications and future directions

The conclusions obtained from the systematic dissection of the single thermodynamic contributions to the overall thermodynamic behaviour of the ISGs phospholipid bilayers seem to be general and applicable to other lipid membranes, including real cell membranes. Indeed, as punctuated in the previous chapters and by the high accordance between the results here reported and literature data, the contribution of other non-lipid components usually present in cell membranes, as proteins, etc., does not seem to compromise the overall thermodynamics of cell membranes.

Hence, the thermodynamic conclusions of this study might be used for interpretation and/or recognition of deviations in terms of thermodynamic stability between cell membranes of healthy and obese/diabetic subjects. Indeed, severally morphological differences are already reported in the literature, but no thermodynamic studies are available today. In this frame, contacts have already been established with the Department of Health Sciences (University of Milan) to investigate calorimetric profiles and lipidomics of platelets' membrane of healthy people and diabetic patients aiming to correlate differences between phospholipid bilayers depending on health conditions.

Moreover, the study on the influence of FFAs on model membranes has revealed that their effects are specific and of different nature and that the chemical structure of the fatty acids plays a crucial role on the thermodynamic

stability of cell membranes. In this context, literature data already reporting that diabetic and/or obese individuals manifest high levels of FFAs might be integrated with a discrimination of blood FFAs distributions in order to help to highlight possible molecular mechanisms hidden behind the relationship between nutrition and health.

Furthermore, the knowledge about the action of FFAs on cell membranes allows to open another branch of investigation about the influence of phospholipid bilayers thermodynamics on the functionality of many transmembrane proteins, as insulin receptor in the frame of type 2 diabetes mellitus.

As for the study of nisin-membrane interaction in presence of FFAs, it paved the way for the thermodynamic and kinetic investigation of vesicles interaction with more complex structures as amyloidogenic peptides (e.g. amylin) allowing the expansion of this approach not only to type 2 diabetes but also to other similar conditions (as for the molecular mechanisms involved) as Alzheimer's and Parkinson's diseases.

Appendices

In the following appendices, some side projects undertaken during the Ph.D. period are reported. They were aimed at deepening the knowledge on thermal analysis and calorimetry, as well as on thermodynamics. Such parallel activities involved the thermodynamics study of biological macromolecules, as proteins in solution (conformational stability, specific and/or aspecific macromolecule - ligand binding phenomena), physicochemical investigation on liposomes thermotropic behaviour for pharmaceutical application, as well as the calorimetric characterization of cultural heritage biomaterials.

Furthermore, a list of publications/communications to scientific meetings and the awards received during the three years are also attached as outcomes of the doctoral research.

A. Side projects

i. *Thermodynamic Stability of Myoglobin-Poly(Ethylene Glycol) Bioconjugates: a Calorimetric Study*



Thermochimica Acta
Volume 671, January 2019, Pages 26-31



Thermodynamic stability of myoglobin-poly(ethylene glycol) bioconjugates: A calorimetric study

Chiara Pelosi ^{a, b, 1}, Francesca Saitta ^{c, 1}, Frederik R. Wurm ^b, Dimitrios Fessas ^c ✉, Maria Rosaria Tinè ^a ✉, Celia Duce ^a

^a Dipartimento di Chimica e Chimica Industriale, Università di Pisa, Via Moruzzi, 56124, Pisa, Italy

^b Max-Planck-Institut für Polymerforschung, Ackermannweg 10, 55128, Mainz, Germany

^c Dipartimento di Scienze per gli Alimenti, la Nutrizione e l'Ambiente, DeFENS, Università degli Studi di Milano, Via Celoria 2, 20133, Milano, Italy

Received 27 September 2018, Revised 30 October 2018, Accepted 4 November 2018, Available online 5 November 2018.



 [Show less](#)

<https://doi.org/10.1016/j.tca.2018.11.001>

[Get rights and content](#)

Highlights

- The **myoglobin** denaturation mechanism remains unaffected upon **PEGylation**.
- PEGylation causes a thermal destabilization of myoglobin but enhances reversibility.
- PEGylation decreases the solvent-exposed surface of the myoglobin denatured state.

Abstract

PEGylated proteins are widely used for therapeutic applications, therefore a fundamental understanding of the conjugates' structure and their behaviour in solution is essential to promote new developments in this field. In the present work, myoglobin-poly(ethylene glycol) conjugates were synthesized and studied by differential scanning calorimetry and UV-visible spectroscopy to obtain information on the bioconjugates' thermodynamic stability, also focusing on PEG's role on the solvent-protein surface interaction. The overall results of this study indicated a thermal destabilization of the protein that follows the extent of the bioconjugation without, however, compromising the native structure which remains functional. Moreover, the myoglobin PEGylation prevented the post-denaturation aggregation phenomena and enhanced the protein thermal reversibility. The thermodynamic interpretation of the data indicated that the bioconjugation influences the solvent-exposed protein surface difference between native and denatured state, contributing to the interpretation of the overall protein modification and functionality.

Keywords: PEGylation, calorimetry, protein unfolding, unfolding reversibility, protein-polymer conjugation.

ii. *pH-responsive chimeric liposomes: from nanotechnology to biological assessment*

Elsevier Editorial System(tm) for
International Journal of Pharmaceutics or its open access mirror
Manuscript Draft

Manuscript Number: IJP-D-19-01421R1

Title: pH-responsive Chimeric Liposomes: From Nanotechnology to
Biological Assessment

Article Type: Research Paper

Section/Category: Pharmaceutical Nanotechnology

Keywords: Chimeric liposomes; pH-responsive; lyotropism; interactions;
micro-DSC

Corresponding Author: Professor Costas Demetzos,

Corresponding Author's Institution: National and Kapodistrian University
of Athens

First Author: Nikolaos Naziris

Order of Authors: Nikolaos Naziris; Francesca Saitta; Varvara
Chrysostomou; Marcin Libera; Barbara Trzebicka; Dimitrios Fessas;
Stergios Pispas; Costas Demetzos

Abstract

The utilization of liposomes in biomedical applications has greatly benefited the diagnosis and treatment of complex diseases. These biomimetic nano-entities have been very useful in the clinical practice as drug delivery systems in their conventional form, comprising lipids as structural components. However, the scientific efforts have recently shifted towards the development of more sophisticated nanotechnological platforms, which apply functional biomaterials, such as stimuli-responsive polymers, in order to aid the drug molecule targeting concept. These nanosystems are defined as chimeric/mixed, because they combine more than one different in nature biomaterials and their development requires intensive study through biophysical and thermodynamic approaches before they may reach *in vivo* application. Herein, we designed and developed chimeric liposomes,

composed of a phospholipid and pH-responsive amphiphilic diblock copolymers and studied their morphology and their behavior based on crucial formulation parameters, including biomaterial concentration, dispersion medium pH and polymer composition. Additionally, their interactions with biological components, pH-responsiveness and membrane thermodynamics were also assessed. Finally, preliminary *in vivo* toxicity experiments of the developed nanosystems were carried out, in order to establish a future protocol for full *in vivo* evaluation. The results have been correlated with the properties of the chimeric nanosystems and highlight the importance of such approaches for designing and developing effective nanocarriers for biomedical applications.

Keywords: Chimeric liposomes, pH-responsive, lyotropism, interactions, micro-DSC.

AWARDED POSTER in Life Science section during the 13th Medicta, 2017.



Application of DSC and Imaging Techniques on the Development of Innovative Chimeric/Mixed Nanosystems



N. Naziris^a, F. Saitta^b, N. Pippa^{a,c}, D. Stellas^{d,e}, V. Chrysostomou^f, S. Pispas^c, M. Libera^f, B. Trzebicka^f, M. Signorelli^b, C. Demetzos^{a,g}, D. Fessas^{b,h}

^aSection of Pharmaceutical Technology, Department of Pharmacy, School of Health Sciences, National and Kapodistrian University of Athens, Panepistimioupolis Zografou, 15771 Athens, Greece

^bDepartment of Food, Environmental and Nutritional Sciences (DeFENS), Università degli Studi di Milano, Via Celeria 2, 20133 Milano, Italy

^cTheoretical and Physical Chemistry Institute, National Hellenic Research Foundation, Vassileos Constantinou Avenue 48, 11635 Athens, Greece

^dBiomedical Research Foundation, Academy of Athens, Soranou Efessiou Street 4, 11527 Athens, Greece

^eVaccine Branch, Center for Cancer Research, National Cancer Institute, National Institutes of Health, Frederick Maryland, MD 21702-1201, USA

^fCentre of Polymer and Carbon Materials, Polish Academy of Sciences, ul. M. Curie-Skłodowskiej 34, 41-819 Zabrze, Poland

*corresponding authors: dimitrios.fessas@unimi.it, demetzos@pharm.uoa.gr

Introduction

Among the biomimetic and bio-inspired drug delivery nanosystems, chimeric/mixed nanostructures are systems composed by different in nature biomaterials. In this frame, self-assembled chimeric lipid/block copolymer nanovesicles include both synthetic and natural building blocks and are surely noteworthy in pharmaceutical field for their remarkable functionalities and properties, such as colloidal stability, biocompatibility, high loading efficiency, stealth properties and controlled and stimuli-responsive release.^[1] However, there is a strict correlation between the exhibited features and the type of copolymer and/or the lipid-to-copolymer ratio. Differential scanning calorimetry (DSC) allows to reveal the thermodynamic phenomena that drive the self-assembly of these mixed nanosystems and that contribute to the membrane properties^[2]. In this study we considered chimeric lipid/block copolymer liposomes containing the lipid L- α -phosphatidylcholine, hydrogenated (Soy) (HSPC) and two amphiphilic diblock copolymers poly(2-(dimethylamino)ethyl methacrylate)-*b*-poly(lauryl methacrylate) (PDMAEMA-*b*-PLMA), at various molar ratios (Fig.1). The DSC technique was applied to evaluate the concentration-dependent thermodynamic properties as well as the influence of the hydrophilic-to-hydrophobic balance of the copolymers. Complementary information as regard the morphological aspects emerged by cryogenic transmission electron microscopy (cryo-TEM).

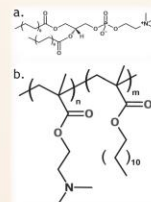


Figure 1. a. HSPC; b. PDMAEMA-*b*-PLMA 1 (m:m=70:30), PDMAEMA-*b*-PLMA 2 (m:m=60:40)

Experimental Methods

Pure and chimeric liposomes were prepared in PBS (pH 7.4) through thin-film hydration^[3] and their physical properties were determined through dynamic, electrophoretic and static light scattering (DLS, ELS and SLS). In addition, their size and morphology were evaluated through atomic force microscopy (AFM) and cryogenic transmission electron microscopy (cryo-TEM). Calorimetric experiments on liposomal suspensions were performed with a Micro-DSC (Micro-DSCIII, Setaram), whereas HSPC bilayers were characterized by using a classic DSC (DSC6, PerkinElmer) (Fig.2). Both systems were stable over two months! (Fig.3)

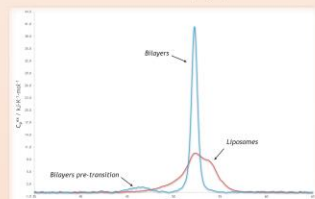


Figure 2. Gel-to-Liquid crystal transition differences for lipid bilayers (blue) and liposomes (red).

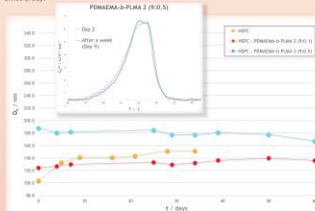


Figure 3. Hydrodynamic diameter (D_n), colloidal stability indexes of pure and mixed nanosystems at various concentrations. On the top, DSC evidence of the stability of such systems.

Results and Discussion

In Fig.4, differences in terms of thermodynamic stability are showed for both systems and at different copolymers concentrations. We observed both enthalpic and entropic (phase separations) effects. In particular, at low copolymer concentration the entropic effects seemed to be dominant ($\Delta H = 40 \pm 2 \text{ kJ} \cdot \text{mol}^{-1}$ for all systems), whereas the enthalpic effects are involved at higher copolymer concentration. However, this last evidence is still under investigation. Indeed, cryo-TEM images showed the presence of other nanoassemblies that deviated from liposomes (polymerosomes, discs and worm-like micelles). Therefore the enthalpy values, that are expressed per mole of lipids involved in gel-to-liquid crystal phase transition, might not be reliable since this extra structures were not taken into account in the normalization. Furthermore, cryo-TEM images confirmed the presence of phase separations, (faceting and density heterogeneity), highlighting a high penetration of the copolymer hydrophobic chains into the hydrophobic core of the membranes.

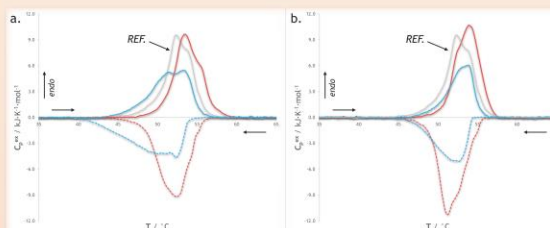


Figure 4. Micro-DSC scans for a. HSPC/PDMAEMA-*b*-PLMA 1 9:0.1 (grey), 9:0.1 (red) and 9:0.5 (blue) b. HSPC/PDMAEMA-*b*-PLMA 2 9:0.1 (grey), 9:0.1 (red) and 9:0.5 (blue) chimeric liposomes in PBS. 150mM pH 7.4. Heating and cooling curves (0.5 °C/min scanning rate) are showed as solid and dashed lines, respectively. Samples concentration: 2.5mg/ml (overall weight).

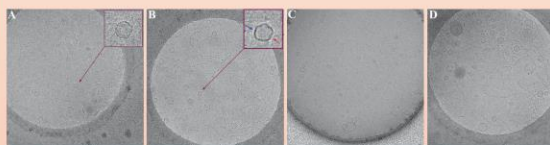


Figure 5. Cryo-TEM images of chimeric nanosystems HSPC/PDMAEMA-*b*-PLMA 1 9:0.01 (A), 9:0.05 (B), HSPC/PDMAEMA-*b*-PLMA 2 9:0.01 (C) and 9:0.05 (D).

Conclusions

DSC revealed the effects of copolymer concentration and hydrophilic-to-hydrophobic ratio on thermodynamic stability of the nanosystems. These information is crucial for the tuning of the physicochemical properties of such new chimeric/mixed nanostructures, making them a versatile matrix for the design of drug carriers with improved and controlled drug loading and release.

References

- Naziris, N. et al. *Curr. Nanomed.*, 6; 2016, 166.
- Gardikis, K. et al. *Colloids Surf. B Biointerfaces*, 81; 2010, 11.
- Kant, S. et al. *Int. Res. J. Pharm.*, 3; 2012, 10.

iii. *The DSC monitoring of oil melting to follow the oil curing*

Abstract presented at the joint CEEC-TAC5&Medicta19, 2019

Silvia PIZZIMENTI¹, Celia DUCE¹, Maria Rosaria TINÈ ¹, Ilaria BONADUCE¹, Francesca SAITTA², Marco SIGNORELLI², Dimitrios FESSAS²

¹ Department of Chemistry and Industrial Chemistry, University of Pisa, Via Moruzzi, 56124, Pisa, Italy

² Department of Food, Environmental and Nutritional Sciences, DeFENS, Università degli Studi di Milano, Via Celoria 2, 20133, Milano, Italy

The drying of an oil paint is due to the polyunsaturations of the oil in the oil paint binder. Polyunsaturated oils dry through an autoxidation process in which the double bonds of linolenic and linoleic acids naturally react with the oxygen present in the atmosphere. The gradual conversion of a liquid oil through a soft gel to a rubbery solid occurs as a result of a multistep free radical chain reaction. During the propagation step, hydroperoxides are formed [1]. A method frequently used to follow the oil curing in the DSC monitoring of the peroxide decomposition peak during time [2, 3, 4]. Taking into account that the oil polymerization affects the crystallinity content of the oil, an alternative method to assess the oil curing is here presented. The melting peak of the linseed oil samples is measured at different time of curing. The comparison between the melting peak behaviour and the peroxide decomposition peak shows that it is possible to correlate the profiles of the peroxide decomposition peaks with the melting peaks and that when the maximum of the peroxide content is reached, the melting peak disappears. The study of the melting peak by DSC is proposed as a valid alternative tool to monitor the curing of the oil paint.

-
- [1] M. Lazzari, O. Chiantore. *Pol. Degrad. Stab.*, 65 (1999) 303-313
- [2] D. Tamburini, D. Sardi, A. Spepi, C. Duce, M.R. Tinè, M.P. Colombini, et al. *Pol. Degrad. Stab.*, 134 (2016) 251-264
- [3] C. Duce, L. Bernazzani, E. Bramanti, A. Spepi, M.P. Colombini, M.R. Tiné *Pol. Degrad. Stab.*, 105, (2014), 48-58
- [4] M.R. Tiné, C. Duce Calorimetric and thermoanalytical techniques in Cultural Heritage In G. Lazzara, R.Fakhrullin (Eds.), *Nanotechnologies and nanomaterials for Diagnostic, Conservation and Restoration of Cultural Heritage*, Elsevier (2018) 79-109.

iv. *Thermodynamic studies of AgamOBP4 and AgamOBP5 from Anopheles gambiae with different semiochemicals*

Abstract presented at the 13th Medicta, 2017.

Francesca Saitta¹, Panagiota G.V. Liggri^{2,3}, Katerina E. Tsitsanou², Christina E. Drakou², Kostas Iatrou⁴, Spyros E. Zographos² and Dimitrios Fessas¹

¹ Department of Food, Environmental and Nutritional Sciences (DeFENS), Università degli Studi di Milano, Via Celoria 2, 20133, Milan, Italy

² Institute of Biology, Pharmaceutical Chemistry and Biotechnology, National Hellenic Research Foundation, 48 Vassileos Constantinou Ave., 11635 Athens, Greece

³ Department of Biochemistry and Biotechnology, University of Thessaly, Viopolis Larissa, Greece

⁴ Insect Molecular Genetics and Biotechnology Group, Institute of Biosciences & Applications, National Centre for Scientific Research "Demokritos", 153 10 Aghia Paraskevi, Athens, Greece

Mosquitoes and other arthropods may transmit infectious agents causing several diseases. In such a context, *Anopheles gambiae* is considered the primary mosquito vector responsible for the transmission of malaria causing more than 1 million deaths each year. The use of repellents is one of the strategies adopted to contrast the spread of such diseases as they reduce the contact frequency between vectors and human targets.

Like for other insects, the olfactory system of mosquitoes is essential for finding food, mates and blood meals and Odorant-binding proteins (OBPs) are the first components of their odor detection unit. Specifically, semiochemicals are captured by OBPs after their interaction with insect's antennae and are delivered to odorant receptors. Therefore, given the crucial role of OBPs, they constitute promising targets for the design of new repellent or attractant molecules and may improve the effectiveness of mosquitos control strategies (1,2).

Here we present a calorimetric study of the thermodynamic stability of AgamOBP4 and AgamOBP5 and their behaviour against several potential ligands. In spite of the great structural resemblance between these two proteins, nanoDSC investigation performed at different pH values (pH 5.0 and 8.0) revealed different pH-dependent thermodynamic profiles and stability. Moreover, AgamOBP5 and AgamOBP4 exhibited different binding affinities for certain molecules suggesting their ability to recognize different classes of odors and that they are likely involved in different pathways of host recognition. Specifically, among the potential ligands tested, AgamOBP4 preferentially binds to artemisia acetate, whereas AgamOBP5 prefers carvacrol, thymol and cuminaldehyde as binders.

References

- (1) Drakou, C.E.; Tsitsanou, K.E.; Potamitis, C.; Fessas, D.; Zervou, M.; Zographos, S.E. *Cell Mol Life Sci* **2017**, *74*, 319.
- (2) Tsitsanou, K.E.; Drakou, C.E.; Thireou, T.; Gruber, A.V.; Kythreoti, G.; Azem, A.; Fessas, D.; Eliopoulos, E.; Iatrou, K.; Zographos, S.E. *J Biol Chem* **2013**, *288*, 33427.

Poster presented at the 13th Medicta, 2017.



Thermodynamic studies of AgamOBP4 and AgamOBP5 from *Anopheles gambiae* with different semiochemicals



Francesca Saitta^{1,*}, Panagiota G.V. Liggri^{2,3}, Katerina E. Tsitsanou², Christina E. Drakou², Kostas Iatrou⁴, Spyros E. Zographos² and Dimitrios Fessas^{1,*}

¹ Department of Food, Environmental and Nutritional Sciences (DeFENS), Università degli Studi di Milano, Via Celoria 2, 20133, Milan, Italy

² Institute of Biology, Pharmaceutical Chemistry and Biotechnology, National Hellenic Research Foundation, 48 Vassileos Constantinou Ave., 11635 Athens, Greece

³ Department of Biochemistry and Biotechnology, University of Thessaly, Viopolis Larissa, Greece

⁴ Insect Molecular Genetics and Biotechnology Group, Institute of Biosciences & Applications, National Centre for Scientific Research "Demokritos", 153 10 Aghia Paraskevi, Athens, Greece

*corresponding authors: francesca.saitta@unimi.it, dimitrios.fessas@unimi.it

Introduction

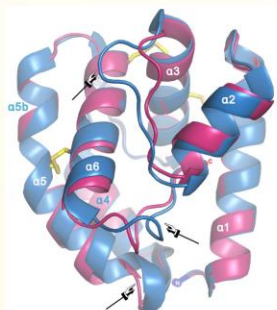


Figure 1. Superimposition of AgamOBP4 (blue) onto AgamOBP5 (magenta). Main differences are indicated by arrow heads.

Anopheles gambiae is considered the primary mosquito vector responsible for the transmission of malaria. The use of repellents is one of the strategies adopted to contrast the spread of such a disease as they reduce the contact frequency between vectors and human targets.

Like for other insects, the olfactory system of mosquitoes is essential for finding food, mates and blood meals and Odorant-binding proteins (OBPs) are the first components of their odor detection unit. Specifically, semiochemicals are captured by OBPs after their interaction with insect's antennae and are delivered to odorant receptors. Given the crucial role of OBPs, they constitute promising targets for the design of new repellent or attractant molecules and may improve the effectiveness of mosquito control strategies^[1-3].

Here we present a calorimetric study of the thermodynamic stability of AgamOBP4 and AgamOBP5 and their behaviour against several potential ligands. In spite of the great structural resemblance between these two proteins, nanoDSC investigation revealed different pH-dependent thermodynamic profiles.



Figure 2. Cartoon representation of AgamOBP5. The binding site is located at the center of a long hydrophobic tunnel represented as a surface.

Results and Discussion

Fig.3&4 show the DSC profiles of AgamOBP4 and AgamOBP5 alone and in presence of ligands at pH 8.0. Despite the structural similarities (Fig.1), OBP4 exhibited higher stability than OBP5 (Tab.1). As for ligands interaction, we observed that all the studied semiochemicals led to proteins stabilization, somehow revealing a protein-ligand interaction (Tab.1). The extent of the interactions depended on the ligand involved. A preliminary comparison between ligands' effects suggested that the small structural differences do not compromise the binding of these classes of ligands (direct ITC binding study is complicated since the tested ligands are not water-soluble). However, such effects are pH-dependent and work is in progress to better highlight these aspects that are strictly correlated with proteins' functionality.

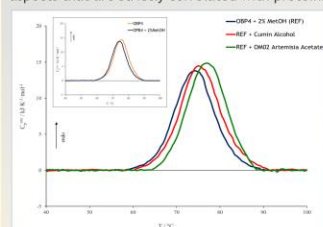


Figure 3. Nano-DSC thermograms for AgamOBP4 in 10mM Tris-HCl, 0.1M NaCl, pH 8.0, in presence of ligands. The box shows the effect of 2% MeOH (-0.5M) on protein stability.

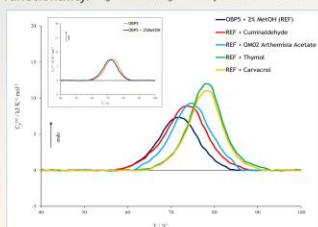


Figure 4. Nano-DSC thermograms for AgamOBP5 in 10mM Tris-HCl, 0.1M NaCl, pH 8.0, in presence of ligands. The box shows the effect of 2% MeOH (-0.5M) on protein stability.

Table 1. Thermodynamic parameters obtained for AgamOBP4 and AgamOBP5 by n-DSC measurements.

System	T_m / °C
OBP4 (REF)	74.2 ± 0.2
REF + Cumin alcohol	75.1 ± 0.2
REF + OMD2 Artemisia acetate	76.9 ± 0.2
OBP5 (REF)	71.7 ± 0.2
REF + Cuminoldehyde	73.4 ± 0.2
REF + OMD2 Artemisia acetate	74.6 ± 0.2
REF + Thymol	78.1 ± 0.2
REF + Carvacrol	78.0 ± 0.2

Materials & Methods

Protein Purification: The proteins were expressed in a high level in the form of inclusion bodies and were purified by a refolding protocol, followed by anion exchange chromatography (Resource Q), cation exchange chromatography (Resource S) and size exclusion chromatography (Superdex 75) as final purification step. Proteins purity was tested by SDS-PAGE electrophoresis.

Differential Scanning Calorimetry (DSC): Calorimetric experiments were performed with a capillary nano-DSC (Nano-DSC 6300, TA) at 0.5 °C/min scanning rate. Protein samples were obtained at pH 5 (150mM sodium acetate, 0.2M NaCl) and pH 8 (10mM Tris-HCl, 0.1M NaCl). Ligands were added to the proteins samples up to a [L]/[P] = 15 (ligands in MeOH; MeOH in protein sample = 2%).

Acknowledgments

This work is supported by a fellowship to P.G.V.L. by the Hellenic State Scholarships Foundation and the action "Support of Human research retention "Support of Human research retention" funded by the Operational Programme Education and Lifelong Learning" co-funded by the European Social Fund (ESF) and National Resources, MIS5000432. Work at I03 station at the Diamond Light Source (Oxford, UK) was supported by the INEXT grant (EU Horizon 2020 project #653706).

Conclusions

AgamOBP5 constitutes a novel target for structure based design of more efficient repellents. The overall AgamOBP5 protein structure is similar to the AgamOBP4 one, as revealed by X-ray studies (Fig.1&2). However, these two proteins showed pH-dependent thermodynamic stabilities and the ligand binding evidences at pH 8.0 also need to be compared at different pH values in order to evaluate whether they are involved in different pathways of host recognition.

References

- [1] Drakou, C.E. *et al.* Cell Mol Life Sci 2017, 74, 319.
- [2] Tsitsanou, K.E. *et al.* J Biol Chem 2013, 288, 33427.
- [3] Suh, E. *et al.* Curr Opin Insect Sci, 2014, 6, 86.

AWARDED POSTER during the 9th HeCrA, 2018.



X-ray crystal structure and binding studies of the Odorant Binding Protein 5 from the malaria vector *Anopheles gambiae*

Panagiota G.V. Liggi^{1,2}, Katerina E. Tsitsanou¹, Francesca Saitta³, Christina E. Drakou¹, Kostas Iatrou⁴, Dimitrios Fessas³, Spyros E. Zograghos^{1*}

¹ Institute of Biology, Pharmaceutical Chemistry and Biotechnology, National Hellenic Research Foundation, 48 Vassilicos Constantinou Ave., 11535 Athens, Greece

² Department of Biochemistry and Biotechnology, University of Thessaly, Voposki Larissa, Greece

³ Department of Food, Environmental and Nutritional Sciences (DaFENS) Università degli Studi di Milano, Via Celonia, 2 – 20133 Milano, Italy

⁴ Insect Molecular Genetics and Biotechnology Group, Institute of Biosciences & Applications, National Centre for Scientific Research "Demokritos", 153 10 Agia Paraskevi, Athens, Greece

Introduction

Like other insects, mosquitoes rely on olfaction to find mates, food and sources of blood meals. Odorant Binding Proteins (OBPs), that mediate the initial step in the transduction cascade of olfactory signals in insects, have been suggested to play an essential role in the detection and transportation of semiochemicals to Odorant Receptors (ORs) [1-4,7]. Therefore, a detailed knowledge of the 3D structures and functionality of OBPs may provide a valuable tool for the structure-based discovery of novel olfactory disruptors of insect host seeking behavior to be used in more effective mosquito control strategies.

The Odorant Binding Protein 5 (AgamOBP5) displays the highest expression levels in the female antennae. Its expression levels are also appear to be affected by the circadian cycle as they dramatically reduce in dark (DD) compared to light dark (LD) circles [6].

Herein, we present the novel 3D crystal structure of AgamOBP5 at 1.43 Å resolution. AgamOBP5 has a similar structure with AgamOBP4 (73% homology, 62.4% identity). Despite their structural similarity, Differential Scanning Calorimetry (DSC) studies at different pH values showed that these proteins exhibit different thermodynamic profiles.

Furthermore, fluorescent displacement assays in the presence of various volatile compounds of natural and synthetic origin [7] indicate that AgamOBP5 and AgamOBP4 exhibit different binding affinities for certain molecules suggesting distinct functionality in host recognition process.

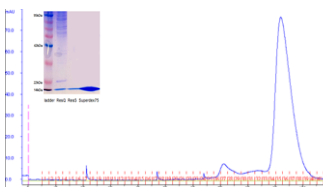


Figure 1. Size exclusion chromatographic profile. Inset: 15% SDS-PAGE electrophoresis gel depicting the purification process.

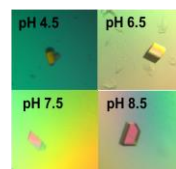


Figure 2. Crystals of AgamOBP5 grown at different pH values.

Table 1. Data collection and refinement statistics

Experiment	AgamOBP5
Wavelength (Å)	0.9763
Resolution range (Å)	53.7- 1.43 (1.51- 1.43)
Space group	P 2 ₁
Unit cell	34.15 36.57 54.83 90.00 101.24 90.00
Total reflections	74201 (9925)
Unique reflections (σ>0)	24431 (3520)
Multiplicity	3.0 (2.3)
Completeness (%)	99.4 (99.6)
Mean I/sigma(I)	17.3 (2.9)
R-merge	0.027 (0.283)
R-meas	0.033 (0.348)
CC 1/2	0.999 (0.943)
R-factor (R free)	0.1455 (0.1959)
Rms Bond Angle (°)	1.5851
Rms Bond Length (Å)	0.0164
Ramachandran favored/outliers	100%/0%

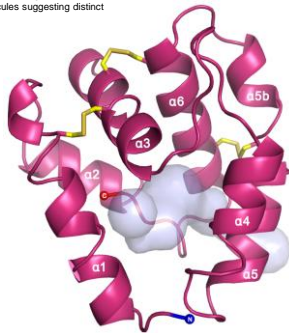


Figure 3. Cartoon representation of AgamOBP5. The binding site is located at the center of a long hydrophobic tunnel represented as a surface. The site is accessible to the solvent via two protein mouths.

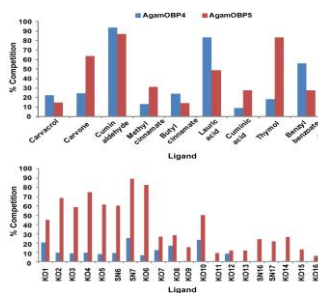


Figure 6. Affinity of natural (upper) and synthetic (down) compounds for AgamOBP4 and AgamOBP5 evaluated experimentally by fluorescence displacement binding assays.

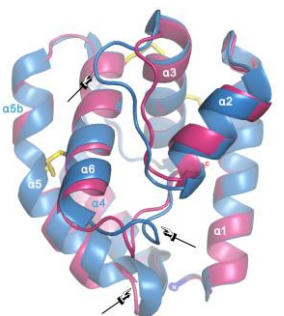


Figure 4. Superimposition of AgamOBP4 (blue) onto AgamOBP5 (magenta). Main differences are indicated by arrow heads.

Results & Discussion

AgamOBP5 constitutes a novel target for structure based design of more efficient repellents. The overall protein structure of AgamOBP5 is similar to that of AgamOBP4. It is comprised of six α helices ($\alpha 1$ - $\alpha 6$) connected by loops, which are arranged around of a central hydrophobic cavity. Three conserved disulfide bonds are formed between the cysteines of helices $\alpha 1$ and $\alpha 3$ (Cys19-Cys50), helix $\alpha 3$ and the top of helix $\alpha 6$ (Cys48-Cys103), $\alpha 6$ and helix $\alpha 5$ (Cys112-Cys92) stabilizing the compact protein structure (Figure 3). The cavity of AgamOBP5 resembles the one of AgamOBP4 with two openings to the protein surface. In both proteins the main opening is formed by the convergence of helices $\alpha 1$, $\alpha 3$ and $\alpha 4$. The second opening of AgamOBP5 is formed by residues from helices $\alpha 5$ and $\alpha 6$ while in AgamOBP4 is formed by residues from the hairpin loop between $\alpha 3$ and $\alpha 4$ helices and residues of the 3_{10} helix $\alpha 5b$ (Figure 4).

Comparison with AgamOBP4 revealed that despite their common structural fold, AgamOBP5 exhibits a binding cavity of quite different environment and shape suggesting different odorant specificities.

Although their structural similarity, Differential Scanning Calorimetry (DSC) studies at different pH values showed that these proteins exhibit different thermodynamic profiles. We found that AgamOBP5 is stable at both tested pH values (pH 5 & pH 8) while AgamOBP4 demonstrates stability only at pH 8 (Figure 5). It has been previously proposed that OBPs undergo pH-induced structural changes in the area of ORs (low pH) causing odor release [8]. Our findings suggest that the two proteins may utilize different release mechanisms of odors.

Furthermore, fluorescent displacement experiments in the presence of various volatile compounds [7] showed that AgamOBP5 and AgamOBP4 exhibit different binding affinities for certain molecules suggesting that they may recognize and bind different classes of odors and in all likelihood are involved in different pathways of host recognition (Figure 6). The detailed characterization of binding specificity of AgamOBP5 in comparison to AgamOBP4 is underway, aiming to improve our understanding of the odor discrimination by female mosquito in molecular level. Importantly, this work amplifying the repertoire of OBPs-targets and thus the number of semiochemicals as weapons in the arsenal against mosquitoes.

Materials & Methods

Protein Purification: The protein was expressed in a high level in the form of inclusion bodies and was purified by a refolding protocol, followed by anion exchange chromatography (Resource C), cation exchange chromatography (Resource S) and size exclusion chromatography (Superdex 75) as the final purification step. The protein was tested for its purity by SDS-PAGE electrophoresis (Figure 1) and concentrated to 12 mg/ml in HPLC water.

Crystallization and Data collection: AgamOBP5 protein crystals (Figure 2) were grown in various pH values (4.5-8.5) by the sitting drop vapor diffusion method using an automated crystallization system (Oryzanol). X-ray data from a single monoclinic crystal (P2₁) at 100K were collected on I03 station at the Diamond Light Source (Oxford, UK) to a maximum resolution of 1.43 Å.

Structure refinement: Data were integrated and scaled with the programs XDS and SCALA of the CCP4 suite. Maximum likelihood refinement (completed of positional minimization, and isotropic and anisotropic B-factor optimization) was performed using the program REFMAC5. Alternate cycles of manual building were performed with the program COOT. Details of data processing and refinement statistics are summarized in Table 1.

Differential Scanning Calorimetry (DSC): Nano Calorimeter Nano-DSC Model 6300 was used for the thermodynamical analysis of both proteins in two different buffer solutions of pH 5 (150mM sodium acetate, 0.2M NaCl) and pH 8 (10mM Tris-HCl, 0.2M NaCl).

Fluorescent displacement assays: Proteins were assayed at 1 μ M final concentration in the presence of 10 μ M 1-NPN probe and 5 μ M compound at a final volume of 200 μ l [7]. Assayed compounds were dissolved in 100% methanol and the final methanol content was 1.5%.

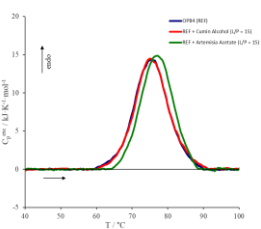


Figure 5. DSC study of AgamOBP4 at pH 8.0 in the presence of ligands. AgamOBP4 is only stable at pH 8.0 (no signal was obtained at pH 5.0), while AgamOBP5 is stable at both pH 5.0 and 8.0 (data not shown).

References

- Drakou CE, et al. (2017) *Curr Mol Life Sci* 74(2): 319-338
- Zograghos SE, et al. (2018) CRC book series: OSAR in Environmental and Health Sciences, Chapter 3, pp. 65-100. ISBN: 978-1483-7418-04
- Tsitsanou KE, et al. (2013) *J Biol Chem* 288(46): 33427-33438
- Tsitsanou KE, et al. (2015) *Cellular Biochem Biophys* 146(2): 203-207
- Blessmann H, et al. (2005) *Insect Molecular Biology* 14(6): 575-589
- Roud SSC, et al. (2013) *BMC Genomics* 14:219
- Thirum T, et al. (2013) *Insect Biochemistry and Molecular Biology* 38, 48-61
- Euroto Suh, et al. (2014) *Insect Science* 2014, 6:86-92

Acknowledgments

We are grateful to Christina N. Petrosidis, who assisted with preliminary protein expression analysis. This work was supported by a Fellowship to P.G.V.L. by the national State Scholarship Foundation and the action "Support of research workers' research through doctoral research" funded by the "Operational Programme Education and Lifelong Learning" and funded by the European Social Fund (ERDF) and National Resources, NSRF(2013). Work at 03 station at the Diamond Light Source (Oxford, UK) was supported by the BE2X grant (EU Horizon 2020 project 101019726).

v. *Mechanism of action of Sakacin-A, a bacteriocin with potential*

Abstract presented at the 60th SIB Congress, 2019.

Motta P.¹, D'Incecco P.¹, Saitta F.¹, Pellegrino S.², Fessas D.¹, Musatti A.¹,
Mapelli C.¹, Pellegrino L.¹, Barbiroli A.^{*,1}

¹ Department of Food, Environmental and Nutritional Sciences (DeFENS), Università degli Studi di Milano, Milano, Italy

² Department of Pharmaceutical Sciences, Università degli Studi di Milano, Milano, Italy

Bacteriocins are ribosomally synthesized peptides with antimicrobial activity against pathogenic Gram positive bacteria. These peptides show a high potency and low toxicity, and are often specific for a few target microorganisms. Sakacin-A is a class IIa bacteriocin produced by *Lactobacillus sakei* with anti-*Listeria* activity, and its use may prevent risks associated to *Listeria monocytogenes* in ready-to-eat foods. Class IIa bacteriocins share a common amphipathic structure: the highly conserved N-terminal structure is hydrophilic, positively charged and contains the YGNGV consensus sequence, whereas the C-terminal portion is hydrophobic and poorly conserved. Anti-*Listeria* activity is exerted by forming pores on the membrane of target cells by binding to the ManPTS receptor.

A better understanding of the molecular mechanisms underlying the specificity and anti-microbial activity of sakacin-A is a prerequisite for a more efficient exploitation of class IIa bacteriocins as food preservative or as an alternative to classical antibiotics.

Incorporation of Sakacin-A into different liposomes highlighted the role of ManPTS and of the nature of the membrane: a negative surface charge is essential for the interaction, but incorporation is not spontaneous in the absence of the receptor. Confocal microscopy was used to assess binding of the isolated N- and the C-terminal domains, conjugated with 5(6)-

carboxyfluorescein, to *Listeria* and other resistant microorganisms. Our data point to a general role of the N-terminal domain in the binding to different Gram positive bacteria, but not to the specific recognition of *Listeria*, suggesting a role of the C-terminal domain. The full length peptide was inserted into liposomes - where the C-term is hidden into the bilayer and the N-term is exposed to the outside - to verify the determinants of specific interactions between sakacin-A and *Listeria* proteins in pulldown experiments

Poster presented at the 60th SIB Congress, 2019.



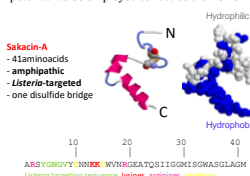
MECHANISM OF ACTION OF SAKACIN-A, A BACTERIOICIN WITH POTENTIAL

Paolo Motta¹, Paolo D'Incecco¹, Francesca Saitta¹, Sara Pellegrino², Dimitrios Fessas¹, Alida Musatti¹, Chiara Mapelli¹, Luisa Pellegrino¹, Alberto Barbiroli¹

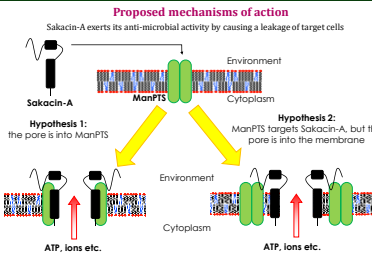
¹DeFENS, ²DISFARM, Università degli Studi di Milano, Milan, Italy -alberto.barbiroli@unimi.it

Introduction

Bacteriocins are a class of short ribosomally synthesized peptides with a strong antimicrobial activity against pathogenic Gram positive bacteria, and are usually specific for only one or a few target microorganisms. They are grouped into three classes based on their biochemical properties. **Sakacin-A** is a class IIa bacteriocin which is produced by the GRAS lactic acid bacterium *Lactobacillus sakei*. It has the potential to be employed to reduce the risk of *L. monocytogenes* poisoning of ready-to-eat food products.



Sakacin-A is reported to bind to a transmembrane sugar transporter (ManPTS) on the surface of target cells, folding into a defined structure, thus causing the formation of pores that lead to cell death. Nevertheless, the precise mechanism of action has yet to be fully elucidated. To gain more insight on this topic, we investigated (i) the role of membrane surface charges on the ability of Sakacin-A to be inserted and to fold in membrane models and (ii) the determinants of its selectivity by analyzing the binding of its two separate domains to different microorganisms.



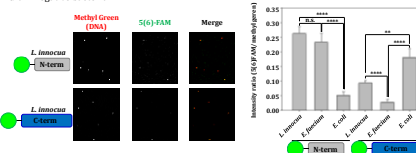
Results

Sakacin-A and its individual domains

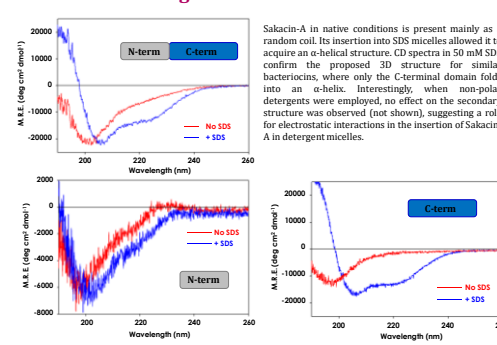
Full length Sakacin-A was purified by RP-HPLC from the culture medium of *Lactobacillus sakei*, with a yield = 1.2 mg/L culture.

Individual domains were produced by chemical synthesis, 'as is' and conjugated to the fluorophore 5(6)-carboxyfluorescein.

Target selectivity
 Fluorescently tagged domains bind on the surface of target cells. The strength of the interaction varies between the N- and C-terminus. The N-terminal domain recognizes ManPTS from phylogenetically different Gram positive microorganisms, resistant to Sakacin-A, but not from Gram negative bacteria.

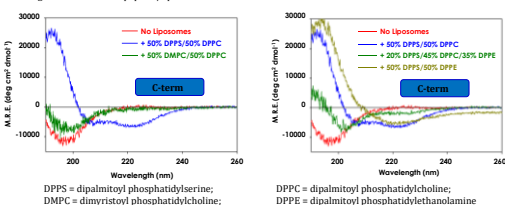


Effect of detergents on Sakacin-A structure



Phospholipid composition affects C-terminal structure

When the C-terminal domain of Sakacin-A is inserted into a phospholipid bilayer, it acquires an α -helical structure only in the presence of a negative charge (DPPE), whose amount affects the amount of acquired secondary structure. In addition, when DPPE is employed in the place of DPPC, the CD spectrum is further different, resembling more a β -sheet structure. Unlike SDS micelles, insertion in liposomes is not spontaneous: no effect was observed without thorough sonication of the peptide/liposomes mixture.



Pull-down experiment

The full length peptide was inserted into liposomes - where the C-term is hidden into the bilayer and the N-term is exposed to the outside - to verify the determinants of specific interactions between sakacin-A and *Listeria* proteins in pull-down experiments.

A: liposome + Sakacin-A + *Listeria* crude extract
 B: liposome NO Sakacin-A + *Listeria* crude extract

Summary

- A negatively charged bilayer is essential to induce Sakacin-A folding, but the insertion is not spontaneous
- The N-terminal domain is responsible for the binding on the surface of cells, but it's not sufficient to select the targets on which to exert the antimicrobial activity of Sakacin-A
- The C-terminal domain binds to a lower extent on target cells
- The binding of the C-terminal domain varies between species and might contribute to the target selectivity of Sakacin-A

Acknowledgements

This work was supported by funds from the Fondazione Cariplo (2015-0464 Nanosak-Nanocellulose-sakacin A conjugates for food packaging purposes)

B. List of publications

Brief summary	
<i>Papers with impact factor</i>	5 (3 published, 1 under revision, 1 in preparation)
<i>Parts in books</i>	5
<i>Personal contributions to scientific meetings</i>	11 (6 oral communications, 5 posters)
<i>Other contributions to scientific meetings</i>	5

i. *Papers with impact factor*

Saitta, F., Signorelli, M., Fessas, D., 2019. Dissecting the effects of free fatty acids on the thermodynamic stability of complex model membranes mimicking insulin secretory granules. *Colloids Surf B Biointerfaces*, 176, 167-175. <https://doi.org/10.1016/j.colsurfb.2018.12.066>

Pelosi, C.*, Saitta, F.*, Wurm, F.R., Fessas, D., Tinè, M.R., Duce, C., 2019. Thermodynamic stability of myoglobin-poly(ethylene glycol) bioconjugates: A calorimetric study. *Thermochim Acta*, 671, 26-31. (*These authors contributed equally to the work) <https://doi.org/10.1016/j.tca.2018.11.001>

Naziris, N., Saitta, F., Chrysostomou, V., Libera, M., Trzebicka, B., Fessas, D., Pispas, S., Demetzos, C., 2019. pH-responsive chimeric liposomes: from nanotechnology to biological assessment. *Int J Pharm*, ACCEPTED. (Manuscript Number: IJP-D-19-01421R1)

Saitta, F., Signorelli, M., Fessas, D., 2019. Hierarchy of interactions dictating the thermodynamics of real cell membranes: following the Insulin Secretory Granules paradigm up to fifteen-components vesicles. *Colloids Surf B*

Biointerfaces, SUBMITTED, UNDER REVISION. (Manuscript Number: COLSUB-D-19-01601)

Saitta, F., Motta, P., Barbiroli, A., Signorelli, M., Janaszewska, A., Klainert, B., Fessas, D., 2019. Influence of free fatty acids on lipid membrane-nisin interaction. *In preparation*.

ii. *Parts in books*

Saitta, F., Fessas, D., 2019. Artificial Insulin Secretory Granules' membranes: thermodynamic stability and interaction with food fatty acids. In: Canuti, V., Dinnella, C., Domizio, P., Fia, G., Lencioni, L., Monteleone, E., Picchi, M., Spinelli, S., Zanoni, B. (Eds.), Proceedings of the XXIV Workshop on the Developments in the Italian PhD Research on Food Science, Technology and Biotechnology, pp. 522-529. ISBN: 9788894467901.

Saitta, F., Signorelli, M., Fessas, D., 2019. ISG-like membrane thermodynamics: a stepwise calorimetric investigation. In: Rotaru, A., Vecchio Cipriotti, S. (Eds.), Book of abstracts of the 5th Central and Eastern European Conference on Thermal Analysis and Calorimetry (CEEC-TAC5) and 14th Mediterranean Conference on Calorimetry and Thermal Analysis (Medicta2019). Academica Greifswald, Germany, pp. 119. ISBN: 9783940237590.

Pizzimenti, S., Duce, C., Tinè, M.R., Bonaduce, I., Saitta, F., Signorelli, M., Fessas, D., 2019. The DSC monitoring of oil melting to follow the oil curing. In: Rotaru, A., Vecchio Cipriotti, S. (Eds.), Book of abstracts of the 5th Central and Eastern European Conference on Thermal Analysis and Calorimetry (CEEC-TAC5) and 14th Mediterranean Conference on Calorimetry and Thermal Analysis (Medicta2019). Academica Greifswald, Germany, pp. 118. ISBN: 9783940237590.

Saitta, F., Fessas, D., 2018. Thermodynamic Assessment of the Interaction of Food Fatty Acids with Pancreatic Model Membranes: Links Between Obesity and T2DM. In: Piga, A., Zara, S., Fadda, C., Del Caro, A., Montanari, L., Deiana, P., Budroni, M., Mannazzu, I., Mangia, N.P., Urgoghe, P.P. (Eds.), Proceedings – XXIII Workshop on the Developments in the Italian PhD Research on Food Science, Technology and Biotechnology, pp. 183-184. ISBN: 9788890767869.

Saitta, F., Fessas, D., 2017. Calorimetric study of new model cell membranes to assess the influence of food fatty acids and Ca^{2+} in the frame of T2DM onset and progression. In: Boselli, E., Brusetti, L., Ferrentino, G., Morozova, K., Scampicchio, M. (Eds.), Proceedings – XXII Workshop on the Developments in the Italian PhD Research on Food Science, Technology and Biotechnology. TG Book, Sandrigo, pp. 87-88. ISBN: 9788898416974.

iii. Communications to scientific meetings

Oral communications

Saitta, F., 2019. Artificial Insulin Secretory Granules' membranes: thermodynamic stability and interaction with food fatty acids. In: *24th Workshop on the Developments in the Italian PhD Research on Food Science, Technology and Biotechnology, September 11th-13th, 2019, Florence (Italy)*.

Saitta, F., 2019. Highly representative model membranes: a stepwise thermodynamic investigation on intrinsic lipid-lipid interactions and influence of food perturbing agents. In: *Short-Cicle Course on Thermal Analysis (Erasmus+ programme), September 02nd-06th, 2019, Rome (Italy)*.

Saitta, F., Signorelli, M., Fessas, D., 2019. ISG-like membrane thermodynamics: a stepwise calorimetric investigation. In: *5th Central and*

Eastern European Conference on Thermal Analysis and Calorimetry and 14th Mediterranean Conference on Calorimetry and Thermal Analysis – CEEC-TAC5&Medicta2019, August 27th-30th, 2019, Rome (Italy).

Saitta, F., Signorelli, M., Fessas, D., 2018. Thermodynamic stability of complex model membranes: the role of composition, morphology and food fatty acids. In: *XL National Conference on Calorimetry, Thermal Analysis and Chemical Thermodynamics – AICAT 2018, December 17th-19th, 2018, Pisa (Italy).*

Saitta, F., Signorelli, M., Fessas, D., 2018. Proteins and Calorimetry: from diluted solutions to food systems. In: *SIB (Gruppo Proteine) Advanced School: "Food Proteins", May 02nd-04th, 2018, Bergamo (Italy).*

Saitta, F., Signorelli, M., Fessas, D., 2017. Metabolic risk of new food technologies: calorimetric study of model cell membranes for the determination of the influence of free fatty acids (FFA) in diabetes mellitus onset. In: *IUMBM Advanced School on "A molecular view of the food-health relationship", May 15th-19th, 2017, Spetses (Greece).*

Poster presentations

Saitta, F., Signorelli, M., Fessas, D., 2019. Calorimetric investigation on the influence of free fatty acids on the stability of Insulin Secretory Granule model membranes. In: *Membrane Lipids, May 09th-10th, 2019, Berlin (Germany).*

Saitta, F., Liggri, P.G.V., Tsitsanou, K.E., Drakou, C.E., Iatrou, K., Zographos, S.E., Fessas, D., 2018. Thermodynamic studies of AgamOBP4 and AgamOBP5 from *Anopheles gambiae* with different semiochemicals. In: *XL National Conference on Calorimetry, Thermal Analysis and Chemical Thermodynamics – AICAT 2018, December 17th-19th, 2018, Pisa (Italy).*

Saitta, F., 2018. Thermodynamic assessment of the interaction of food fatty acids with pancreatic model membranes: links between obesity and T2DM. In: *23rd Workshop on the Developments in the Italian PhD Research on Food Science, Technology and Biotechnology, September 19th-21st, 2018, Oristano (Italy)*.

Naziris, N., Saitta, F., Pippa, N., Stellas, D., Chrysostomou, V., Pispas, S., Libera, M., Trzebicka, B., Signorelli, M., Demetzos, C., Fessas, D., 2017. Application of DSC and Imaging Techniques on the Development of Innovative Chimeric/Mixed Nanosystems. In: *13th Mediterranean Conference on Calorimetry and Thermal Analysis – Medicta 2017, September 24th-27th, 2017, Loano (Italy)*. (AWARDED)

Saitta, F., 2017. Calorimetric Study of New Model Cell Membranes to Assess the Influence of Food Fatty Acids and Ca²⁺ in the Frame of T2DM Onset and Progression. In: *22nd Workshop on the Developments in the Italian PhD Research on Food Science, Technology and Biotechnology, September 20th-22nd, 2017, Bozen (Italy)*.

Other communications to scientific meetings

Motta, P., D'Incecco, P., Saitta, F., Pellegrino, S., Fessas, D., Musatti, A., Mapelli, C., Pellegrino, L., Barbiroli, A., 2019. Mechanism of action of Sakacin-A, a bacteriocin with potential. In: *60th Congress of the Italian Society of Biochemistry and Molecular Biology (SIB), September 18th-20th, 2019, Lecce (Italy)*.

Pizzimenti, S., Duce, C., Tinè, M.R., Bonaduce, I., Saitta, F., Signorelli, M., Fessas, D., 2019. The DSC monitoring of oil melting to follow the oil curing. In: *5th Central and Eastern European Conference on Thermal Analysis and Calorimetry and 14th Mediterranean Conference on Calorimetry and*

Thermal Analysis – CEEC-TAC5&Medicta2019, August 27th-30th, 2019, Rome (Italy).

Motta, P., D’Incecco, P., Saitta, F., Fessas, D., Pellegrino, S., Rollini, M., Musatti, A., Mapelli, C., Barbiroli, A., 2019. Insights on the mechanism of action of class IIa bacteriocins. In: *44th FEBS Congress – From molecules to living systems, July 06th-11th, 2019, Krakow (Poland).*

Pelosi, C., Saitta, F., Wurm, F.R., Fessas, D., Tinè, M.R., Duce, C., 2018. Evaluation of thermal stability of model protein-polymer conjugates. In: *XL National Conference on Calorimetry, Thermal Analysis and Chemical Thermodynamics – AICAT 2018, December 17th-19th, 2018, Pisa (Italy).*

Liggri, P.G.V., Tsitsanou, K.E., Saitta, F., Drakou, C.E., Iatrou, K., Fessas, D., Zographos, S.E., 2018. X-ray crystal structure and binding studies of the Odorant Binding Protein 5 from the malaria vector *Anopheles gambiae*. In: *9th International Conference of the Hellenic Crystallographic Association (HeCrA), October 05th-07th, 2018, Patras (Greece). (AWARDED - POSTER)*

C. Honours and awards





D. Other activities

Scientific visits to Italian and foreign universities

- Training period for liposomes-model membranes preparation and characterization for applications in food and biological fields at the Laboratory of Pharmaceutical Technology, Section of Pharmaceutical Technology, Department of Pharmacy of the School of Health Sciences, **National and Kapodistrian University of Athens, Greece**, from 29/11/2016 to 10/12/2016 (Supervisor: Prof. Costas Demetzos);
- Training period focused on possible applications of FT-IR spectroscopy and atomic force microscopy (AFM) for studying model cell membranes and their interaction with pore-forming and amyloidogenic peptides at the Laboratory of Physical Chemistry for Biological Systems, Department of Chemical Sciences, **Università degli Studi di Catania, Catania**, from 16/03/2019 to 31/03/2019 (Supervisor: Prof. Carmelo La Rosa);
- Research period focused on the application of fluorescence spectroscopy (fluorescence anisotropy) and dynamic light scattering for studying model cell membranes and their interaction with a pore-forming peptide at the Department of General Biophysics, Faculty of Biology and Environmental Protection, **University of Lodz, Poland**, from 12/05/2019 to 15/06/2019 (Supervisor: Prof. Barbara Klajnert-Maculewicz).

Courses

- Sensing technologies and chemometrics (Supervisor: Prof. Alamprese)
- June 2018 (20 h, 3 cfu)
- Bioprocesses for the valorisation of agrifood by-products and residues (Supervisor: Prof. Molinari) - June 2018 (10 h, 2 cfu)

- Advanced spectroscopic methods in food systems (Supervisor: Prof. Bonomi) - February 2019 (22 h, 3 cfu)

Seminars

- Prof. Barbarossa: "Taste physiology and food choice" - 26/01/2017
- Prof. Demetzos: "Pharmaceutical nanotechnology: advanced liposomal drug delivery nanosystems" - 06/06/2017
- Prof. Šaponjac: "Food industry by-products: assessing the opportunities for their utilization" - 12/12/2017
- Prof. Valli: "Overlap of the physical chemistry approach in Unisalento and (bio)applications" - 23/05/2018
- Prof. Giancane: "Multifaceted approaches in sensing of targeted analytes" - 23/05/2018
- Prof. Bettini: "Design and development of tailored nanoparticles and their involvement in biotechnology and agrifood" - 23/05/2018
- Prof. Klapper: "Mathematical modelling of biofilms" - 10/05/2018
- Prof. Frazzon: "PRINT / CAPES / UFRGS program at the Institute of Food Science and Technology, Porto Alegre, Brazil" - 16/07/2019

Transferable skills (5 out of 5)

- "Open access – open data e il mondo delle pubblicazioni" - 21/11/2017 (4 h)
- "La valutazione della ricerca: indicatori bibliometrici e peer review" - 22/01/2018 (4 h)
- "Research Integrity" - 31/05/2018 (4 h)
- "Come scrivere un progetto di ricerca - parte 1 & 2. Le 100 cose che avrei voluto sapere quando ero un dottorando" - 09/07/2018 & 18/09/2018 (4+4 h)

Meetings

- Journal club: 6 out of 7 meetings (20 h)
- Ph.D. final exams: 1 out of 4 meetings (2 h)
- Opening of academic years: 2 out of 3 (4 h)
- Visit of students from the Wageningen University (4 h)
- One-day Seminar “Calorimetry for Food” (8 h)

Acknowledgments

Scientific acknowledgments

I have never been good in expressing my thanks, but at the end of this course I would like to dedicate this thesis to the many people who have made it possible by their work and support, each in their own way.

First of all, I would like to start by expressing my deep sense of gratitude to my tutor Prof. Dimitrios Fessas, who has followed me and my work in the past three years. I would like to thank you because you trusted in me even without knowing me. Thank you for the expertise, assistance, guidance and patience throughout these years and for continuously supporting my scientific growth. I would also like to thank Dr. Marco Signorelli for the competence and the significant help in laboratory work organization.

I would like to extend my sincere gratitude to Prof. Carmelo La Rosa from the University of Catania for the time spent in teaching during my short but inspiring scientific visit. I am also grateful to Prof. Costas Demetzos, Dr. Natassa Pippa and Dr. Nikolaos Naziris from the National and Kapodistrian University of Athens (Greece) and to Prof. Barbara Klajnert-Maculewicz and Dr. Anna Janaszewska from University of Lodz (Poland) for the stimulating and fruitful research and for the pleasant time spent in their laboratories allowing me to improve my expertise as a researcher. Many thanks also to

Prof. Alberto Barbiroli, Dr. Paolo Motta, Prof. Luciano Piergiovanni and Prof. Alberto Schiraldi from the University of Milan for the help and for allowing me to enrich my Ph.D. research with interesting details.

Last in my scientific acknowledgments but not least, I submit my heartiest gratitude to Prof. Giuseppe Arena from the University of Catania. Although we were not involved in a concrete scientific collaboration during my Ph.D., you have always been present, you have continuously watched over my scientific and professional growth as always done throughout my university career. But my acknowledgments are not merely scientific. I owe you part of the person and the researcher I am today. Thank you so much for encouraging me to move to Milan, for listening to my doubts and my worries and for pushing me to believe more in myself and in my abilities. I will never forget it.